PCCP

View Online
Dynamic Article Links

Cite this: *Phys. Chem. Chem. Phys.*, 2011, **13**, 15350–15383

www.rsc.org/pccp

PERSPECTIVE

Molecular transport in nanopores: a theoretical perspective

Suresh K. Bhatia,* Mauricio Rincon Bonilla and David Nicholson

Received 13th April 2011, Accepted 15th June 2011
DOI: 10.1039/c1cp21166h

Molecular transport in nanopores plays a central role in many emerging nanotechnologies for gas separation and storage, as well as in nanofluidics. Theories of the transport provide an understanding of the mechanisms that influence the transport and their interplay, and can lead to tractable models that can be used to advance these nanotechnologies through process analysis and optimisation. We review some of the most influential theories of fluid transport in small pores and confined spaces. Starting from the century old Knudsen formulation, the dusty gas model and several other related approaches that share a common point of departure in the Maxwell–Stefan diffusion equations are discussed. In particular, the conceptual basis of the models and the validity of the assumptions and simplifications necessary to obtain their final results are analysed. It is shown that the effect of adsorption is frequently either neglected, or treated on an ad hoc basis, such as through the division of the pore flux into gas-phase and surface diffusion contributions. Furthermore, while it is commonplace to assume that cross-sectional pressure is uniform, it is demonstrated that this violates the Gibbs–Duhem relation and that it is the chemical potential that essentially remains constant in the cross-section, as near-equilibrium density profiles are preserved even during transport. The Dusty Gas model and Maxwell–Stefan model for surface diffusion are analysed, and their strengths and weaknesses discussed, illustrating the use of conflicting choices of frames of reference in the former case, and the importance of assigning appropriate values for the binary diffusivity in the latter case. The oscillator model, developed in this laboratory, which is exact in the low density limit under diffuse reflection conditions, is shown to represent an advance on the classical Knudsen formula, although the latter frequently appears as a fundamental part of many transport models. The distributed friction model, also developed in this laboratory for the study of multi-component transport at any Knudsen number is discussed and compared with previous approaches. Finally, the outlook for theory and future research needs are discussed.

1. Introduction

The problem of modeling the transport of fluids in narrow pores and confined spaces has attracted considerable attention

School of Chemical Engineering, The University of Queensland, Brisbane, QLD 4072, Australia. E-mail: s.bhatia@uq.edu.au

Suresh K. Bhatia

Suresh Bhatia is Professor of Chemical Engineering, and Australian Professorial Fellow, at the University of Queensland. He received his BTech from the Indian Institute of Technology, Kanpur, and MSE and PhD degrees in Chemical Engineering from the University of Pennsylvania. His research interests focus on theoretical modelling and simulation of adsorption and transport in nanoporous materials and in heterogeneous reaction engineering, where he has authored over 180 scientific articles in learned journals. He is a Fellow of the Academy of Technological Sciences and Engineering in Australia, and of the Indian Academy of Sciences.

Mauricio Rincon Bonilla

Mauricio is a PhD candidate at the University of Queensland, Australia, working under the direction of Professor Suresh Bhatia. He received his BSc and MSc degrees in chemical engineering from the National University of Colombia, Medellin in 2004 and 2007, respectively. After a brief career in industry, Mauricio received the UQIRTA scholarship to join Bhatia's group, where his current research is focused in theoretical modelling and simulation of transport in nanoporous materials, at both the single pore and macroscopic levels.

among scientists and engineers for over a century, due to its importance to a variety of applications of industrial interest. These include heterogeneous catalysis, gas–solid reactions, adsorptive separations, electrochemical processes and a host of other systems involving the infiltration of fluids in porous materials. The topic has gained renewed attention in the last two decades as a consequence of the explosive development of a wide array of novel nanoporous materials such as carbon nanotubes,[1,2] metal organic frameworks,[3–5] and periodic mesoporous materials such as MCM-41 and its analogues,[6–10] as well as zeolite based membranes.[11,12] Complementing their development, there has been a large on-going international effort aimed at exploiting these materials in novel applications, such as in hydrogen[13,14] and electrochemical energy storage[15] and lab-on-a chip technology and nanofluidics,[16–18] besides the conventional applications indicated above. All of these applications involve the movement of fluids through highly confined spaces, and success in designing and optimizing both the materials and processes relies critically on the understanding of how the fluid molecules are transported within the structure, under the action of concentration and pressure gradients and the possible influence of an adsorption field.

Research on transport in confined spaces has a long history, dating back to the works of Knudsen[19–23] and von Smoluchowski[24,25] during the first decade of the 20th century. While the area has been active ever since because of its numerous applications, only limited progress was achieved until recently, with models and theories relying heavily on variations of the early results of almost a century ago. Knudsen and Smoluchowski focused their attention on the low density hard sphere gases, thereby omitting the effect of fluid–fluid intermolecular and gas–wall interactions on the transport. An important feature of the original Knudsen model was the assumption that hard spheres reflected at the wall lost all memory of their original tangential momentum. This assumption of 'diffuse reflection' in Knudsen's original equation was modified by Smoluchowski to account for the possibility that a fraction of the collisions was purely specular (the rest being purely diffuse), in a refinement of the Knudsen equation.

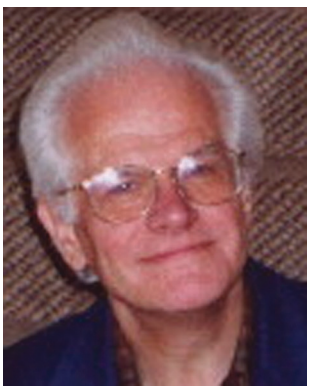

David Nicholson

David Nicholson is Emeritus Reader in Physical Chemistry at Imperial College of Science, Technology and Medicine, London, from where he retired in 2001. Since 2003 he has been Honorary Visiting Professor in the School of chemical Engineering at The University of Queensland. His main research interests are in the theory and simulation of interfacial systems, and in the use molecular dynamics simulation in predicting transport properties. He has over 180 publications in learned journals, and has served as an elected member of the International Adsorption Society during 2001–2005.

The mechanism of wall reflection still remains largely unresolved, especially for molecular species. A few decades later this treatment was refined by Pollard and Present,[26] who extended the theory to higher densities, albeit retaining the non-interacting hard-sphere gas and hard-wall assumptions. The dusty gas model (DGM), later developed by Evans, Watson and Mason[27–29] based on the Chapman–Enskog theory of transport[30] and subject to further re-derivations by Mason *et al.*[31–33] has been the most popular approach to the modeling of multicomponent transport in porous media, and has been widely used in interpreting experimental results of fluids flow through adsorbents and catalysts.[34,35] The DGM relies on the assumption that the wall-mediated contribution to transport can be described by the Knudsen model, thereby inheriting the weaknesses of the century old approach. Furthermore, the division of the flux vector into a diffusive and a viscous non-segregative contribution has been recently called into question.[36,37] As a consequence, semi-empirical fitting parameters are often introduced in this model to obtain better agreement with experimental data,[38,39] explaining the apparent success of the approach.

The introduction of intermolecular forces from rigorous statistical mechanical considerations based on kinetic theory of dense fluids has been attempted,[40,41] although such models become rapidly intractable when many-body systems are considered and have found only limited application.[42] Generally, models derived from simplified forms of the Maxwell–Stefan equations, such as the dusty gas model, have been preferred,[43,44] leading to more tractable approaches, albeit at the expense of dispersive interactions between the wall and the fluid, and of the fluid inhomogeneities. The role of adsorption forces was recognized after the 1940's, for example by Wicke and Kallenbach[45] and Barrer and co-workers[46,47] who invoked the concept of surface 'diffusion' to explain the extra flow (*i.e.* in excess of the Knudsen prediction) experimentally observed in microporous compacts. In essence this concept relied on the supposition that gas phase and surface phase flows were separable; the former being treated as pure Knudsen flow. Krishna and co-workers[48,49] have developed a Maxwell–Stefan-type model for transport of mixtures at the nanopore level, that includes surface transport. The terms "activated diffusion" or "surface diffusion" are often found in the literature to describe the diffusion in cases where the presence of a strongly adsorbed phase clearly contributes to transport, and the use of a Knudsen diffusion coefficient empirically modified by an Arrhenius type factor to better capture the effect of temperature is common place in the description of this phenomenon.[50,51] The approach of Krishna, based on the more rigorous Maxwell–Stefan approach, relies on the empirical specification of the mutual-diffusion parameters from the individual transport coefficients, while the fluid inhomogeneities seen in mixture equilibrium adsorption simulations are overlooked.

Molecular dynamics (MD) simulations on the other hand, do not suffer from the uncertainties arising from the assumptions and simplifications introduced for tractability of the theoretical models. In molecular dynamics, an approximate solution to the molecular many-body problem is developed using techniques such as the Gear or Verlet algorithms, based

on truncated Taylor expansion of the molecular coordinates; by a suitable choice of time step (typically of the order of a femto second) it is then possible to obtain sufficiently accurate phase space trajectories to represent the time evolution in real systems.[52,53] The description of physical reality is then only limited by the accuracy of the force fields describing the interactions in the system, the spatial representation of the porous matrix, and the limitations imposed by finite computing resources. The last constraint in particular restricts its use for the analysis of experimental permeation data in macroscopic solids, as well as for process design and optimization purposes. While invaluable as a research tool, MD also serves as a powerful basis to assess the validity of the theoretical models, and of the underlying assumptions and simplifications. This is of particular importance in those cases when experiments are either impossible or inadequate.

In recent years, new models to deal with the problem of transport in nano and mesoporous materials have emerged from this laboratory, namely the oscillator model[54,55] and the distributed friction model.[56,57] In these models, the fluid–solid interaction potential is explicitly considered in the calculation of the transport coefficients. While the oscillator model is exact under diffuse reflection conditions in the low density limit, and therefore represents an important advance over the Knudsen formulation for hard-spheres, the distributed friction model provides a novel framework for the analysis of transport of multicomponent mixtures in narrow pores at any density. As opposed to earlier approaches, the distributed friction model takes account of the fluid inhomogeneities arising from the interactions with the wall, and introduces the wall-mediated contribution to transport through a phenomenological friction coefficient that can be precisely estimated by means of the oscillator model. The resulting model is fully predictive, and provides a bridge between tractability and theoretical rigor.

In this article we survey the theories developed for the study of transport in confined spaces, starting from the classical work of Knudsen. It is shown that available experimental and simulation data found in the literature do not support the Knudsen hypothesis of a hard-sphere non-interacting gas, but instead indicate that molecular transport is strongly affected by the fluid–wall potential. This potential leads to a significant reduction in the diffusion coefficient compared to that obtained with the Knudsen formulation. The widely-used dusty gas model is analyzed and key conceptual flaws in its derivation are outlined. Other theories based on the Maxwell–Stefan diffusion equations are also discussed. While problems in the dusty gas formulation have been recognized,[37,44,58] the modifications put forth have overlooked fluid inhomogeneity, and are principally appropriate for relatively large pores. The extension of the Maxwell–Stefan equations to the study of surface diffusion is also analyzed, and the advantages and disadvantages of the oscillator and distributed friction models with respect to the preceding theories discussed. Although not all of the available theories are presented in depth in this focused review, given the vast amount of literature on the subject, it is hoped that the most influential approaches, in particular those that are widely used and have provided the framework for the development of many other models and theories, are covered.

2. The Knudsen model

First derived in 1909,[19] the Knudsen model of the diffusion of a rarefied gas under confinement in a tube has formed the most widely used point of departure in our understanding of transport in narrow pores at low density. In his pioneering analysis of the transport of non-interacting hard sphere molecules while undergoing diffuse reflection on the tube surface, Knudsen recognized that, at a density low enough for the mean free path λ to be large compared to the tube diameter, the frequency of molecular collisions would be small relative to that of molecule–wall collisions. Molecule–wall collisions would therefore govern gas diffusion under the action of a pressure gradient along the tube. Knudsen's original analysis, based on momentum conservation arguments, was soon after refined by Smoluchowski[24] through a detailed treatment of molecular trajectories to provide the now classic equation

$$D_{\mathrm{k}} = \frac{d}{3}\sqrt{\frac{8k_{\mathrm{B}}T}{\pi m}} \tag{1}$$

for the diffusion coefficient in tube of effective diameter d, where m is the molecular mass and T is temperature. This diffusion coefficient differs from the original Knudsen result[19] by a factor of $3\pi/8$, and permits the estimation of flux based on a pressure gradient driving force, through the phenomenological model

$$J = -\frac{D_{\mathrm{k}}}{RT}\nabla p \tag{2}$$

where J and ∇p are molar flux and pressure gradient, respectively. Pollard and Present[26] extended Smoluchowski's analysis for the case when the mean free path is smaller than the tube dimensions. Their theory accurately predicts the self-diffusion coefficient for non-interacting molecules at all densities, and reduces to eqn (1) in the low density limit (large Knudsen numbers, $\mathrm{Kn} = \lambda/d \rightarrow \infty$) and the kinetic theory limit[59] for the self-diffusivity at high pressures ($\mathrm{Kn} \rightarrow 0$), $D_{\mathrm{self}} = (1/3)\bar{v}\lambda$, where $\bar{v}(= \sqrt{8k_{\mathrm{B}}T/\pi m})$ is the mean molecular velocity.

2.1 Momentum accommodation

Key to the above developments is the assumption of diffuse reflection, which was vindicated by Knudsen's experiments,[19,20] in his matching of theory and experiment using tubes of 0.0033–0.0145 cm diameter. As a result it has become common to use this assumption even in molecular dynamics simulations.[54–57,60–62] In practice, this assumption may well be reasonable for disordered carbons, where diffusivity values estimated from fits of experimental uptake kinetics,[63,64] of the order of 10^{-8}–10^{-7} $\mathrm{m^2\ s^{-1}}$, are of similar range of magnitudes as simulation results for the transport coefficient in slit carbon nanopores based on diffuse reflection.[62] Similarly, permeabilities for various gases in a DDR zeolite membrane[11] have also been matched by theory considering diffuse reflection,[65] and transport coefficients for gases in various zeolites[66] are of the order of 10^{-8}–10^{-10} $\mathrm{m^2\ s^{-1}}$, and in the range of values predicted by theory and MD considering diffuse reflection in nanopores.[55] Such results suggest the diffuse reflection assumption to be reasonable for oxide surfaces (where gas–solid interaction is dominated by the surface oxygen). However, for ordered

carbon surfaces such as those of graphitic slit pores and carbon nanotubes, atomistic simulations[67–69] have yielded extremely high diffusivities, of the order of 10^{-5}–10^{-4} m^2 s^{-1}, suggesting nearly specular reflection, attributed to their smooth energy landscape. The momentum accommodation (fraction of tangential momentum lost to the wall) in such cases is small, leading to rapid transport. Partial momentum accommodation on wall collision was first considered as early as 1879 by Maxwell,[70] and later incorporated in his trajectory analysis by Smoluchowski[24] by defining a fraction, α, of diffuse collisions with the remainder $(1 - \alpha)$ being specular. This led to the corrected result for the diffusion coefficient

$$D_k(\alpha) = \frac{2-\alpha}{\alpha} D_k(1) \quad (3)$$

where $D_k(1)$ is the diffuse reflection result in eqn (1), arising when $\alpha = 1$. Recently, Arya and co-workers[71] extended Smoluchowski's treatment by analyzing the trajectories of hard spheres in rough slit-shaped pores, obtaining,

$$D_k(\alpha) = \left[1 - \frac{2\pi(1-\alpha)}{\alpha \ln \varepsilon}\right] \ln \varepsilon D_k(1) \quad (4)$$

where $\varepsilon = mv_c^2/2k_BT$ and v_c is a cut-off velocity that must be introduced due to the fact that, in ideal slit-shaped pores, infinitely long trajectories for molecules travelling parallel to the walls are possible, leading to unbounded diffusion coefficients in the low density limit. Such a cut-off is physically reasonable since for large, though finite, Knudsen numbers the probability of molecule–molecule collisions is not entirely zero. Besides, in real systems with slit-like shapes the pores are finite and may not be straight. These issues were also discussed earlier by Hiby and Pahl.[72] Cylindrical pores, on the other hand, impose a natural geometrical cut-off.

The Knudsen theory was rapidly adopted in vacuum technology applications, such as the development of diffusion pumps,[73–76] molecular beam research[77] or viscosity gauge theory.[78,79] In the majority of these applications the gas container critical dimension is usually of the order of a few micrometres, and eqn (1) offers a good estimate of the diffusion coefficient since wall–fluid interactions are negligible for most of the tube volume. The Knudsen model has also been widely adopted for the analysis of transport in porous catalysts and reactive porous solids,[34] as well as the permeation of membranes and adsorbents with pores above the IUPAC limit of microporosity (>2 nm).[35] Nevertheless, most of the modern applications of Knudsen theory on transport in porous media are usually embedded into the framework of the dusty gas model.[27,32]

2.2 Failure of the Knudsen model due to adsorption-related effects

Although the Knudsen equation has shown good agreement with experiments carried out under vacuum conditions in relatively wide cylinders of a few micrometres diameter,[19,77] direct experimental verification of its validity at the mesopore level (2 nm–50 nm) has proven elusive. This is largely because common mesoporous solids such as silicas and aluminas are highly disordered and may possess a complex multi-scalar structure[80] that makes it difficult to isolate molecular transport at the single pore level. Nevertheless, for mesopores, one expects that, below a certain temperature which increases with decreasing pore size and increasing gas–solid interaction strength, the molecular trajectories will not be rectilinear, as is inherent to hard sphere systems envisioned in the Knudsen and Smoluchowski analyses, since the molecules will not have enough kinetic energy to escape from the wall attraction field in the vicinity of the pore wall. Thus, adsorption is expected to lead to deviations from the Knudsen model, especially for gases with a strong affinity for the solid, at low temperatures and under stringent confinement.

The role of adsorption strength at low pressure can be readily visualized through the Henry law equilibrium constant. Consider for instance a cylindrical pore with the wall–fluid interaction following the well-known hypergeometric potential,[81]

$$\frac{\phi_{fs}(r)}{\varepsilon_{fs}} = 4\rho_s[\sigma_{fs}^{12} I_1 - \sigma_{fs}^6 I_2] \quad (5)$$

where

$$I_1 = \frac{63\pi}{128 d_{cc}^{10}(1-\beta^2)^{10}} F(-4.5, -4.5, 1; \beta^2) \quad (6)$$

$$I_2 = \frac{3\pi}{4 d_{cc}^{4}(1-\beta^2)^{4}} F(-1.5, -1.5, 1; \beta^2) \quad (7)$$

Here $\phi_{fs}(r)$ is the fluid–solid potential, r is the radial coordinate, ε_{fs} and σ_{fs} are the Lennard Jones (LJ) fluid–solid well depth and collision diameter, respectively, d_{cc} is the (center to center) diameter of the pore, ρ_s is the surface atomic density and $\beta = 2r/d_{cc}$. The equilibrium constant is given by

$$K = \frac{8}{d_{cc}^2} \int_0^{d_{cc}/2} r e^{-\phi_{fs}(r)/k_BT} dr \quad (8)$$

and can be expressed as a function of an energy parameter, $\theta = k_BT/\varepsilon_{fs}\rho_s\sigma_{fs}^2$, representing the ratio of kinetic to potential energy for a fluid molecule, and a size parameter $s = d_{cc}/\sigma_{fs}$. Fig. 1a depicts the variation of K with θ at different values of s. For sufficiently wide pores, K approaches unity as θ increases. This is because in systems with high values of θ ($\theta \gtrsim 3.2$), molecules will have sufficient kinetic energy to overcome the strength of dispersive van der Waals forces exerted by the wall, thus retaining the bulk density inside the pore and making adsorption negligible. The region in which Knudsen-like diffusion occurs must then be embedded within the interval $(3.2 < \theta < \infty)$. On the other hand, for small values of θ ($\theta \lesssim 1$) adsorption is significant and molecules tend to be concentrated in the vicinity of the pore wall, with their trajectories restricted to a region around the minimum of the potential field. In that case, the Knudsen hypothesis of hard-sphere solid–fluid interaction will no longer be a good approximation and eqn (1) will surely fail. In the intermediate region $(1 < \theta < 3.2)$ the adsorption strength depends on the size parameter s. For example, for $\theta = 1.5$, adsorption is weak in a system with $s = 30$ but very significant in a system with $s = 8$, from which one expects the Knudsen model to perform poorly in predicting the transport coefficient of the latter and relatively better in predicting the diffusivity of the former. Let us take as an

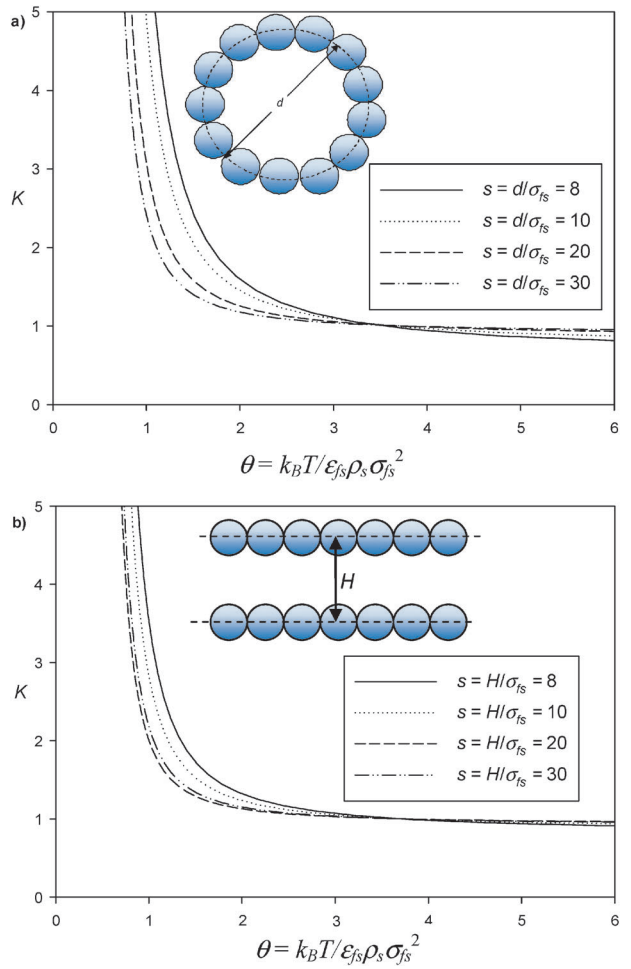

Fig. 1 Equilibrium constant as a function of the energy parameter $\theta = k_B T/\varepsilon_{fs}\rho_s\sigma_{fs}^2$ for (a) a cylindrical pore at different values of $s = d_{cc}/\sigma_{fs}$, and (b) a slit-like pore at different values of $s = H/\sigma_{fs}$. When K deviates significantly from a value of 1 the Knudsen equation is not recommended. For $\theta \gtrsim 3.2$ the Knudsen equation is likely to provide a reasonable first-estimation of the low density diffusivity for pores larger than the considered pore size.

example the adsorption of He and CH_4 in MCM-41 silica, with solid–solid LJ interaction parameters estimated from Neimark *et al.*[82] as $\sigma_{ss} = 0.28$ nm, $\varepsilon_{ss}/k_B = 492.7$ K, and $\rho_s = 10.47$ nm^{-2}. The fluid–solid parameters are calculated from the Lorentz–Berthelot rule, using for the fluid–fluid interactions $\sigma_{ff} = 0.381$ nm and $\varepsilon_{ff} = 148.1$ K in the case of methane and $\sigma_{ff} = 0.2551$ nm and $\varepsilon_{ff} = 10.22$ K in the case of helium. For He at 298 K, $\theta = 5.3$ and the Knudsen model is likely to provide a reasonable estimation of the low density diffusion coefficient at any pore size in the mesopore region. On the other hand, for a more strongly adsorbed species such as CH_4, for which θ (298 K) = 0.973, even for pores as large as 12 nm (about 30 times the molecule LJ size) the Knudsen model is likely to fail. In order to reach the point of negligible adsorption strength the temperature should be about 650 K for a 12 nm diameter pore and 960 K for a 3 nm pore. For a single walled carbon nanotube (SWNT) the parameters given by Nguyen *et al.*[83] are $\sigma_{cc} = 0.34$ nm, $\rho_c = 38.2$ nm^{-2} and $\varepsilon_{cc}/k_B = 36$ K, where the value of ε_{cc}/k_B reflects the interaction enhancement due to curvature effects. At 298 K, we have $\theta = 0.82$ for CH_4 and $\theta = 1.85$ for H_2 where, for H_2, $\sigma_{ff} = 0.2551$ nm and $\varepsilon_{ff} = 38.0$ K have been taken.[83] That is, even for the weakly adsorbed H_2 the adsorption strength is not negligible at all pore sizes in the mesopore region at 298 K. Only for $s > 20$ is it reasonable to neglect the wall adsorption field. A value of $\theta > 3.2$ is reached at 1150 K for CH_4 and 550 K for H_2, so that, below these threshold temperatures, the analysis of transport in mesoporous carbon nanotube membranes through the Knudsen theory can lead to serious error.

Fig. 1b depicts the Henry law constant for a slit-like pore comprised of one atomic layer, calculated by

$$K = \frac{1}{s}\int_0^s e^{-\phi_{fs}(x)/k_B T}dx \qquad (9)$$

where $s = H/\sigma_{fs}$, with H the pore width. The fluid–solid interaction is assumed to have the form of the Steele potential[84] for a graphitic slit pore with single layer walls,

$$\phi_{fs}(x) = \frac{2\pi}{\theta}\left\{\left[\frac{2}{5}\left(\frac{1}{x}\right)^{10} - \left(\frac{1}{x}\right)^{4}\right] + \left[\frac{2}{5}\left(\frac{1}{s-x}\right)^{10} - \left(\frac{1}{s-x}\right)^{4}\right]\right\} \qquad (10)$$

The plot resembles that obtained for cylindrical pore, although it is slightly less steep. As a consequence, the same basic conclusions will apply to the slit-like shape, albeit requiring a velocity cut-off in estimating low pressure diffusivity when adsorption is neglected.[71]

The failure of the Knudsen model in the presence of adsorption is evident from a multitude of available experimental and theoretical results. A suitable point of departure for investigating adsorption effects is the corrected flux model

$$J = -D_o\nabla\rho_t = -\frac{KD_o}{RT}\nabla p \qquad (11)$$

where D_o is the low density transport coefficient, ρ_t is mean molar density of the adsorbed phase and p is the pseudo-bulk pressure at which the bulk fluid would be in equilibrium with the adsorbate at density ρ_t, assuming a linear isotherm (*i.e.* sufficiently low pressure). In practice, however, it is the macroscopic permeability of the adsorbent that it is extracted from permeation experiments. Since the detailed topology of the pore network is often unknown, the results are usually correlated through a phenomenological equation of the form of eqn (11), replacing the local values of K and D_o by effective values and introducing the factor ε_p/γ, where ε_p is the particle porosity, typically extracted from independent sorption experiments and γ is the tortuosity, which is frequently left as an adjustable parameter. In general, the effective values of K and D_o are obtained from the corresponding single pore relations, such as in eqn (1) and (8), evaluated at a representative pore radius $\bar{r}_p$. In that case, the permeability b is given by,

$$b = J^{mac}/(-\Delta p/L) = \frac{\varepsilon_p K(\bar{r}_p)D_0(\bar{r}_p)}{\gamma RT} \qquad (12)$$

where J^{mac} is the macroscopic measured flux and L is the sample thickness in the direction of the macroscopic pressure gradient. Eqn (12) is often employed to extract the system

tortuosity, with $\bar{r}_p$ estimated from the ratio of the void volume to the surface area. When $D_o(r_p)$ is evaluated by the Knudsen model in eqn (1), $K(r_p)$ is most commonly taken as unity,[85,86] equivalent to assuming that the fluid is an ideal gas, and that no adsorption occurs.

Qiao and Bhatia[87,88] have measured the low pressure diffusivities of a series of paraffins (nC_6–nC_{10}) in mesoporous MCM-41 silica of pore diameter 3.79 nm, over a range of temperatures, using the zero-length column (ZLC) method. For the straight parallel channels of MCM-41, $\gamma = 3$,[89] as the crystallites are randomly oriented[80] and eqn (12) predicts the Knudsen permselectivities (neglecting adsorption, *i.e.* using $K = 1$)

$$(b_1/b_2)_{\text{Knudsen}} = \frac{D_{o1}}{D_{o2}} = \sqrt{\frac{M_2}{M_1}} \qquad (13)$$

Fig. 2a depicts the Knudsen permselectivity (relative to hexane) *versus* the square root of the molecular weight ratio, $(M_{hex}/M)^{1/2}$, for the various paraffins, based on the data of Qiao and Bhatia. The temperature range in the parenthesis indicates the maximum and minimum temperature of the measurements. The highest temperature corresponds in all cases to the point closer to the Knudsen limit, whereas the lowest temperature is associated with the furthest one. It is clear that Knudsen theory fails to explain transport of these paraffins in the silica sample. Further, *n*-decane and *n*-octane, which are more strongly adsorbed than *n*-heptane, exhibit a more pronounced deviation from the Knudsen line. As temperature is increased, a larger fraction of molecules can overcome the potential barrier near the wall and the Knudsen model becomes a better approximation. Qiao and Bhatia[87,88] also determined the equilibrium constants of the different alkanes at the temperatures used. Following eqn (12) the apparent permselectivities, $KD_o/KD_{o,hex}$, which correspond to the actual low pressure permselectivity b/b_{hex} with respect to *n*-hexane when the tortuosity is the same for all species, may then be plotted against $(M_{hex}/M)^{1/2}$. Fig. 2b depicts the result for the same temperature intervals indicated in Fig. 2a. At high temperature, the apparent permselectivities for *n*-heptane and *n*-octane are in agreement with the predicted Knudsen permselectivities given by the $(M_{hex}/M_x)^{1/2}$ relationship, where x represents either heptane or octane. However, as temperature decreases and adsorption effects become more significant, the data for *n*-heptane and *n*-octane begin to deviate from the Knudsen value towards higher apparent permselectivities. In contrast, the apparent permselectivity data for *n*-decane reveals that adsorption effects are so considerable for this species to produce a substantial deviation from the Knudsen prediction at any of the investigated temperatures. Nevertheless, a tendency in the direction of the Knudsen permselectivity is evident as temperature is increased. The predominantly positive deviation in the apparent permselectivity with respect to the Knudsen estimation lies in the fact that, as temperature is lowered, the adsorption equilibrium constant increases at a faster rate than that at which the diffusion coefficient decreases, and such tendency is more significant for the more strongly adsorbed species.

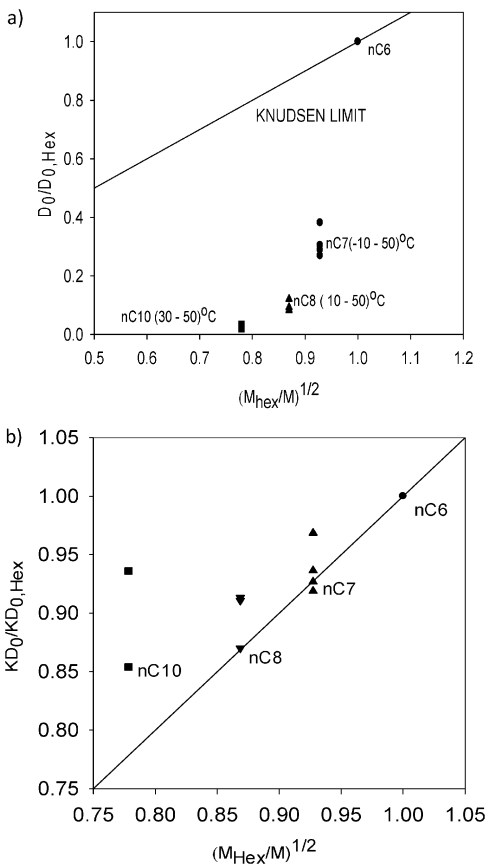

Fig. 2 (a) $D_o/D_{o,Hex}$ for different linear alkanes in MCM-41 based on the data of Qiao and Bhatia.[87,88] The values are measured over the temperature range indicated in parenthesis. The straight line represents the Knudsen limit. (b) $KD_0/KD_{0,Hex}$ for the same data set. It is clear that at sufficiently high temperature this ratio approaches the Knudsen limit.

Similar conclusions are evident from numerous experimental results in the literature, for mesopores as well as micropores. In recent work, Huang *et al.*[90] investigated the transport of toluene and *n*-heptane in SBA-15 silica at low pressures. Despite having similar molar masses ($(M_{tol}/M_{hept})^{1/2} = 0.92$) the diffusivity of heptane was twice as much the diffusivity of toluene at room temperature. The isosteric heat of adsorption of *n*-heptane and toluene were quite large, at 48 kJ mol^{-1} and 59 kJ mol^{-1}, respectively, which supports the hypothesis that adsorption reduces the mobility of the gas molecules significantly. Similar results have been obtained in other materials with ordered morphologies, where transport behavior at the single pore level is somewhat less obscured by the topological complexities of the solid. For instance, Cavalcante *et al.*[91] reported low pressure diffusivities of the order of 10^{-10} m^2 s^{-1} for several linear paraffins, in mesoporous zeolite Y with an average pore size of 7 nm. These results are far below the Knudsen theoretical value, indicating once more the strong influence of adsorption in confined transport. The effect of adsorption is more evident in micropores. Chong and co-workers[92] measured the diffusivity of ethane in silicalite by means of neutron scattering. At room temperature, the diffusivity at infinite dilution was 6×10^{-9} m^2 s^{-1} for an average pore size of 0.5 nm, two orders of magnitude below the predicted Knudsen diffusion. In other work, Kärger *et al.*[93] obtained low concentration self-diffusivities of methanol in the zeolite ferrierite of the order of 10^{-12} m^2 s^{-1} at 298 K using infrared

microimaging and interference microscopy. Ferrierite is composed of perpendicular 8 and 10 rings nanochannels that permit diffusion in two dimensions. However, flow along the 10 ring channels proved to be highly restricted and essentially only one-dimensional flow through the 8 rings channels was observed. The measured values are at least one order of magnitude below the Knudsen estimate, due to the effect of significant adsorption in the single file diffusion regime. Jobic *et al.*[94] and Heink *et al.*[95] have measured the low density self-diffusion of *n*-alkanes in MFI-zeolite by quasi-elastic neutron scattering and pulse field gradient (PFG) NMR, respectively, with both techniques obtaining values of the order of 10^{-9} m^2 s^{-1}, much smaller than their Knudsen counterparts.

For disordered materials, the issue of testing the validity of the Knudsen model is obscured by the unknown tortuosity factor, which can no longer be taken as 3. In such materials, the tortuosity will also depend on the pore size distribution and connectivity features of the porous network. A convenient way to model the behavior in such systems is offered by the combination of effective medium theory (EMT) of Kirkpatrick[96] and the correlated random walk theory (CRWT) of Bhatia,[89] the hybrid EMT–CRWT model,[97] which has been shown to yield an apparent tortuosity[65]

$$\gamma = \frac{3\pi(N+1)\langle r_p^2 l\rangle K(\bar{r}_p) D_0(\bar{r}_p)}{(N-1)\langle l\rangle \kappa_e} \qquad (14)$$

for a network of coordination number N. Here $\bar{r}_p$ is a suitably defined mean pore radius, l is pore length, and κ_e is an effective network conductance given by the solution of

$$\left\langle \frac{\kappa(r_p) - \kappa_e}{\kappa(r_p) + \left(\frac{N}{2} - 1\right)\kappa_e} \right\rangle = 0 \qquad (15)$$

where the κ (r_p) is the conductance of a pore with radius r_p and is given by

$$\kappa = \frac{\pi r_p^2 K(r_p) D_0(r_p)}{l} \qquad (16)$$

$\langle \bullet \rangle$ represents a number average over the pore size distribution. When the Knudsen model in eqn (1) is applicable, $K = 1$, and eqn (1), (14)–(16) yield a tortuosity of $3(N+1)/(N-1)$ that is independent of species molecular weight and temperature, and is purely a structural constant.[65] For most porous solids, one obtains values of N in the region of 3–4,[98] leading to tortuosities of 3–6 for uniform networks. Since real solids exhibit a pore size distribution and a complex morphology, the actual tortuosity can reach higher values, normally in the range of 3 to 10.[65] A detailed examination of the recent data of Markovic *et al.*[86] for the permeability of various gases in mesoporous glass membranes has yielded[65] abnormally high tortuosities in the range of 15–20 when the Knudsen model in eqn (1) is used for D_o, with $K = 1$. These tortuosities were also found to be dependent on the diffusing gas, increasing with increase in adsorption strength, contrary to the expectations that the tortuosity is purely a structural constant if the Knudsen model is valid. The trends were found to be consistent with those predicted[65] using the Oscillator model from this laboratory,[54,55] which takes account of adsorption through van der Waals interactions. Furthermore, ignoring adsorption

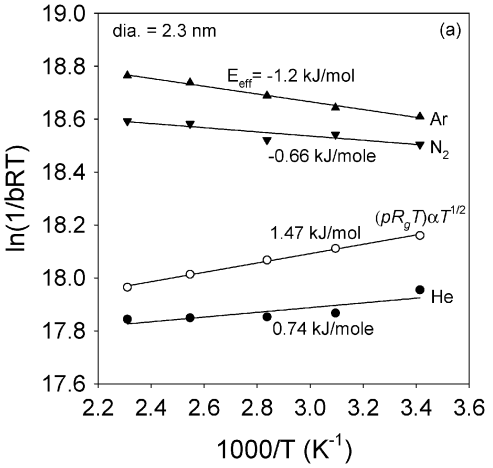

Fig. 3 Variation of $\ln(1/bRT)$ with $1/T$ in permeation of Ar, He and N_2 through a mesoporous glass membrane with 2.3 nm average pore size.[65] The negative slope for the linear fittings of Ar and N_2 data reflects the importance of adsorption. For He, the positive slope is almost half of the corresponding Knudsen theoretical slope.

leads to serious inconsistencies with the temperature variation of their experimental data.[65] Indeed, considering $K \propto \exp(-\Delta H_D)$, where ΔH_D is the adsorption enthalpy change, and $D_o \propto \exp(-E_D)$, where E_D is an activation energy, eqn (12) leads to a linear relationship between $\ln(1/bRT)$ and $1/T$, with slope $\Delta H_D + E_D$. Therefore, in the absence of adsorption ($\Delta H_D = 0$) the slope of the $\ln(1/bRT)$ *vs.* $1/T$ line should be positive, with the theoretical value for the Knudsen model approximately 1.47 kJ mol^{-1}. Fig. 3 depicts the variation of $\ln(1/bRT)$ with $1/T$ for Ar, He and N_2 based on the data of Markovic *et al.*[86] in a 2.3 nm average pore size membrane. Strikingly, the slope of the linear fit of the Ar and N_2 data is in fact negative. For the weakly adsorbed He the slope is only slightly positive, and its value is only about half of the theoretical one. Similar results were obtained for the 3.1 nm and 4.2 nm average pore size membranes, demonstrating the importance of considering adsorption in modeling transport.

At the micropore level (<2 nm), the importance of adsorption in transport has in fact been widely recognized.[38,50] However, it has usually been incorporated in the traditional Knudsen formulation through an empirical Arrhenius-type term[39,99] or by an empirical temperature dependent effective pore size.[85] Alternatively, the oscillator model developed in this laboratory,[54,55] which is exact for soft spheres under diffuse reflection conditions at the low density limit, incorporates adsorption in a rigorous way and performs equally well at the micro and mesopore levels. This model will be discussed in a later section.

In a recent defence of the Knudsen model, Ruthven and co-workers[100] report a tortuosity of 3.2 when their permeation data for light gases in supported silica membranes is correlated through the Knudsen equation. Their approach has been criticized[101] based on the fact that flow through the support is arbitrarily assumed to be viscous, while an elementary comparison of the relative magnitudes of Poiseuille-viscous and Knudsen-diffusive resistances indicates that the viscous contribution is negligible, even for pore sizes 10 times larger than the reported average pore size. The assumption of dominant

viscous flow through the support leads to significant overestimation of its resistance, thus transferring part of the active layer resistance to the support. As a result, the tortuosity value extracted from the correlation artificially falls within the reasonable tortuosity range for these materials.

2.3 Comparison with molecular dynamics simulations

MD offers an alternative route to test theoretical results, without the unavoidable uncertainty associated with experiments on real samples. Topological defects, blocked pores, pore throats or surface heterogeneity may create unexpected transport resistances which make it difficult to assess fundamental diffusion models. MD on the other hand, permits the isolation of specific transport resistances in a very realistic manner, limited only by quality of the assumptions made about the molecular geometry, the surface topology and the force fields. Clearly, MD simulations cannot replace experiments, but provides valuable insight into whether a theoretical approach is headed in the right direction. Since we do not review MD methods in detail in this article, which is focused on theoretical methods, the reader is referred to Allen and Tildesley[52] and Frenkel and Smit[53] for an elaborate discussion of the subject. Reviews of MD techniques and applications to nanoporous materials are available elsewhere.[102–105]

Transport coefficients can be extracted from MD simulations in a variety of ways. Both equilibrium and non-equilibrium methods are possible.[52] In the latter the fluid is driven either by a force field or by a chemical potential gradient. In the former no driving field is applied, but it can be observed that the fluid nevertheless streams back and forth with respect to a reference frame anchored in the solid adsorbent. It has been demonstrated that all these techniques yield equivalent results.[106,107]

From equilibrium molecular dynamics (EMD) two diffusion coefficients can be extracted. The better known is the self-diffusion coefficient which is derived from the decay of the single particle autocorrelation function:[52,102]

$$D_s = \frac{1}{Nd^*}\int_0^\infty \sum_i \langle \mathbf{u}_i(0)\cdot\mathbf{u}_i(t)\rangle dt \qquad (17)$$

Here d^* is the dimensionality of the system and $\mathbf{u}_i$ is the molecular velocity vector of molecule i out of a population of N molecules. In a cylindrical system for example, $d^* = 1$ and only the axial component of the vector is used in the dot product (diffusion in the other two directions decays to zero). D_s can also be calculated from the long time limit of the mean square displacement *via* the Einstein relation:

$$D_s = \frac{1}{Nd^*}\lim_{t\to\infty}\frac{1}{t}\sum_i \langle \Delta r_i^2\rangle \qquad (18)$$

The collective or transport diffusion coefficient D_o can be calculated from similar expressions for the streaming velocity $\mathbf{v}$ and the centre of mass displacement $\mathbf{R}$, where

$$\mathbf{v} = \sum_i \mathbf{u}_i/N \text{ and } \mathbf{R} = \sum_i r_i m_i \Big/ \sum_i m_i \qquad (19)$$

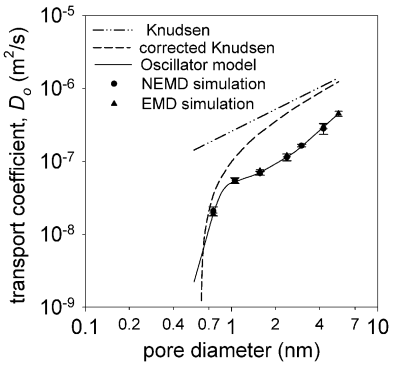

Fig. 4 Variation of the low-density transport coefficient with pore diameter, for methane at 450 K in cylindrical silica pores, estimated through MD and various theoretical methods.[55]

For example,

$$D_o = \frac{N}{d^*}\int_0^\infty \langle \mathbf{v}(0)\cdot\mathbf{v}(t)\rangle dt \qquad (20)$$

It is readily shown from the last two expressions that D_o can be decomposed into the sum of two terms:

$$D_o = D_s + D_\xi \qquad (21)$$

where D_s comes from the diagonal self-correlation terms and D_ξ from cross correlations between distinct molecules. Clearly D_o becomes equal to D_s in rarefied systems where cross correlations decay to zero.

Comparisons with MD have indicated that the Knudsen equation significantly overestimates the low density diffusion coefficient in nanopores by as much as an order of magnitude, depending on the strength of the fluid–wall interaction.[55,108] As an example, Fig. 4 depicts the variation of the low-density transport coefficient with pore diameter for methane at 450 K in silica cylindrical pores,[55] showing considerable overprediction compared to both equilibrium and nonequilibrium molecular dynamics (NEMD) simulations even at a pore diameter as large as 7 nm. On the other hand the Oscillator model from this laboratory, to be discussed later, which considers the fluid–wall interaction, gives excellent agreement with the simulations. The overprediction by the Knudsen model is significantly reduced at very small pore diameters, by empirically modifying the effective pore diameter to $d = d_{cc} - 2(0.92\sigma_{sf})$, in eqn (1) to account for the repulsive region. Nevertheless, considerable overprediction remains at pore sizes above 1 nm due to neglecting the dispersive solid–fluid interactions.

Krishna and van Baten[109,110] have independently found the Knudsen approach to overpredict significantly the MD simulation results for the low density diffusivity. Fig. 5, from Krishna and van Baten,[110] shows the variation of the MD low density diffusivity with the Knudsen diffusivity at several temperatures for methane and argon in silica pores of 2 nm and 3 nm. The plot shows that deviations are more significant at low temperature, but as temperature increases the MD diffusivities converge to the Knudsen values, in agreement with the discussion of Fig. 1. A similar analysis has been made by Fernandes and Gavalas[111] who performed MD simulations of

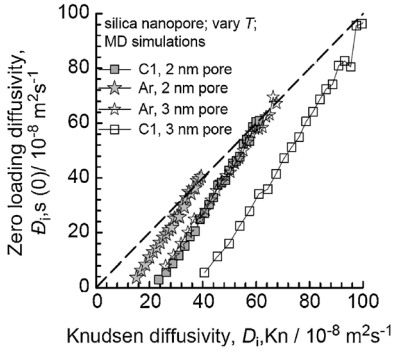

Fig. 5 Correlation between the MD low density diffusivity and the Knudsen diffusivity at several temperatures for methane (C1) and argon in silica mesopores.[110]

nitrogen and isopropane in silica pores at large Knudsen numbers. Some of their results are depicted in Fig. 6. In Fig. 6a the variation of the normalized diffusivity $D_o v^{-1}$ is shown, where v is the average molecular speed, with temperature in a 2 nm pore. It is again clear that only in the high temperature limit do the Knudsen and the MD diffusivities coincide; for the more strongly adsorbed isopropane that limit is not reached in this material even at temperatures as high as 800 K, whereas

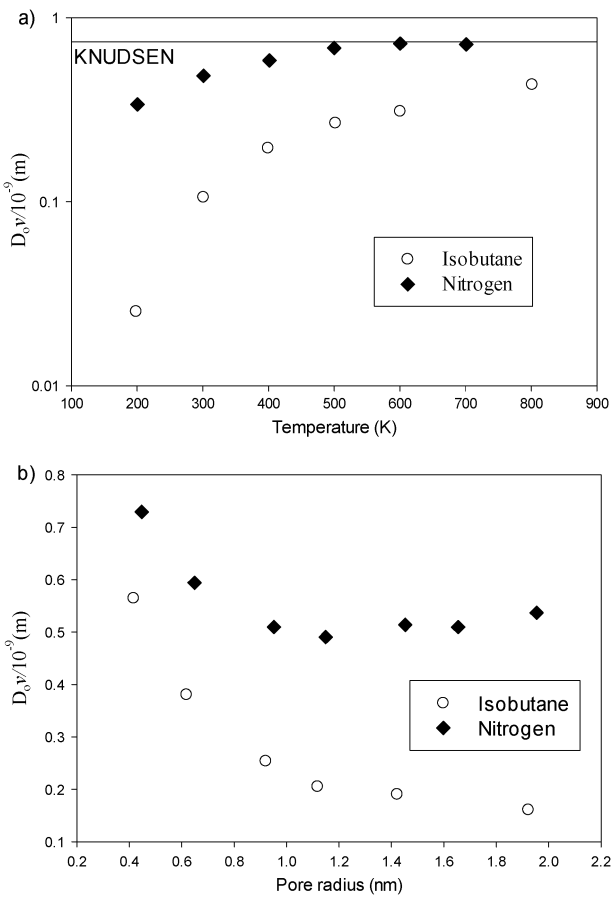

Fig. 6 (a) Variation of the normalized MD low density diffusivity $D_0 v^{-1}$ with temperature in a 2 nm silica pore. (b) Ratio of the MD low density diffusivity to the Knudsen diffusivity as a function of pore radius. From Fernandes and Gavalas.[111]

for nitrogen the limit is reached at around 500 K. In Fig. 6b the variation with pore radius of the MD low density diffusivity to Knudsen diffusivity ratio at 393 K for the same two gases is shown. Interestingly, although the ratio is always below unity for the pore radii studied, a peak is observed at about 0.4 nm for both species. This is associated with the so-called levitation effect[112] which occurs when there is a transition from two to one minima in the wall potential field as the pore width is decreased. This effect is readily explained through the oscillator model,[113] but is of course out of the reach of the Knudsen description. At the micropore level, Skoulidas and Sholl[66,114] have calculated room temperature MD low density diffusivities for several light gases in silicalite, ITQ-7, ITQ-3 and ZSM-12 zeolites of the order of 10^{-8} m^2 s^{-1}; that is, an order of magnitude below the corresponding Knudsen value. Only when the Knudsen formula is corrected by $0.92\sigma_{fs}$ do the values approach the order of magnitude of the MD results, although the quantitative agreement is still unsatisfactory.

In summary, experimental and simulation data on diffusion of low density gases in nano and mesoporous media indicate that the century old Knudsen approach leads to over-prediction of D_o, particularly when significant adsorption occurs. In the case of experimental data, the deviation from the Knudsen formula is usually masked within the tortuosity factor, which turns out to be significantly above the theoretically expected values.

3. Bulk and wall-mediated diffusion in macro and mesopores

In most practical applications, fluid densities exceed the Knudsen limit (Kn $\gg$ 1) and locate the system in the bulk-diffusion regime (Kn $\ll$ 1) or in the transition regime (Kn $\approx$ 1), where viscous effects may also be of importance. Much effort has been devoted to the development of a theory for multicomponent transport in porous materials valid at any Knudsen number and applicable under the potential influence of pressure gradients, the origin of viscous flow. In general, the most successful approaches have followed the lines of the Maxwell–Stefan (MS) description of mass transfer rather than those of Fick's law, which cannot explain some phenomena such as reverse ("uphill") or osmotic diffusion, experimentally observed in many systems of practical interest.[50] By far the most widely used MS-type "unifying approach" is the dusty gas model,[32] and for that reason the majority of this section is dedicated to the analysis of this model. Some other Maxwell–Stefan type modeling approaches adopting a "frictional approach" are also discussed, emphasizing in all cases the strengths and limitations of the models arising from the assumptions and conceptual framework employed in their derivation. The Onsager description of multicomponent transport has been shown to be equivalent to the Maxwell–Stefan approach,[115–117,50] although the latter has generally been preferred as the starting point in engineering analysis, while the former is relevant for theoretical and computational purposes. We will focus our attention on the Maxwell–Stefan type models only in the absence of external body forces, as the inclusion of these forces is not generally problematic because

they are very naturally included in the diffusion and momentum equations.

The generalized Maxwell–Stefan diffusion equations have been derived by Chapman and Enskog[30] and Hirschfelder–Curtiss–Bird[115] from kinetic theory and irreversible thermodynamics principles, respectively. Their initial derivations do not allow for shear forces because, in the former, the Boltzmann equation was solved considering only first order fluctuations with respect to the mass-averaged velocity and, in the latter, because of the restrictions imposed by Curie's theorem.[118] Zhdanov *et al.*[119] later introduced the shear term through the thirteen-moment approximation to the Boltzmann equation, although this term is very commonly dropped arguing that its contribution is negligible compared to that of other terms.[35,50] Alternative forms of the equations were later derived by several authors[120–122] and all are, in general, equivalent, except for the particular expressions for the shear term and the constitutive equations for the diffusion coefficients. The complete form of the generalized Maxwell–Stefan equations for an n-components mixture reads,

$$\sum_{\substack{j=1,\\ i\neq j}}^{n}\frac{x_i x_j(\mathbf{v}_i-\mathbf{v}_j)}{Đ_{ij}}+\sum_{\substack{j=1,\\ i\neq j}}^{n}x_j x_i\left(\frac{D_i^T}{\rho_i^{\mathrm{m}}}-\frac{D_i^T}{\rho_j^{\mathrm{m}}}\right)\nabla T=\mathbf{d_i}\;\; i=1,\ldots,n \tag{22}$$

where x_i is the mol fraction of i, $\mathbf{v}_i$ its mean local velocity, D_i^T its thermal diffusion coefficient, ρ_i^{m} its mass density, and $Đ_{ij}$ is the Maxwell–Stefan binary diffusion coefficient of species i and j. The first term in the left hand side is called the "mutual diffusion" or "Maxwell–Stefan" term and represents the drag exerted by the molecules of species j on the molecules of species i. The second one is the "thermal diffusion term" and accounts for thermal segregation phenomena ("Soret" and "Dufour" effects) related to temperature gradients in the fluid. Finally, the term on the right hand side is the so-called "diffusion driving force" which can be written, ignoring inertial effects, as

$$\begin{aligned}\rho_t RT\mathbf{d_i}\;&=\rho_i\nabla_{T,p}\mu_i+(\phi_i-\omega_i)\nabla p-(\nabla\cdot\boldsymbol{\tau}_i-\omega_i\nabla\cdot\boldsymbol{\tau}_i)\\&\quad-\left(\rho_i F_i-\omega_i\sum_{i=1}^{n}\rho_j F_j\right)\;\; i=1,\ldots,n\end{aligned} \tag{23}$$

Here ρ_i is the molar density of i, μ_i its chemical potential, $\bar{V}_i$ its partial molar volume, ω_i its mass fraction, $\boldsymbol{\tau}_i$ is the shear stress tensor associated to viscous momentum exchange with molecules of i, F_i is the force per unit mol acting on species i and ρ_t is the mixture molar density. The first term on the right hand side represents the so-called ordinary diffusion, the second term represents the pressure diffusion, the third one is the stress-gradient diffusion[123] and the last one is the forced diffusion term. It is worth mentioning that the above equations can be derived from purely linear momentum and mass conservation arguments,[124] although the particular form of the mutual and thermal diffusion terms can only be obtained through the statistical-mechanical or irreversible thermodynamics derivations. The constitutive expression relating $\boldsymbol{\tau}_i$ to the velocity gradients is also beyond the domain of a continuum mechanical derivation, requiring a statistical-mechanical treatment.[121] The models considered below all result from simplified forms of the above generalized Maxwell–Stefan equations.

3.1 The dusty gas model (DGM)

3.1.1 Gas phase transport. The DGM is probably the most widely used approach for modeling of multicomponent transport in porous media.[34,35,116] Initially developed by Evans and co-workers[27–29] it was later refined by Mason *et al.*[31] with the goal of accounting within a unified framework for combined wall mediated and bulk diffusion of gases in porous systems. However, besides having the weakness of incorporating the Knudsen model which, as shown above, fails under conditions of practical importance, its formulation has fundamental flaws, and the theory fails to accurately predict the behaviour of even a simple diffusion experiment widely known as the Stefan tube.[58] While there has been some recent criticism of the DGM, the discussion has been somewhat obscured in a plethora of derivations,[37,44,58,125] and there is considerable lack of clarity on the issue. Its apparent success in application is largely due to the presence of fitting parameters such as tortuosity, which mask model errors. Here we present a fresh perspective on this classic model, illuminating key flaws in the derivation that have hitherto been largely unrecognised.

The principle behind the DGM is in fact quite simple and originates from the concept of the Lorentz gas where one component of a binary mixture is taken to the limit of extremely heavy and therefore immobile molecules.[30] Thus, in the DGM, the pore wall is assumed to consist of uniformly distributed giant "dust" molecules of infinite molar mass, held fixed in space by some external 'clamping' force that counteracts the drag exerted by the fluid. This is equivalent to fixing the frame of reference on the dust. This dust is then taken as a pseudo-species in the Maxwell–Stefan diffusion equations, which are employed to relate the fluxes and diffusion driving forces. The final expression for isothermal diffusion of an ideal gas mixture of n species, in the absence of external forces reads,

$$\sum_{\substack{j=1\\ i\neq j}}^{n}\frac{x_j\bar{J}_i-x_i\bar{J}_j}{\rho_t Đ_{ij}^{\mathrm{e}}}+\frac{\bar{J}_i}{\rho_t D_{\mathrm{io}}^{\mathrm{e}}}=-\frac{1}{p}\frac{dp_i}{dz}-\frac{x_i B_0}{\eta D_{\mathrm{io}}^{\mathrm{e}}}\frac{dp}{dz}\;\; i=1,\ldots,n \tag{24}$$

where p_i is the partial pressure of species i, η is the mixture viscosity, B_0 is the viscous permeability coefficient and z is the diffusion coordinate. The effective binary diffusion coefficient $Đ_{ij}^{\mathrm{e}}$ is given by $(\varepsilon_{\mathrm{p}}/\gamma)Đ_{ij}$ where $(\varepsilon_{\mathrm{p}}/\gamma)$ is the common porosity to tortuosity correction factor associated with the particular medium morphology. $D_{\mathrm{io}}^{\mathrm{e}}$ is an effective diffusion coefficient arising from the drag exerted by the dust (medium) on species i. It is customary to take $D_{\mathrm{io}}^{\mathrm{e}}=(\varepsilon_{\mathrm{p}}/\gamma)D_{\mathrm{k}i}$, with $D_{\mathrm{k}i}$ the Knudsen diffusion coefficient of i. $\bar{J}_i$ is the pore cross-section averaged molar flux, which, for a cylindrical pore of radius r_{p} is given by

$$\bar{J}=\frac{2}{r_{\mathrm{p}}^2}\int_0^{r_{\mathrm{p}}}r\rho_i(r)v_i(r)dr \tag{25}$$

$v_i(r)$ is the axial velocity of i and r is the radial coordinate. To illustrate the shortcomings of the model it is pertinent to briefly outline key steps in its formulation, identifying the flaws. The reader is referred to Jackson[34] for a more detailed derivation.

The starting point is the generalized Maxwell–Stefan diffusion eqn (22) and (23) applied to an ideal gas mixture comprising n gas species and the solid as the $(n + 1)$th component (the dust). The very assumption of an ideal gas mixture including the solid "dust" particles would appear problematic, as in real porous solids the gas and solid phases are segregated in different regions of the particles—*i.e.* the gas molecules and dust particles are not randomly mixed. Nevertheless, upon using the condition that $J_{n+1} = 0$ and that the total clamping force on the dust particles per unit volume must match the pressure gradient, a series of algebraic manipulations, detailed elsewhere,[34] yields

$$\sum_{j=1}^{n} \frac{\rho_j \bar{J}_i - \rho_i \bar{J}_j}{\rho_t \mathcal{D}_{ij}} + \frac{\bar{J}_i}{D_{io}} = -\frac{1}{RT}\frac{dp_i}{dz} \tag{26}$$

in which the diffusivity D_{io} relates to the binary gas–dust mutual diffusion coefficient, and is taken as the Knudsen diffusivity D_{ki}. Further, the gas phase pressure and the molar densities of all species are assumed uniform over the pore cross-section, ignoring inhomogeneities and density gradients that arise due to gas–wall interactions. This places considerable restrictions on the applicability of the approach in nanoscale pores, where adsorption and gas–wall interactions play a strong role as discussed above. Besides these limitations, there has been some controversy regarding the nature of the fluxes in eqn (26). Evans and co-workers divide the total flux, *i.e.*, the flux with respect to a framework of reference fixed to the walls (as $J_{n+1} = 0$), into an additive viscous (non-segregative) contribution $\bar{J}_{\mathrm{vis},i}$ and a diffusive contribution $\bar{J}_{\mathrm{diff},i}$, according to

$$\bar{J}_i = \bar{J}_{\mathrm{vis},i} + \bar{J}_{\mathrm{diff},i} \tag{27}$$

and then assert that fluxes in eqn (26) correspond to the diffusive contribution only. That is, eqn (26) must be really written as,

$$\sum_{j=1}^{n} \frac{\rho_j \bar{J}_{\mathrm{diff},i} - \rho_i \bar{J}_{\mathrm{diff},j}}{\rho_t \mathcal{D}_{ij}} + \frac{\bar{J}_{\mathrm{diff},i}}{D_{io}} = -\frac{1}{RT}\frac{dp_i}{dz} \tag{28}$$

The viscous part is given by $J_{\mathrm{vis},i} = x_i J_{\mathrm{vis}}$, where $\bar{J}_{\mathrm{vis}}$ is assumed to follow a Darcy-type law,

$$\bar{J}_{\mathrm{vis}} = \rho_t \bar{v}^{\mathrm{ns}} = -\frac{\rho_t B_0}{\eta}\frac{dp}{dz} \tag{29}$$

The permeability B_0 is characteristic to the medium and, in general, must be determined experimentally. For instance, in a cylindrical pore, the classical non-slip Poiseuille flow relationship provides $B_0 = r_p^2/8$. $\bar{v}^{\mathrm{ns}}$ is the cross-section average of the mass-averaged velocity $v = \sum \rho_i^{\mathrm{m}} v_i / \rho_t^{\mathrm{m}}$, and the superscript ns indicates that the mass-averaged velocity here is calculated under the assumption of no wall slip. Finally, combining eqn (27)–(29) leads to the DGM eqn (24). It must be recalled that fluxes in the final result in eqn (24) are *total fluxes* and include both the viscous and diffusive contributions.

Kerkhof[44] has criticized this treatment on the grounds that expressing the total flux as the sum of a viscous and a diffusive part is artificial. According to Kerkhof, eqn (26) is complete in the sense that both viscous and diffusive contributions are already included in the fluxes, which means that adding a viscous term on the right hand side leads to double-counting of the viscous effects. The rationale for Kerkhof's arguments is, however, not clear; nevertheless, the main problem with the approach may be readily traced to conflicting choices for the frame of reference in different steps.

The arbitrary replacement of the flux $\bar{J}_i$ in eqn (26) by the diffusive component $\bar{J}_{\mathrm{diff},i}$, to obtain eqn (28) would appear to create an internal contradiction, and is in serious error. The motivation for the substitution is that only velocity differences are involved in the Maxwell–Stefan formulation in eqn (22), the starting point of the analysis, hence the choice of reference frame is arbitrary. However, on the one hand, the condition $J_{n+1} = 0$ employed in the derivation automatically locates the frame of reference for the fluxes on the pore walls (*i.e.* the solid phase), while on the other hand eqn (28) implies that $\bar{J}_{\mathrm{diff},i}$ represents the flux measured with respect to a frame of reference located at the fluid centre of mass. Replacing $\bar{J}_i$ by $\bar{J}_{\mathrm{diff},i}$ in eqn (26) therefore yields the physically incorrect result that the solid phase and the fluid centre of mass have the same velocity, and therefore $\bar{J}_{\mathrm{vis},i} = 0$, since the dust (solid phase) is stationary (as $J_{n+1} = 0$). Conversely, the substitution of $\bar{J}_i$ by $\bar{J}_{\mathrm{diff},i}$ leads to the extraordinary conclusion that the pore walls are moving at a cross-section averaged velocity $\bar{v}^{\mathrm{ns}}$ with respect to themselves!

Thus, it is clear that gas velocities, v_i, in the DGM must be measured relative to the pore walls, rather than the fluid centre of mass; that is, the fluxes in eqn (26) are total rather than diffusive only. Even though the foregoing argument is quite elementary, it has not been discussed so far in the literature. The problem, as some authors have pointed out,[37,44] lies mainly in the abundance of terminology and definitions for the flux contributions that is found in the literature. The lack of a standard framework makes it difficult to judge and compare the different available transport models from a theoretical stand-point. In the present case, eqn (27) is no more than a particular definition for $\bar{J}_{\mathrm{diff},i}$ which, as we shall see, does not actually correspond to the usual statistical-mechanical definition for the diffusion velocity.

The previous discussion is also valid for the more refined derivation by Mason *et al.*[31] where the shear term in the generalized Maxwell–Stefan diffusion equations, written as a function of the mass-averaged velocity, is eliminated through the mixture equation of change. In this work, Mason *et al.*[31] write for the single gas case,

$$\bar{J}_{\mathrm{diff}} = -\frac{D_o}{RT}\frac{dp}{dz} \tag{30}$$

and the coefficient D_o is subsequently taken to be the Knudsen diffusion coefficient. Since the total flux corresponds to the summation of the diffusive and viscous contributions, according to eqn (27), they finally obtain,

$$\bar{J} = -\frac{1}{RT}\left(D_k + \frac{pB_0}{\eta}\right)\frac{dp}{dz} \tag{31}$$

This corresponds to the well-known viscous slip equation for diluted gases. Now, the usual statistical-mechanical definition of the diffusion velocity of species i, $v_{\mathrm{diff},i}^{\mathrm{SM}}$ is given by

$$v_i = v + v_{\mathrm{diff},i}^{\mathrm{SM}} \tag{32}$$

That is, $v_{\mathrm{diff},i}^{\mathrm{SM}}$ is simply the velocity with respect to the mass-averaged velocity. The benefit of such a definition is that $\sum_i \rho_i^{\mathrm{m}} v_{\mathrm{diff},i}^{\mathrm{SM}} = 0$, since $\sum_i \rho_i^{\mathrm{m}} v_i = \rho_t^{\mathrm{m}} v$. Consequently, the total "diffusive flux" derived from the statistical-mechanical definition, $J_{\mathrm{diff}}^{\mathrm{SM}} = \sum_i \rho_i^{\mathrm{m}} v_{\mathrm{diff},i}^{\mathrm{SM}}$ is *always* zero. It is this definition that is used in both the Chapman–Enskog and Zhdanov derivations of the diffusion equations, from where the DGM is deduced. However, J_{diff} is clearly non-zero in eqn (30) and therefore, J_{diff} cannot correspond to $J_{\mathrm{diff}}^{\mathrm{SM}}$. If the statistical-mechanical convention is followed and the correct flux used, eqn (30) provides the total flux rather than its diffusive part, and one has,

$$\bar{J} = -\frac{D_{\mathrm{o}}}{RT}\frac{dp}{dz} \tag{33}$$

Therefore, D_{o} cannot correspond to the Knudsen diffusivity, but is a coefficient combining Knudsen and viscous effects, as in eqn (31). To see this, consider for simplicity a cylindrical pore of radius r_{p}. The solution of the Navier–Stokes equation under the Maxwell slip and symmetry boundary conditions,

$$v(r_{\mathrm{p}}) = -\xi \left.\frac{dv}{dr}\right|_{r=r_{\mathrm{p}}} \left(\frac{dv}{dr}\right)_{r=0} = 0, \tag{34}$$

yields the following cross-section average of the mass-averaged velocity[126]

$$\bar{v} = \frac{r_{\mathrm{p}}^2}{8\eta}\left[1 + \frac{4\xi_{\mathrm{s}}}{r_{\mathrm{p}}}\right]\left(-\frac{dp}{dz}\right) \tag{35}$$

where ξ_{s} is the Maxwell slip modulus. In the derivation of eqn (35) a radially uniform pressure was assumed. Combining eqn (33) and (35) provides,

$$D_{\mathrm{o}} = \frac{\rho r_{\mathrm{p}}^2}{8\eta}\left[1 + \frac{4\xi_{\mathrm{s}}}{r_{\mathrm{p}}}\right] \tag{36}$$

Thus, when the flux in the DGM is taken to be the total rather than the diffusive and the usual statistical-mechanical convention in eqn (32) is employed, the resulting coefficient D_{o} combines viscous and wall-mediated diffusion effects, the latter embedded in the Maxwell slip modulus ξ_{s}. Maxwell[127] derived an expression for ξ_{s} in the case of hard sphere gases, assuming the pore wall to be constituted by closely packed spheres

$$\xi_{\mathrm{s}} = C\lambda \tag{37}$$

where constant $C \approx 1.4$ according to the measurements performed by Knudsen[19] on transport of several light gases through glass capillaries. In practice, C is a function of the momentum accommodation coefficient and varies with the specific material and diffusing gas. Taking this particular value and expressing the mean free path in terms of other physical variables, one can finally obtains

$$\bar{J} = -\frac{1}{RT}\left(D_{\mathrm{k}}^{*} + \frac{pB_0}{\eta}\right)\frac{dp}{dz} \tag{38}$$

where $D_{\mathrm{k}}^{*} = 0.89 D_{\mathrm{k}}$. The 0.89 factor is required to fit the Knudsen experimental data.[58]

3.1.2 Fluids at high density. The extension of the DGM to non-ideal and dense fluids was done by Mason and Viehland[128] and Mason and del Castillo,[33] starting from the Bearman–Kirkwood formulation for the microscopic momentum balance,[120] but again suffers from the weaknesses of its low-density predecessor. For an isothermal system in the absence of body forces, the resulting DGM equation is,

$$\sum_{\substack{j=1\\ i\neq j}}^{n} \frac{x_j\bar{J}_i - x_i\bar{J}_j}{\mathcal{D}_{ij}^{e}} + \frac{\bar{J}_i}{D_{io}^{e}} = -\frac{\rho_i}{RT}\left[\left(\frac{d\mu_i}{dz}\right)_{T,P} + \bar{V}_i\frac{dp}{dz}\right] - \frac{\alpha_i'\rho_i B_0}{\eta D_{io}^{e}}\frac{dp}{dz}\quad i = 1,\ldots,n \tag{39}$$

where μ_i is the chemical potential of i, $\bar{V}_i$ its molar volume and α_i' its viscous selectivity factor, introduced to allow for the possibility of "segregative viscous flow" in semipermeable membranes. This coefficient can take values greater than or less than unity, and depends on both the species and the particular medium. A value below unity applies for example to molecules that "stick" to the wall and slip, whereas a value greater than unity applies to relatively large molecules of size near to the pore diameter; such molecules tend to move along the pore center-line.[50] Kerkhof[44] has carried out a careful deconstruction of the derivation of eqn (39), finding again that the addition of a viscous term in the right hand side leads to some inconsistencies. For example, the single component version of eqn (39) for a liquid-medium system with $\alpha' = 1$ reads

$$\bar{J} = -\left(\frac{D_{\mathrm{o}}}{RT} + \frac{\rho_i B_0}{\eta}\right)\frac{dp}{dz} \tag{40}$$

which is contradictory since, for a single Newtonian liquid, no viscous slip at the wall is anticipated. On the other hand, elimination of the viscous term in the right hand would lead, upon solution of the Navier–Stokes equation with non-slip boundary condition, to

$$\bar{J} = -\frac{D_{\mathrm{o}}}{RT}\frac{dp}{dz} \tag{41}$$

with

$$D_{\mathrm{o}} = RT\frac{\rho_i B_0}{\eta}\frac{dp}{dz} \tag{42}$$

showing that the correct selection of the flux in the derivation (total instead of diffusive) along with the statistical-mechanical convention yields a fully viscous transport coefficient. Although the ratio of the viscous to the slip term (assuming that $D_{\mathrm{o}} = D_{\mathrm{k}}$) in eqn (40) is in general large for liquids, *i.e.* $\sim$50 for water and $\sim$73 for acetic acid at 298 K in a 1 μm capillary, there are cases in which the two terms are comparable, *i.e.* $\sim$13 for phenol and $\sim$2 for propylene glycol at the same temperature, even though the density is high enough in all cases to hold a large amount of intermolecular collisions near the wall and guarantee the non-slip condition.

3.1.3 Alternate perspective on the DGM. It is clear from the above discussion that as usually derived the DGM suffers from conflicting choices of the frame of reference used for different terms in the analysis. A second equally serious error lies in the frequent use of the expression $B_0 = r_p^2/8$ for the intrinsic permeability, which is based on simple Poiseuille flow in a tube; as it conflicts with the spatial averaging behind eqn (24), in which it is assumed that the solid particles are intimately mixed with the fluid rather than being confined to the tube surface. In this section we analyze the DGM from a new perspective, avoiding the above inconsistencies, but with a different assumption, and find that unphysical consequences still arise. The starting point of our analysis is the microscopic momentum balance,[120] or equivalently the generalized Maxwell–Stefan equations

$$RT\sum_{\substack{j=1\\ i\neq j}}^{n}\frac{\rho_j\rho_i(v_i-v_j)}{\rho_t\mathcal{D}_{ij}} = -\rho_i\left(\frac{d\mu_i}{dz}\right)_T - \frac{1}{r}\frac{d(r\tau_{rz,i})}{dr}\quad i=1,\ldots,n \tag{43}$$

written for a cylindrical pore of radius r_p, where v_i is the local axial velocity of i and $\tau_{rz,i}$ is the rz component of its shear stress tensor, representing the rate of z-momentum transferred in the r direction due to radial gradients of the axial velocity of i. Upon defining a wall friction coefficient, $\xi_{s,i}$, such that $\tau_{rz,i}(r_p) = \xi_{s,i}\rho_i v_i^w$, and performing a cross-sectional averaging over eqn (43) while considering the species densities and chemical potential gradients to be radially uniform, we obtain

$$\sum_{\substack{j=1\\ i\neq j}}^{n}\frac{\rho_j(\bar{v}_i-\bar{v}_j)}{\rho_t\mathcal{D}_{ij}}+\frac{v_i^w}{D_{io}} = -\frac{1}{RT}\left(\frac{d\mu_i}{dz}\right)_T\quad i=1,\ldots,n \tag{44}$$

where $\bar{v}_i$ is the cross-section averaged velocity of species i, v_i^w its velocity at the wall, and $D_{io} = RTr_p/2\xi_{s,i}$. The friction coefficient $\xi_{s,i}$ is expected to be specific to component i and the medium, as will D_{io}. Comparing the definition of $\xi_{s,i}$ with that of the Maxwell modulus in eqn (34), and taking the latter to be 1.4λ, one finally gets $D_{io} \approx 0.89D_k$. We can rewrite eqn (44) in terms of the molar fluxes,

$$\sum_{\substack{j=1\\ i\neq j}}^{n}\frac{x_j\bar{J}_i - x_i\bar{J}_j}{\mathcal{D}_{ij}}+\frac{J_i^w}{D_{io}} = -\frac{\rho_i}{RT}\left(\frac{d\mu_i}{dz}\right)_T\quad i=1,\ldots,n \tag{45}$$

where J_i^w represents the molar flux of i at the wall. J_i^w is obtained by an approximation, in conjunction with the Navier–Stokes equation, by first solving for the mass-averaged velocity, following

$$\frac{\eta}{r}\frac{d}{dr}\left(r\frac{dv}{dr}\right) = \frac{dp}{dz} \tag{46}$$

with boundary conditions $dv/dr = 0$ at $r = 0$ and $v = v^w$ at $r = 0$. The mixture viscosity η is taken to be uniform in the radial coordinate r. Assuming a radially uniform axial pressure gradient (which is consistent with the assumption of radially uniform density and axial chemical potential gradient, used in the averaging behind eqn (45)), solution of eqn (46) yields the cross-sectional averaged velocity

$$\bar{v} = v^w - \frac{r_p^2}{8\eta}\frac{dp}{dz} \tag{47}$$

To obtain the flux of component i at the wall, consider,

$$J_i(r) = \rho_i v_i(r) = \rho_i v(r) + J_{diff,i}(r) \tag{48}$$

where $J_{diff,i}$ is a local diffusive flux relative to the local centre of mass velocity, v, such that $\sum_i M_i J_{diff,i} = 0$. Now, if the diffusive part of the flux of each species is assumed to be uniform over the whole pore cross section, *i.e.* $J_{diff,i}^w = J_{diff,i}(r) = \bar{J}_{diff,i}$, eqn (47) and (48) provide

$$J_i^w = \bar{J}_i - \bar{J}_{vis,i} \tag{49}$$

where $\bar{J}_{vis,i}$ is given by the no-slip Poiseuille equation,

$$\bar{J}_{vis,i} = -\frac{\rho_i r_p^2}{8\eta}\frac{dp}{dz} \tag{50}$$

in agreement with the DGM definition of $\bar{J}_{vis,i}$. Inserting eqn (49) in eqn (45) yields

$$\sum_{\substack{j=1\\ i\neq j}}^{n}\frac{x_j\bar{J}_i - x_i\bar{J}_j}{\mathcal{D}_{ij}}+\frac{\bar{J}_i-\bar{J}_{vis,i}}{D_{io}} = -\frac{\rho_i}{RT}\left(\frac{d\mu_i}{dz}\right)_T\quad i=1,\ldots,n \tag{51}$$

Upon substituting

$$\left(\frac{d\mu_i}{dz}\right)_T = \left(\frac{d\mu_i}{dz}\right)_{T,P} + \bar{V}_i\frac{dp}{dz} \tag{52}$$

and using $B_0 = r_p^2/8$ for a cylindrical pore, eqn (50) and (51) yield the DGM eqn (39), with $\alpha_i' = 1$.

There are several interesting aspects of the above formulation. First of all, it was necessary to suppose that the species densities are radially uniform, as in the traditional derivation in Sections 3.1.1 and 3.1.2. On the other hand, simulation results, for example for methane in silica pores,[106,129] show layering effects and strong density gradients in nanopores as large as 5 nm diameter, with significant localization of the adsorbate near the potential energy minimum even at temperatures as high as 450 K, as shown in Fig. 7. Thus, the DGM can only be applicable to sufficiently large nanopores where adsorption-induced density gradients have an insignificant influence. This holds even if the wall coefficient D_{io} is modified, for example, through an activation energy factor to empirically capture adsorption effects on the diffusivity. The introduction of the viscous selectivity α_i' coefficients by Mason and del Castillo[33] seems to be more of an artifact to expand the scope of the model to those cases where dispersive interactions between the fluid and the wall are of importance. In fact, the statistical-mechanical origin of α_i' has been challenged.[44] Finally, the assumption of uniform diffusive flux, and therefore of separative effects, over the cross section would appear to be an internal contradiction. On the one hand the Navier–Stokes equation is used to determine mass-averaged velocity profiles for the mixture, while on the other the diffusive part of the velocity of any component is assumed uniform over the cross section. Such an assumption leads to the rather unusual

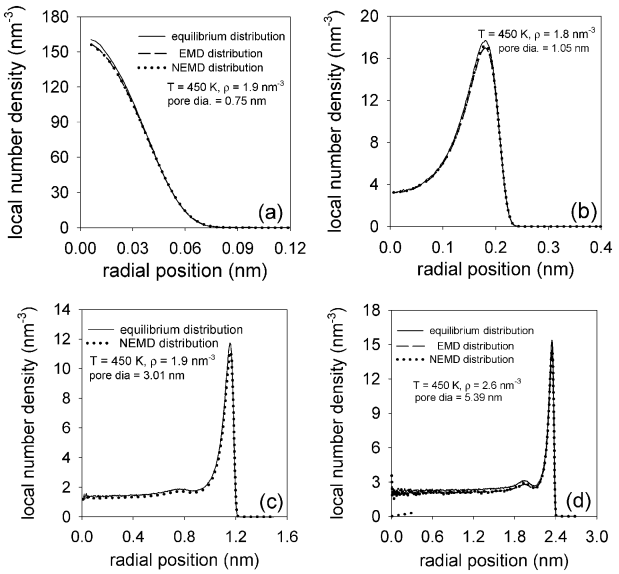

Fig. 7 Radial density profiles at 450 K for various pore sizes and densities for methane in silica cylindrical pores. Solid lines represent GCMC-determined equilibrium density profiles, while dashed lines represent profiles from EMD and dotted lines those from NEMD. The silica was represented as having infinitely thick walls of closed packed LJ sites, with ε_s = 290 K and σ_s = 0.29 nm. In the NEMD simulations a constant axial acceleration is exerted on all particles. From Bhatia *et al.*[55]

conclusion that the velocity profiles of all species are parallel to each other, *i.e.* the velocity gradients of all species are identical, since for radially uniform densities

$$v_i(r) - v_j(r) = \left(v(r) + \frac{J_{\mathrm{diff},i}}{\rho_i}\right) - \left(v(r) + \frac{J_{\mathrm{diff},j}}{\rho_j}\right) = \frac{J_{\mathrm{diff},i}}{\rho_i} - \frac{J_{\mathrm{diff},j}}{\rho_j} = \text{const.} \quad (53)$$

Such behaviour is unlikely in the general case, casting serious doubts on the validity of the DGM even under conditions of negligible adsorption.

3.2 Interfacial friction-based models

Frictional models also have their basis in the Maxwell–Stefan diffusion equations. However, the fluid–wall momentum exchange is usually approached through an interfacial friction coefficient active at the pore surface and introduced directly into the diffusion equations, or through the slipping modulus in the solution of the equation of change with slip boundary condition. The friction coefficient embeds viscous and wall–molecule collisions effects, although the final form of the equations is sometimes put in such a way that the friction coefficient is not directly visible. The DGM can be in fact derived from a frictional approach, as we have shown above. Nevertheless, except for the Lightfoot model,[43] the models described below are not equivalent to the DGM.

The starting point for the Lightfoot model[43] is the irreversible thermodynamics formulation of the diffusion driving force. For the isothermal case, in the absence of external body forces, Lightfoot's model reads

$$\sum_{\substack{j=1\\ i\neq j}}^{n} \frac{x_j\bar{J}_i - x_i\bar{J}_j}{E_{ij}} + \frac{\bar{J}_i}{E_{io}} = -\frac{1}{RT}\left[\left(\frac{d\mu_i}{dz}\right)_{T,P} + \bar{V}_i\frac{dp}{dz}\right] \quad i = 1,\ldots,n \quad (54)$$

The fluxes here are total rather than diffusive only. Lightfoot's derivation is in spirit similar to that of the DGM, in the sense that the membrane is taken as a pseudo-component held in place by a clamping force. The main difference lies in the fact that it is the membrane that is taken as the frame of reference, rather than the fluid centre of mass. The binary and unary diffusion coefficients E_{ij} and E_{io} obviously do not correspond to $\mathcal{D}^{e}_{ij}$ and D^{e}_{io} in eqn (35). According to Mason and del Castillo,[130] the Lightfoot coefficients, commonly referred to as "augmented coefficients", embed both diffusive and viscous contributions. The two models are however algebraically equivalent; *i.e.* well defined functions f and g exist such that $E_{io} = f(\{D^{e}_{io}\},\{\mathcal{D}^{e}_{ij}\},\{\alpha'_i\},B_0)$ and $E_{ij} = g(\{D^{e}_{io}\},\{\mathcal{D}^{e}_{ij}\},\{\alpha'_i\},B_0)$.[130]

It can be proved that, when the viscous term is dropped ($B_0 = 0$) the Lightfoot and DGM coefficients become equivalent.[50] Mason and co-workers assert that $\mathcal{D}^{e}_{ij}$ are the real effective Maxwell–Stefan coefficients, while E_{ij} contains both binary momentum exchange and viscous contributions, making the Lightfoot model less convenient since E_{ij} cannot be directly determined from binary diffusion measurements. Following the previous analysis, and in agreement with Kerkhof's discussion,[44] we conclude that the Lightfoot binary coefficients are in fact diffusion coefficients rather than "augmented" expressions. The DGM coefficients on the other hand are altered because they must absorb the effect of the extra viscous term. However, in the majority of applications both models require empirical specification of the transport parameters to fit the experimental or molecular simulation results. Examples include: Hejtmánek *et al.*[131] on transport of binary and ternary mixtures of light gases in mesoporous commercial catalysts; Moon *et al.*[132] on separation analysis of H_2/CO mixtures in mesoporous silica/alumina membranes; Chang and Lee[133] on the determination of DGM parameters for diffusion of light gases in silica by MD; or Todd *et al.*[134] on the determination of DGM and structural parameters through uptake experiments in zeolites; interpretations of experimental data through the Lightfoot model have been carried out by Keurentjes *et al.*[135] in the study of dialysis membranes using water/2-propanol solutions and Scattergood and Lightfoot[136] in ion-exchange membranes. In summary, the need to resort to empirical parameters, in addition to their algebraic equivalence, makes these two approaches equally convenient (with the same strengths and weaknesses) for the interpretation of experiments. The two models are not suitable for predictive purposes due to the ultimately empirical nature, and therefore non-transferability, of their parameters, neither are they appropriate for the analysis of nanopores, where fluid inhomogeneities are of paramount importance in the description of transport.

A different approach known as the mean transport pore model (MTPM) was developed by Rothfeld[137] for binary gas mixtures, and later extended by Schneider[138] to the multicomponent case.

In this model the pore is assumed to be cylindrical and the flux is also arbitrarily partitioned into a viscous and a diffusive part, as in eqn (27). The viscous term is determined by the solution of the Navier–Stokes equation with slip boundary condition for each species, writing the shear stress as

$$\tau_{rz,i} = -\eta \frac{dv_i}{dr} \tag{55}$$

Thus, the shear stress is proportional to the species velocity rather than the mass average velocity. The species 'partial viscosity' is taken to be equal to the mixture viscosity, η. The slip velocity is determined through the calculation of the rate of momentum transferred to the wall, which is in turn obtained by interpolation of the momentum transfer rates at the low density and continuum limit, taking the Knudsen number as the interpolation parameter. The final expression for this model is,

$$\sum_{\substack{j=1 \\ i\neq j}}^{n} \frac{x_j \bar{J}_i - x_i \bar{J}_j}{\mathcal{D}_{ij}^{e}} + \frac{\bar{J}_i}{D_{ki}^{e}}$$

$$= -\rho_t \frac{dx_i}{dz} - \left[\frac{B_i}{\mathcal{D}_{ki}^{e}} + \sum_{\substack{j=1 \\ i\neq j}}^{n} \frac{B_i}{\mathcal{D}_{ki}^{e}} x_j (1 - B_i/B_j) \right] x \frac{d\rho_t}{dz} \quad i = 1, \ldots, n \tag{56}$$

The B_i's are species specific permeability coefficients given by,

$$B_i = D_{ki}^{e} \frac{\omega_i \sqrt{M_i/\bar{M}} + Kn}{1 + Kn} + \frac{\varepsilon_p}{\gamma} \frac{\langle r^2 \rangle p}{8\eta} \quad i = 1, \ldots, n \tag{57}$$

The superposition of the viscous and diffusive contributions used in the derivation of eqn (56) and (57) is, however, arbitrary. Furthermore, assuming the partial viscosities to be equivalent to the mixture viscosity is incorrect, as it violates the condition that the sum of the shear stresses on all the components must match the total shear stress on the mixture. In spite of its weaknesses, the near-wall kinetic theory analysis in the MTPM has inspired the development of more physically sound models, such as the binary friction model (BFM),[44] the velocity profile model (VPM)[139] and the cylindrical pore interpolation model (CPIM).[37]

We will refer now to the VPM, as this model is an improvement over the previous BFM approach. The starting equation is, for a cylindrical capillary,

$$\frac{\eta_i}{r} \frac{\partial}{\partial r} \left(r \frac{\partial v_i}{\partial r} \right) = \rho_i \frac{\partial \mu_i}{\partial z} + p \sum_{\substack{j=1 \\ i\neq j}}^{n} \frac{x_j x_i (v_i - v_j)}{\mathcal{D}_{ij}} \quad i = 1, \ldots, n \tag{58}$$

Eqn (58) is equivalent to the momentum balance in eqn (43) with the component rz of the shear stress tensor for species i defined as

$$\tau_{rz,i} = -\eta_i \frac{\partial v_i}{\partial r} \tag{59}$$

As in the MTPM,[140] the species velocity rather than the mass-averaged velocity is considered in the specification of the shear term. The physical justification for this is as follows: consider a cylindrical volume element $\delta V(r)$ with a mean streaming velocity $v_i(r)$ for species i, as depicted in Fig. 8.

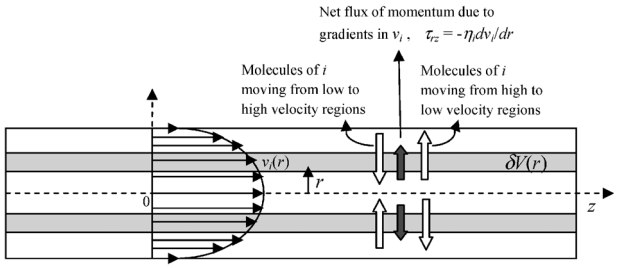

Fig. 8 Illustration of the momentum transfer mechanism due to species velocity gradients. Since there is not radial velocity component, the number of molecules of i moving from the pore center to the wall and *vice versa* is the same. However, the existence of gradients in $v_i(r)$ leads to a net flux of momentum in the direction of $(-dv_i/dr)$.

Under steady-state conditions, and in the absence of a radial partial pressure profile and external body forces, the change in the z-momentum of i within $\delta V(r)$ produced by the joint effect of the pressure force $-dp_i/dz$ and the $i - j$ ($i \neq j$) collisions, must be balanced by the rate of momentum lost/gained due to the exchange of molecules of i with the adjacent volume elements $\delta V(r \pm dr)$ having mean streaming velocities $v_i(r \pm dr)$. Such exchange is represented by the shear term and will on average lead to a net z-momentum flux of species i from the regions with high z-velocity of i to those with low z-velocity of i. The shear term should then logically be proportional to the gradient in the velocity of i rather than the gradient in the mass-averaged velocity, as the momentum exchanged in i–j collisions is already accounted for in the mutual diffusion term. This is similar to the idea behind the early work of Schneider,[140] though the latter does not provide any physical justification.

An analytical solution of eqn (58) was derived by Kerkhof and co-workers[139] for a two component mixture using a slip boundary condition, similar to that in eqn (34). Averaging of this solution over the pore cross section gives,

$$\rho_i \frac{d\mu_i}{dz} = -\rho_t RT g_D \frac{x_1 x_2}{\mathcal{D}_{ij}} (\bar{v}_i - \bar{v}_j) - \rho_t RT \beta_{i0} \bar{v}_i \quad i = 1, 2 \tag{60}$$

where the friction coefficient β_{i0} is a function of the partial viscosities and the Maxwell slip modulus. The correction factor g_D arises because, apparently, the average of the difference in velocities is not exactly equal to the difference in the average velocities. However, this correction was found to vary between 1 and 1.3 for liquids and it is approximately unity for gases. Kerkhof and Geboers[58,125] have generalized the idea behind the VPM by solving the Boltzmann equation around the average velocity of each species, as opposed to the common solution around the mass-averaged velocity.[30,115] In effect, when the mixture components have very different mobilities, the velocity profiles of the separate species may differ significantly from that of the mass-averaged velocity. In that case, the assumption that the species' diffusion velocities are small fluctuations around the mass-averaged velocity leads to incorrect results. This problem is avoided when the expansion of the velocities is performed around the species average velocity; when this is done, eqn (59) for the shear-stress arises naturally from the analysis. The drawback of the VPM approach is that an equation of change for each species arises, and the resulting system must be solved simultaneously

in order to find the velocity profiles. Moreover, no simple expression is provided by Kerkhof and Geboers for the calculation of the partial viscosities.

In summary, the different approaches to describe in a unified framework bulk and wall-mediated diffusion in porous media are not fully satisfactory from a theoretical standpoint. Some errors in the derivations arise from *ad-hoc* superposition of the viscous and diffusive contributions to the total flux, where the definition of the latter is not always in agreement with the statistical-mechanical convention. In addition, some of the models assume uniform diffusive flux, which seems to be a rather convenient but unlikely situation. The VPM, which is probably the theoretically neatest approach, introduces partial viscosities which are difficult to access from theoretical or experimental methods. Moreover, the cross-section averaged form of the equations, rely on the assumption of uniform pressure and composition in the cross-section, which is not the case when adsorption is present.

4. Transport in the presence of adsorption fields

The models discussed above introduce the effect of the pore walls through the Knudsen diffusion coefficient that considers a hard sphere system, and consequently neglect the effect of adsorption. At the nanopore level adsorption cannot be ignored. The fluid molecules can never escape from the force field of the pore walls, and transport is often empirically treated as an "activated process".[38] In the discussion of the Knudsen model in Section 2 it was clearly shown that, at this size scale, ignoring adsorption leads to diffusion coefficients usually orders of magnitude above those determined by experimental and simulation methods. However, to argue that adsorption is important only at the nanopore level ($d < 2$ nm) is certainly incorrect, as the definition of "nanopore" is arbitrary. The discussion of this section also applies to larger (often much larger) pores where adsorption effects on transport can still be significant.

The consideration of more realistic van der Waals interactions at low density, to overcome limitations of the Knudsen model, was performed by Nicholson and coworkers,[141–144] who numerically solved the equations of motion for a Lennard-Jones particle moving under the action of the adsorbent field in a slit pore. In their 'molecular path tracing' method the trajectories yielded path lengths which were incorporated into a statistical mechanical averaging to obtain self-diffusivities. The theory was successful in explaining experimentally observed temperature minima in the relative permeability.[145] Several attempts have been made to derive a rigorous statistical mechanical description of the transport of fluids in nanopores at high density, while allowing for van der Waals fluid–fluid and fluid–wall intermolecular interactions. However, they have largely been intractable due to the complexity of describing the dynamical evolution of a many body system, and have not yielded models that can be routinely applied in interpreting experimental data. Pozhar and Gubbins[146] developed a kinetic theory approach based on the generalized Langevin equation, and later[147] a more refined version based on the Enskog theory. Starting from the Liouville equation and utilizing the Zwanzig–Mori[148,149] projection operator technique, Pozhar[150] and Pozhar and Gubbins[41] developed a master equation for the set of collective variables that is sufficient for a complete characterization of a system's behavior. However, besides being computationally intensive, the final equations for the kinetic coefficients rely on gas–solid contact pair distributions that are obtained by molecular dynamics simulations, as a result of which the method is not predictive. The agreement with simulation results is also modest, with errors in predicted self-diffusivity of methane in carbon slit pores as large as 60% in some cases,[42] while viscosities can be similarly inaccurate, particularly near the wall.[151] A similar issue of intractability and requirements of estimating contact distributions is inherent to other kinetic theory based approaches.[40] Some of these problems are avoided in recent treatments by Guo and co-workers[152,153] and Marconi and Melchionna,[154] based on the Boltzmann equation, with the collision term being represented by the well-known Bhatnagar–Gross–Krook (BGK)[155] relaxation approximation. However, the BGK approximation is known to be crude, in which the relaxation time is taken as the reciprocal of the collision frequency, and is therefore inaccurate for a nanoscale system where strong density gradients exist and mean free paths are density-dependent and not small in comparison to the pore size. No quantitative comparison of the transport properties with those from MD simulations in nanopores is reported in these papers, and the results of Guo *et al.*[153] show only rough qualitative consistency in trends of the change of slip-length with interaction energy parameter. In an attempt to overcome the problem of a centre of mass-based frame of reference Kerkhof and Geboers[125] modified the Enskog solution of the Boltzmann equation for dilute gases by expanding around the species average velocity based frame of reference. However, their solution is only valid for a uniform bulk gas, as it does not account for inhomogeneities that occur in nanopores, or for the influence of finite Knudsen number. Indeed, any analysis treating binary collisions in a manner similar to the conventional kinetic theory,[59] must be inaccurate in nanopores, even at low density, because the *a priori* assumption of molecules approaching each other from infinite separation is no longer valid at the length scales involved.

In recent years new approaches based on modifications of the Maxwell–Stefan (MS) theory in eqn (22) and (23) have arisen, providing tractable models for transport under conditions when adsorption is important. These are the generalized MS theory of Krishna and co-workers at Amsterdam, and the statistical mechanics based approach from the Bhatia group at the University of Queensland. In what follows we discuss these approaches and their merits and limitations.

4.1 Generalized Maxwell–Stefan approach

Krishna and co-workers[48,49,156] extended the Maxwell–Stefan formulation in the spirit of the DGM by introducing a model for surface diffusion. An important aim of the approach is to be able to determine individual species fluxes in multicomponent system, based only on information on pure component diffusivities. Thus, the approach does not explicitly incorporate adsorption fields; however, these are indirectly considered through the pure component transport coefficients,

which may be obtained from experiment or MD simulation. In the same spirit, the approach also implicitly considers inhomogeneity, whose effect at the pure component level of description is inherent to diffusivity values used as input. In their derivation, molecules are assumed to hop from one adsorption site to the other, and the adsorption site to which a molecule jumps may be vacant or occupied by another molecule. Jumping to a vacant site leads to an exchange of momentum between the "vacant" site and the molecule which, for species i, is characterized by a surface diffusion coefficient $Đ_i^s$. If a molecule of i jumps to a site occupied by a molecule of j and displaces the latter, a net change in the momentum of i will arise from this process. Such change is characterized by a Maxwell–Stefan binary surface diffusion coefficient, $Đ_{ij}^s$. Obviously, if the site is already occupied by a molecule of i, on the average no net momentum change for species i will occur when the molecule is replaced by another molecule of i. When a porous solid is considered rather than a single straight pore, it is implied that $Đ_i^s$ and $Đ_{ij}^s$ already contain the factor ε_p/γ.

If the vacant sites are assumed to be the $(n+1)$th component of a mixture containing n-adsorbates, the Maxwell–Stefan equations produce, after some manipulation,

$$\sum_{\substack{j=1\\ i\neq j}}^{n}\frac{\theta_j\mathbf{J}_i^s-\theta_i\mathbf{J}_j^s}{\varepsilon_p\rho_p q_{sat}Đ_{ij}^s}+\frac{\mathbf{J}_i^s}{Đ_i^s}=-\frac{\theta_i}{RT}\nabla_T\mu_i\ i=1,\ldots,n \qquad (61)$$

θ_i is the fractional coverage of i defined as

$$\theta_i=\frac{q_i}{q_{sat}} \qquad (62)$$

where q_i is the concentration of i in the adsorbed phase, usually expressed in mmol g^{-1} and q_{sat} is the saturation surface concentration. ρ_p is particle density, ε_p is particle porosity and J_i^s is the "surface flux" given by,

$$\mathbf{J}_i^s=\rho_p\varepsilon_p q_{sat}\theta_i\mathbf{v}_i \qquad (63)$$

where $\mathbf{v}_i$ is the surface (diffusion) velocity of species i. It is generally more convenient to rewrite the chemical potential gradients in terms of the coverage gradients,

$$\frac{\nabla_T\mu_i}{RT}=\sum_{j=1}^{n}\Gamma_{ij}\nabla\theta_j;\ \Gamma_{ij}=\frac{\partial\ln f_i}{\partial\theta_j} \qquad (64)$$

where f_i is the fugacity of i in the bulk fluid mixture. The quantity Γ_{ij} is the so-called "thermodynamic factor" and can be computed from the adsorption isotherm obtained, for example, by grand canonical Monte-Carlo (GCMC) simulation methods (see the recent review by Tylianakis and Froudakis[157]). When the system pressures are not too high, $f_i\approx p_i$ and the thermodynamic factor is easily calculable from classical adsorption isotherms, *e.g.* the extended Langmuir equation,

$$\theta_j=\frac{b_ip_i}{1+\sum_{j=1}^{n}b_jp_j} \qquad (65)$$

Through which the thermodynamic factor is simply given by

$$\Gamma_{ij}=\delta_{ij}+\frac{\theta_i}{1-\sum_j\theta_j};\ \delta_{ij}=\begin{cases}1 & \text{if } i=j\\ 0 & \text{if } i\neq j\end{cases} \qquad (66)$$

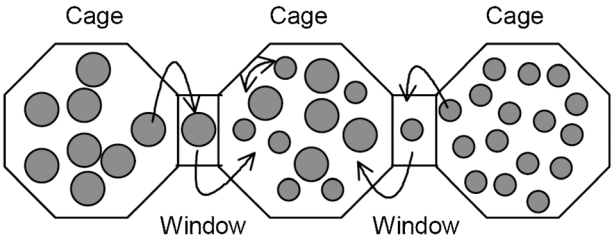

Fig. 9 Diffusion in cage-type zeolites. A molecule diffuses through jumps to the nearest vacant cages. When the window size allows one jump at a time the rate of the process will be dominated by the species with the lowest hopping frequency. From Krishna and Baur.[159]

Krishna and co-workers have extensively employed this approach for the study of several adsorbate–adsorbent systems, particularly zeolites.[109,158–160] In the analysis of zeolites with cage-type structures, such as faujasite or zeolite Y, "the active sites" correspond to the crystal cages, which can hold one or more molecules simultaneously. Molecules jump to the nearest sites through narrow channels, or windows, interconnecting the cages (Fig. 9). The windows may be narrow enough to allow for the transit of one molecule at a time only, in which case single-file diffusion occurs through the windows. In the original formulation of the Maxwell–Stefan equations for surface diffusion, it is implicitly assumed that only one molecule per site is allowed. As this is not the case for zeolites and, moreover, the saturation loading (maximum number of molecules per cage) may vary from one species to the other, eqn (61) must be modified (see Keil *et al.*,[161] for details):

$$\sum_{\substack{j=1\\ i\neq j}}^{n}\frac{q_j\mathbf{J}_i^s-q_i\mathbf{J}_j^s}{\varepsilon_p\rho_p q_{i,sat}q_{j,sat}Đ_{ij}^s}+\frac{\mathbf{J}_i^s}{Đ_i^s}=-\frac{\theta_i}{q_{i,sat}}\sum_{j=1}^{n}\Gamma_{ij}\nabla\theta_j\ i=1,\ldots,n \qquad (67)$$

where a particular saturation loading $q_{i,sat}$ (taken as molecules per cage in zeolites) is allowed for every species and the fractional coverage is redefined as $\theta_i=q_i/q_{i,sat}$. Much effort has been devoted to find expressions for the mutual surface diffusivities $Đ_{ij}^s$ in terms of the single component surface diffusivities $Đ_i^s$. Krishna and Wesselingh have proposed an extended Vignes interpolation formula,[50]

$$Đ_{ij}^s=(Đ_i^s)^{q_i/(q_i+q_j)}(Đ_j^s)^{q_j/(q_i+q_j)} \qquad (68)$$

The coefficient $Đ_i^s$ must in general be estimated experimentally or through simulation techniques, although these authors suggest,

$$Đ_i^s=Đ_i^s(0);\quad \text{for weakly confined adsorbates (small molecules)} \qquad (69)$$

$$Đ_i^s=Đ_i^s(0)\left(1-\textstyle\sum_j\theta_j\right);\quad \text{for strongly confined adsorbates (small molecules)} \qquad (70)$$

A variation of eqn (68) was later proposed by Skoulidas *et al.*[162] considering the transport of CH_4/CF_4 mixtures in MFI zeolites:

$$q_{j,sat}Đ_{ij}^s=(q_{j,sat}Đ_i^s)^{q_i/(q_i+q_j)}(q_{i,sat}Đ_j^s)^{q_j/(q_i+q_j)} \qquad (71)$$

This formula apparently provides better agreement with simulations than eqn (68) for diffusion of alkanes in some zeolitic structures.[160]

For one-dimensional transport in the z direction, eqn (67) can readily be recast as a Fickian expression,

$$\mathbf{J}^{\mathrm{s}} = \varepsilon_{\mathrm{p}}\rho_{\mathrm{p}}(\mathbf{q}_{\mathrm{sat}})(\mathbf{D})\frac{d}{dz}\boldsymbol{\theta} \tag{72}$$

where $\boldsymbol{\theta} = (\theta_1,\ldots,\theta_n)^T$, $\mathbf{J}^{\mathrm{s}} = (J_1^{\mathrm{s}},\ldots,J_n^{\mathrm{s}})^T$, $\mathbf{q}_{\mathrm{sat}} = \mathrm{diag}(q_{1,\mathrm{sat}},\ldots,q_{n,\mathrm{sat}})$ and $\mathbf{D}$ is the nxn generalized Fickian diffusivities matrix. The superscript T in the vector quantities indicates "transpose". Matrix $\mathbf{D}$ is given by the product of a diffusive and a thermodynamic contribution, represented by the nxn matrices $\mathbf{B}$ and $\boldsymbol{\Gamma}$, respectively,

$$\mathbf{D} = \mathbf{B}^{-1}\boldsymbol{\Gamma} \tag{73}$$

Here, $\boldsymbol{\Gamma}$ is the matrix of thermodynamic factors with $(\boldsymbol{\Gamma})_{ij} = \Gamma_{ij}$, while $\mathbf{B}$ is given by

$$B_{ii} = \frac{1}{Đ_i^{\mathrm{s}}} + \sum_{\substack{j=1\\ i\neq j}}^{n}\frac{\theta_j}{Đ_{ij}^{\mathrm{s}}};\quad B_{ij} = \frac{\theta_j}{Đ_{ij}^{\mathrm{s}}} \tag{74}$$

An entirely equivalent treatment can be carried out to cast the DGM equations in a compact matrix form.[50,117] Fig. 10 depicts the components of matrix $\mathbf{D}$, calculated by Krishna[158] using eqn (68) and (73) for a CH_4/CF_4 mixture in faujasite, along with those obtained from MD. Fig. 11 shows essentially the same calculations using eqn (71) and (73) for the same mixture in MFI.[162] Both interpolation equations, (68) and (71), provide qualitatively good results, although it is apparent that the interpolation formula must be adapted depending on the particular zeolite. As a matter of fact, the mutual diffusion coefficient $Đ_{ij}^{\mathrm{s}}$ must depend on the binary cross-interactions, and expressing it as a function of the unary diffusivities $Đ_i^{\mathrm{s}}$ artificially reduces the transport degrees of freedom established from irreversible thermodynamics principles,[163] indicating that a physically sound basis for the determination of $Đ_{ij}^{\mathrm{s}}$ is still lacking.

Many authors have employed the DGM formulation and Krishna model of surface diffusion simultaneously for the calculation of the total fluxes in mesopores, with the premise that the former describes appropriately the transport in the "quasi-bulk" phase located in the pore core whereas the latter describes molecular transport at the surface (*cf.* Fig. 12). In these works[132,164–166] the total flux is expressed by

$$\bar{J}_i = \bar{J}_i^{\mathrm{DGM}} + \bar{J}_i^{\mathrm{GMS}} \tag{75}$$

where $\bar{J}_i^{\mathrm{DGM}}$ is the contribution to the flux from the dusty gas model, in which adsorption is ignored, and $\bar{J}_i^{\mathrm{GMS}}$ is the contribution from the generalized Maxwell–Stefan model for surface diffusion from Krishna. There is considerable ambiguity in the way in which the total loading is partitioned between the two transport mechanisms, while eqn (75) has no real fundamental justification. If the pore core is to be considered as being a bulk-like phase, the introduction of the "dust" is not

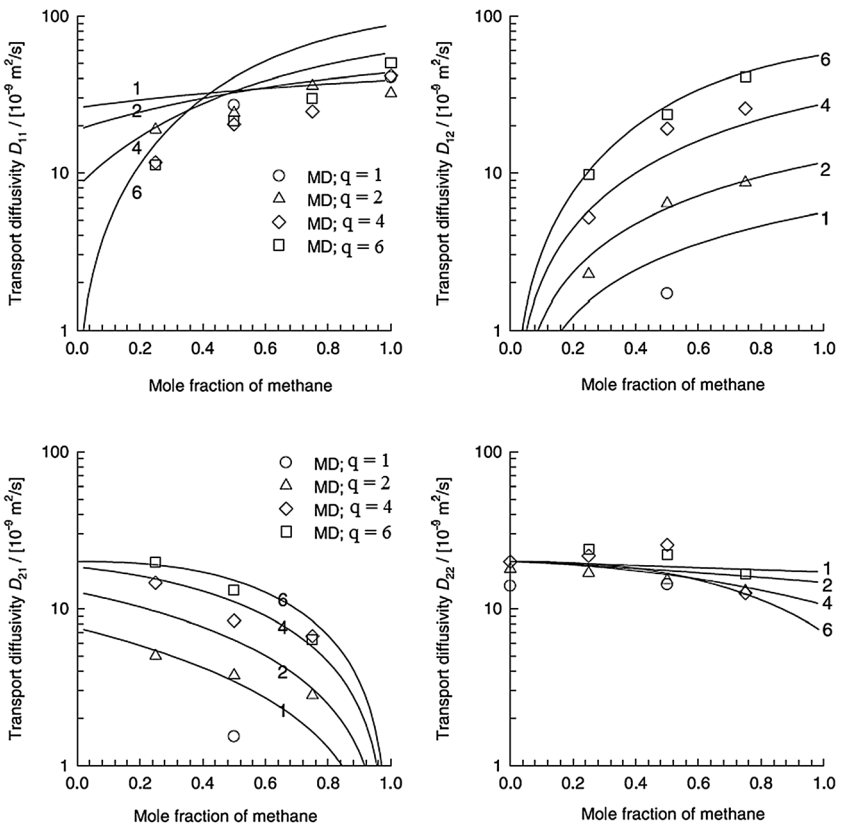

Fig. 10 Comparison of the elements of the Fick matrix $\mathbf{D}$ calculated by MD simulations (symbols) with those calculated through eqn (73) using the correlation in eqn (68) for the estimation of the MS mutual diffusivity (continuous line), for a mixture of CH_4/CF_4 in faujisite at 300 K and different loadings (q). From Krishna.[158]

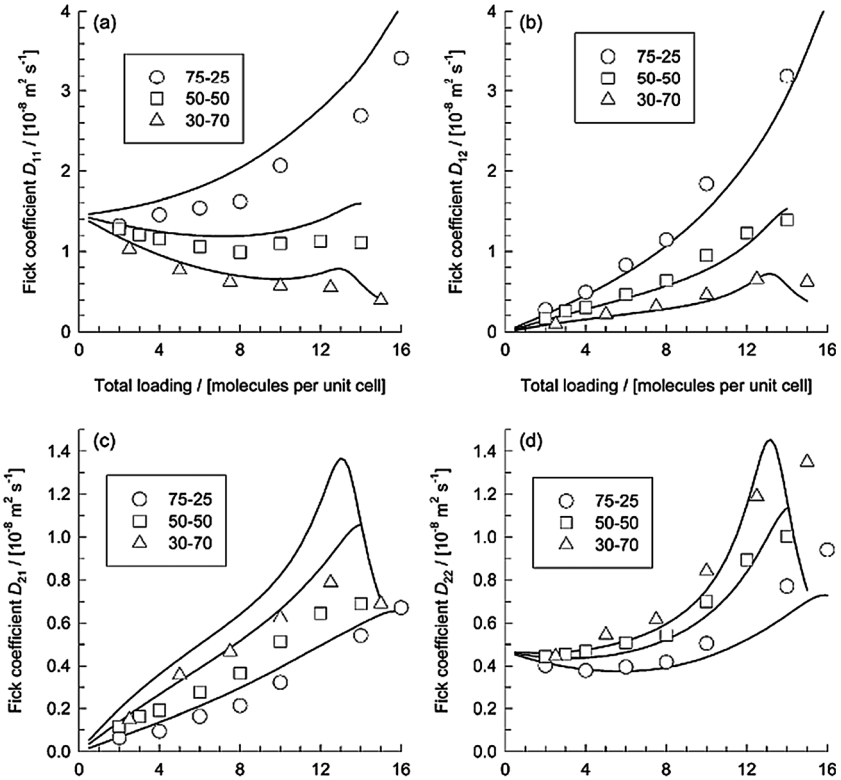

Fig. 11 Comparison of the elements of the Fick matrix **D** calculated by MD simulations (symbols) with those calculated through eqn (73) using the correlation in eqn (71) for the estimation of the MS mutual diffusivity (continuous line), for a mixture of CH_4/CF_4 in MFI zeolite at 298 K and at different CH_4/CF_4 proportions. From Skoulidas *et al.*[162]

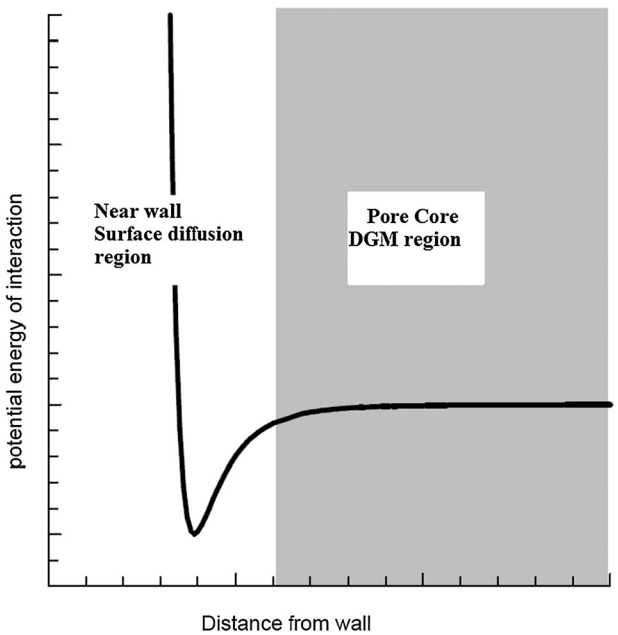

Fig. 12 The surface diffusion model of Krishna is often used along with the DGM to describe transport in nano and mesoporous materials where viscous and bulk diffusion effects are thought to be considerable. The idea behind this treatment is assuming that a fraction of the molecules, moving in a monolayer near the wall, obey the surface diffusion description, while the fraction in the core, where the potential energy of interaction is negligible, obeys the DGM description. From Krishna and van Baten.[109]

justified as the wall effect would be included in the surface term (unless the adsorbed layer moving along the surface is considered as "the wall" for the bulk particles, in which case the nature of $Đ_{io}$ is uncertain). However, most of the theories using this approach display very good agreement with experimental data. The apparent success can be traced to the large number of parameters to be adjusted. In fact, some authors introduce an activation energy factor in the Knudsen diffusion in the DGM, in this way increasing the chances for the model to fit the laboratory results. A more consistent attempt to unify surface and bulk diffusion in porous media has recently been given by Krishna and van Baten.[109] Their approach resembles the Lightfoot model, described in the previous section, in the sense that the fluxes draw together surface and bulk diffusion effects. However, their model still relies on the empirical specification of the binary surface diffusion coefficients $Đ_{ij}^s$ based on the unary coefficients $Đ_i^s$ and $Đ_j^s$.

It is pertinent to mention that the division of the pore flux into separate contributions from surface diffusion and Knudsen diffusion has a long history, with early work detailed in a comprehensive review nearly two decades ago.[167] Over the years the approach has continued to find much favor,[99,168–170] with the total flux being represented as a weighted average of the surface and Knudsen diffusivities. The weighting factors for a given phase are taken to be the fraction of molecules in that phase, based on the adsorption isotherm and an assumption of the surface layer thickness.[170] This division of the pore fluid between the surface and gas phases, while removing some element of ambiguity present in many earlier works does

require detailed justification based on a more fundamental molecular approach. Moreover, layer thickness ultimately rests on an equilibrium concept of a Gibbs dividing surface that may have little relevance to dynamics and which in any case is subject to uncertainties where phases do not have an infinite extent on either side of the interface.[171] Molecular dynamics simulations[172] do reveal a monolayer region of high adsorbate density and low diffusivity near the wall, corresponding to molecules undergoing slow surface diffusion, with the bulk of the flux dominated by molecules in the interior of the pore. However, such simulations do not offer a recipe or precise estimate of the partitioning of the pore fluid into gas and surface phases. As a matter of interest, Argönül and Keil[173] have numerically shown that when the surface flow is a substantial fraction of the total flow, the approach of superposing independent gas and surface fluxes while using the adsorption isotherm can yield improper estimates. They find that under such conditions the assumption of local equilibrium can be incorrect, and that instead models for rates of adsorption and desorption should be introduced.

4.2 The oscillator model

The statistical mechanical 'Oscillator Model', developed in this laboratory[54,55,62] provides an analytical result for the low-density transport coefficient of a LJ fluid in a confined space, whose particles are oscillating between diffuse wall collisions under the action of a conservative one-dimensional fluid–solid interaction potential. This represents a significant advance over the earlier Knudsen formulation which considers only hard sphere interactions, and can be applicable only to sufficiently large pores where adsorption effects are negligible, as shown in Section 2. In this sense, it is also superior to other approaches where adsorption effects are empirically added through an activation energy factor. Not being limited by any assumptions regarding the strength of the LJ fluid–solid interaction, the new Oscillator model is valid for all pore sizes, from nanopores to macropores, without requiring any empirical activation energy corrections. Since the method treats the pore fluid as a whole it is also a major advance over the approaches that divide the pore flux into gas and surface flow contributions, avoiding the empiricism associated with this partitioning.

4.2.1 Basic formulation. In the low density limit, the molecular trajectories are subject solely to the force field from the adsorbent wall and can be described by Newtonian equations of motion. For example, in a cylindrical pore with wall potential $\phi_{fs}(r)$ the Hamiltonian for a single molecule is

$$H = \phi_{fs}(r) + \frac{p_r^2}{2m} + \frac{p_\theta^2}{2mr^2} + \frac{p_z^2}{2m} - zF \qquad (76)$$

where p_r, p_θ and p_z are the cylindrical components of the momentum vector, m is the molecule mass and F is an external driving force in the z direction. In the conservative force field of the adsorbent the (r,θ) part of the Hamiltonian is constant, and for a particle having radial and angular momenta p_r and p_θ, respectively, at some position r, one obtains for the radial momentum when the particle is at position r'

$$p_r^2(r', r, p_r, p_\theta) = 2m[\phi_{fs}(r) - \phi_{fs}(r')] + \frac{p_\theta^2}{r^2}\left[1 - \left(\frac{r}{r'}\right)^2\right] + p_r^2(r) \qquad (77)$$

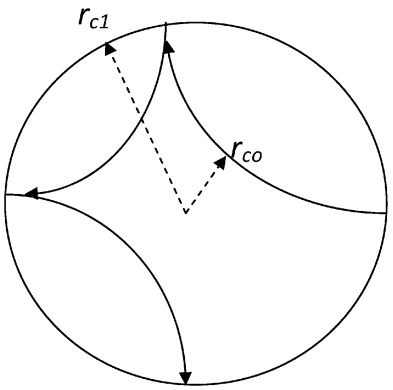

Fig. 13 Schematic of trajectories of an oscillating molecule projected onto the pore cross section.[55]

The radial momentum of a molecule becomes zero at positions $r_{c0}(r, p_r, p_\theta)$ and $r_{c1}(r, p_r, p_\theta)$, where the molecule reverses its radial direction in the external adsorbent field. Thus, the radial bounds of the trajectory, r_{c0} (r, p_r, p_θ) and r_{c1} (r, p_r, p_θ) can be found from the solution of

$$p_r(r', r, p_r, p_\theta) = 0 \qquad (78)$$

Outside the interval $[r_{c0}\ r_{c1}]$, the radial momentum will be imaginary. As a consequence, the molecular motion will be periodic in the radial coordinate, as depicted in Fig. 13. The oscillation time τ can be obtained from integration of the reciprocal of $p_r(r', r, p_r, p_\theta)$ over the interval in which it is real,

$$\tau(r, p_r, p_\theta) = 2m \int_{r_{c0}(r,p_r,p_q)}^{r_{c1}(r,p_r,p_q)} \frac{dr'}{p_r(r', r, p_r, p_\theta)} \qquad (79)$$

Now, the average steady state axial velocity of the fluid can be related to the external force through the phenomenological relation,

$$\langle v \rangle = \frac{D_o^{LD}}{k_B T} F \qquad (80)$$

where k_B is the Boltzmann constant and D_o^{LD} is the low-density diffusion coefficient, implying that the equation is now specifically applied to molecular streaming and takes no account of intermolecular collisions. The driving force maintaining the steady state regime can be a chemical potential gradient $(-\nabla\mu)$ or alternatively a gravitational force, as in a non-equilibrium molecular dynamics (NEMD) simulation.[174] The force is related to the average axial momentum change between reflections by $F = m\langle v \rangle / \langle \tau \rangle$, leading to,

$$D_o^{LD} = \frac{k_B T}{m} \langle \tau \rangle \qquad (81)$$

When the hopping time given by eqn (79) is averaged with respect to a canonical distribution of the energy, given by the

conserved part of the Hamiltonian in eqn (76), the low density transport coefficient is obtained as,

$$D_{\mathrm{o}}^{\mathrm{LD}} = \frac{2}{\pi mQ}\int_0^\infty e^{-\beta\phi(r)}dr\int_0^\infty e^{-\beta p_r^2/2m}dp_r\int_0^\infty e^{-\beta p_\theta^2/2mr^2}dp_\theta \times\int_{r_{c0}}^{r_{c1}}\frac{dr'}{p_r(r',r,p_r,p_\theta)} \quad (82)$$

where $\beta = (k_{\mathrm{B}}T)^{-1}$ and $Q = \int_0^\infty re^{-\beta\phi_{\mathrm{fs}}(r)}dr$. A similar result for slit-like pore geometries can be found elsewhere.[54] It is noted that the canonical averaging over the energy distribution incorporates the exponential density profile, $\rho(r) \propto \exp[-\beta\phi_{\mathrm{fs}}(r)]$, expected at low density. In doing so it overcomes the significant limitation of a uniform density profile inherent to the Knudsen model and the DGM as well its sister models discussed earlier.

The above derivation assumes that that the molecules undergo diffuse reflection and are thermalised upon colliding with the wall, as in the Knudsen analysis, so that only the time spent between successive collisions contributes to the streaming velocity. Thus, successive trajectories are uncorrelated. The idealized diffuse reflection model for the surface is not necessarily a precise representation of a real solid pore wall, as demonstrated in MD simulations of atomically detailed surfaces.[67,129,175] Reflection from smooth surfaces such as the graphene-like wall of a carbon nanotube is very close to being specular, leading to almost frictionless flow of small molecules.[176,177] Even from rough surfaces, reflection can be more than 50% specular. However, this assumption is not a limitation since the theory can be readily extended to accommodate partially specular reflection through the tangential momentum accommodation coefficient, α, while the idealised diffuse reflection condition is sufficient to illustrate the main ideas of the model derivation. As noted earlier, the diffuse reflection hypothesis was also embedded in the Knudsen theory of the transport coefficient in confined hard sphere systems, and a correction factor for partial specular reflection was introduced by Smoluchowski. The studies cited above, using atomically detailed pore walls, have considered defect-free surfaces, which is probably unrealistic in practice. Most real porous carbons, for example, are highly defective with a large degree of disorder, as confirmed in laboratory analysis and interpretation of X-ray diffraction patterns of heat-treated carbons.[178–180] Moreover, carbon structures determined by the reverse Monte Carlo method, based on the interpretation of X-ray-scattering structure factors,[181–183] as well as transmission electron microscopy studies, disclose the presence of a high degree of disorder in carbons and suggest that a large number of rings have less than six members. In such materials, the fraction of specular reflections is expected to be significantly less than that from defect-free surfaces, and selection of suitable boundary conditions is to some extent ambiguous. Even in defect-free surfaces the accommodation coefficient is a strong function of the interaction energy and the surface lattice parameter of the solid, and can be far from specular (*i.e.* α is of the order of unity), as is evident in Fig. 14,

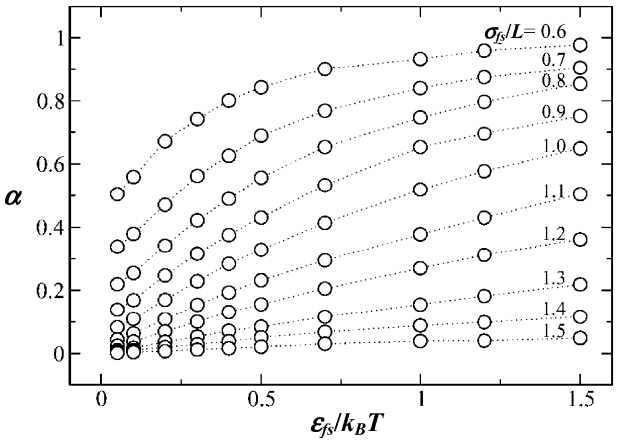

Fig. 14 Variation of the accommodation coefficient with fluid solid interaction parameter $\varepsilon_{\mathrm{fs}}/k_{\mathrm{B}}T$, for various values of the lattice parameter $\varepsilon_{\mathrm{fs}}/L$. From Arya *et al.*[184]

which depicts the effect of lattice spacing and fluid–solid interaction energy on the accommodation coefficient determined by Arya *et al.*[184] based on simulation of fluid solid collisions.

It has been shown that, in the high temperature limit, $D_{\mathrm{o}}^{\mathrm{LD}}$ converges to the Knudsen diffusion coefficient,[55] demonstrating the consistency of this approach. Moreover, no previous assumptions are made regarding the form of the fluid–wall interaction potential other than that it is a function exclusively of the radial coordinate (or the coordinate perpendicular to the wall in the slit-shape pore), indicating the great versatility of the model. For spherical molecules reflecting diffusely from the wall the theory is *exact* in the low density limit. For more realistic molecular geometries at high but finite Knudsen numbers the theory certainly becomes an approximation, but its performance is still expected to exceed that of the classical Knudsen model. This is indeed the conclusion extracted from comparison of the low-density diffusion coefficients obtained from MD simulation with D_{k} and with $D_{\mathrm{o}}^{\mathrm{LD}}$ calculated from eqn (82). For methane in cylindrical silica pores at 450 K this comparison has already been depicted in Fig. 4. Recalling the discussion in Section 2, we note that the Knudsen diffusivity represents an upper limit which can only be reached when $\beta\phi_{\mathrm{fs}}(r) = 0$. The oscillator model on the other hand agrees very well with the MD results at all pore sizes, in both the micro and the mesopore region. Further comparison in slit-like nanopores is depicted in Fig. 15, where this model is seen to accurately capture the variation of $D_{\mathrm{o}}^{\mathrm{LD}}$ with pore size estimated by MD simulations, for methane adsorbed at 300 K in graphitized carbon slit-pores. The inset in Fig. 15 illustrates that, for a 1.4 nm width carbon slit pore, the streaming velocity profile predicted by the theory and that estimated by MD agree very well, with the deviations associated mostly with the statistical noise inherent in the simulations.

4.2.2 Levitation effect. MD simulations have revealed the existence of a levitation (also called floating molecule) or superfast diffusive regime in which the diffusivity shows a maximum when the adsorbate molecular size approaches the pore size.[112,185–187] This has also recently found experimental support from quasi-elastic neutron scattering experiments.[188]

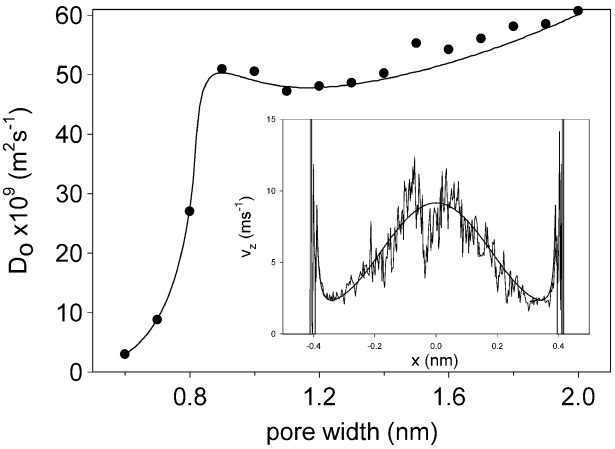

Fig. 15 Variation of transport coefficient with slit width for the adsorption of methane at 300 K in carbon slit pores. The line corresponds to model predictions and symbols to simulation data. The inset shows a comparison of the velocity profiles predicted by the model and generated by the simulation, for a pore of 1.4 nm width. From Jepps *et al.*[54]

The oscillator model provides a fundamental basis to explain this puzzling phenomenon that had previously not been well understood from a theoretical viewpoint. Fig. 16 depicts MD simulation values and oscillator model calculations of the transport coefficient of CF_4 in cylindrical silica pores.[113] It can be noted that, at a center to center pore diameter $d_{cc} \approx 1$ a local maximum in the diffusivity occurs. The maximum is accurately predicted by the oscillator model, and occurs approximately in the region where the overlapping wall potential fields merge from two to one minimum in as the pore width is reduced. As a rule of thumb, it was proposed that the pore diameter at which levitation occurs is twice the equilibrium separation based on the LJ pair interaction[112]

$$d_{cc} = 2(2^{1/6})\sigma_{fs} \tag{83}$$

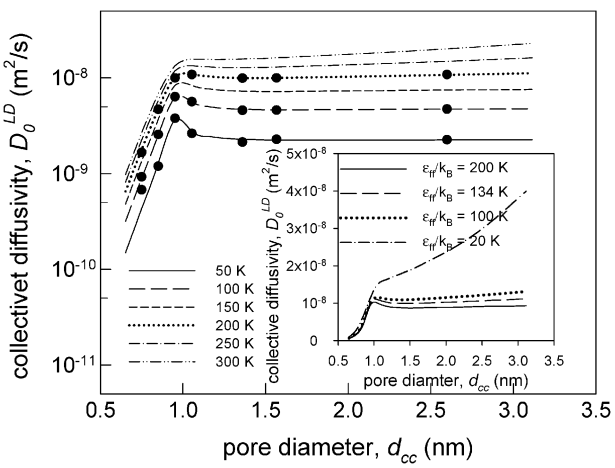

Fig. 16 Variation of diffusivity of CF_4 with pore diameter at various temperatures. The lines represent theoretical values and the symbols molecular dynamics simulations. The dependence of the levitation effect on the fluid–fluid interaction strength, ε_{ff}, is shown in the inset. From Anil Kumar and Bhatia.[113]

However, this criterion does not account for the observed temperature dependence of levitation, where it is noted that the maximum in the diffusivity becomes progressively weaker with increasing temperature and eventually disappears. The inset in Fig. 16, where the interaction strength ε_{fs} is varied at fixed σ_{fs}, for a molecule of the same mass as CF_4, shows that weakening the fluid–solid interaction strength has the same effect as increasing the temperature. A shift in the levitation diameter towards slightly higher pore sizes is observed as temperature increases. This occurs because, as the adsorbate molecules gain kinetic energy, a larger fraction of them can escape from the local energy minimum near the pore surface at larger pore sizes (in analogy with a rocket gaining sufficient escape velocity to leave the earth's gravitational field). These molecules have longer trajectories because they traverse the pore cross section during an oscillation, increasing the hopping time and thereby the diffusivity.

4.2.3 Extension of oscillator model for finite density in narrow nanopores. Since the Oscillator model is developed for low density, any extension to transport at finite density must consider the dynamics of a many body system, which is rendered intractable by the large number of degrees of freedom involved. For nanopores that can accommodate at most two molecules in their cross-section (*i.e.* a monolayer on the pore surface), Bhatia and Nicholson[189] have circumvented this problem by performing a nearest neighbor analysis, considering a 3-particle system in a cylindrical pore as depicted in Fig. 17. In such a system multilayers cannot form, and the conventional concepts of viscous flow do not apply. In strong confinement the interaction between neighboring particles can hinder their oscillations, leading to a decrease in diffusion coefficient with density. The Oscillator model is applied to obtain the collective diffusion coefficient, but with the fluid–wall interaction replaced by the total effective interaction potential $\phi_{eff}(r)$ given by

$$\phi_{eff}(r) = \phi_{ff}(r) + \phi_{fs}(r) \tag{84}$$

where the fluid–fluid interaction potential $\phi_{ff}(r)$ includes the nearest neighbor interactions for arbitrarily located neighbors, as shown in Fig. 17, following

$$\phi_{ff}(r) = 2\int_0^{2\pi}\int_0^{r_p}\int_0^{2\pi}\int_0^{r_p}\int_0^{d} r'r''\phi_{LJ}(b(r,z,r',\theta'))p(z,r',\theta',r'',\theta''/r) \times dz dr' d\theta' dr'' d\theta'' \tag{85}$$

Here $b(r,z,r',\theta')$ is the distance between the target particle at r and its immediate neighbour at (z,r',θ'), and $p(z,r',\theta',r'',\theta''/r)$ is the joint probability density for a particle at (z,r',θ') and another at (d,r'',θ''), given a target particle at r. This joint probability density is related to the equilibrium pair distributions by a superposition approximation.[59]

Fig. 18a[189] depicts the variation of the collective diffusivity, D_o, with density, for CH_4 and CF_4 in a 1.26 nm cylindrical pore in silica at 300 K, obtained using eqn (82) with the fluid–solid interaction energy replaced by the total potential energy following eqs (84) and (85). Here the pore density

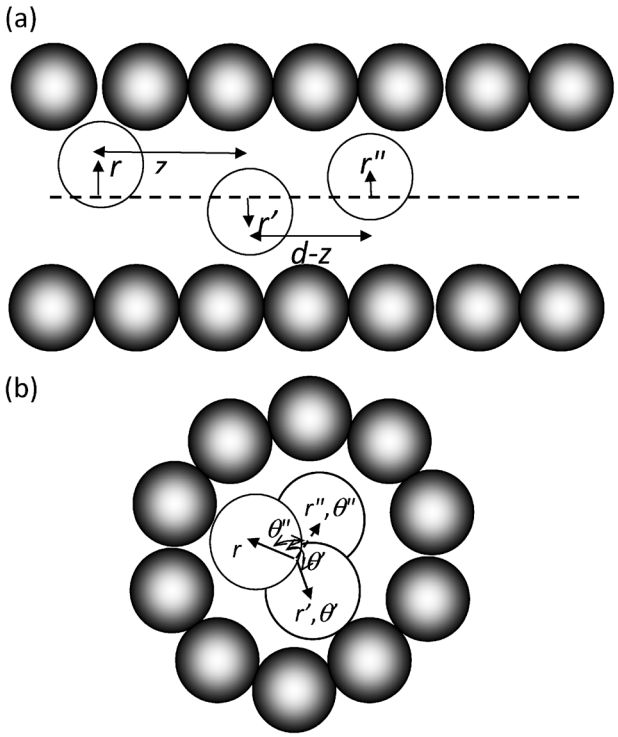

Fig. 17 Illustration of nearest neighbor particles in cylindrical pore. Dark circles represent solid atoms and empty circles the adsorbate particles. (a) Side view showing three particles at radial positions of r, r' and r'', and (b) cross-sectional view showing the polar angle between particles, measured relative to the particle at r. From Bhatia and Nicholson.[189]

represents the overall cross-sectionally averaged value

$$\bar{\rho} = \frac{2}{r_p^2}\int_0^{r_p} r\rho(r)dr \qquad (86)$$

with the non-uniform density profile, $\rho(r)$, obtained by Monte Carlo simulation. Further, in eqn (82), the exponential density profile, $\rho(r) \propto \exp[-\beta\phi_{fs}(r)]$, was replaced by the actual simulation-based profile $\rho(r)$. Alternatively, this profile may be theoretically obtained by density functional theory.[105,190,191] Both the theory and NEMD simulation results, while in excellent agreement, show a decrease in diffusivity with increase in density, contrary to what was found for larger pores[55] where an increase in diffusivity with increase in density was reported. This behavior is due to the formation of a repulsive core in the pore in which oscillating neighbors undergo a repulsive interaction, as shown in Fig. 18b[189] for CF_4 in a 1.26 nm pore (which accommodates exactly one monolayer of CF_4). Thus, the critical role of the non-uniformity of the density profile in nanopores is clearly evident. A further finding from the results is that agreement of theory with MD simulations is found when the pair distribution function between second nearest neighbors is periodic, suggesting that the molecules are moving in a highly correlated manner in the narrow confinement at this pore size. Thus, multiparticle dynamics plays a significant role under these conditions, though the simple 3-particle system used

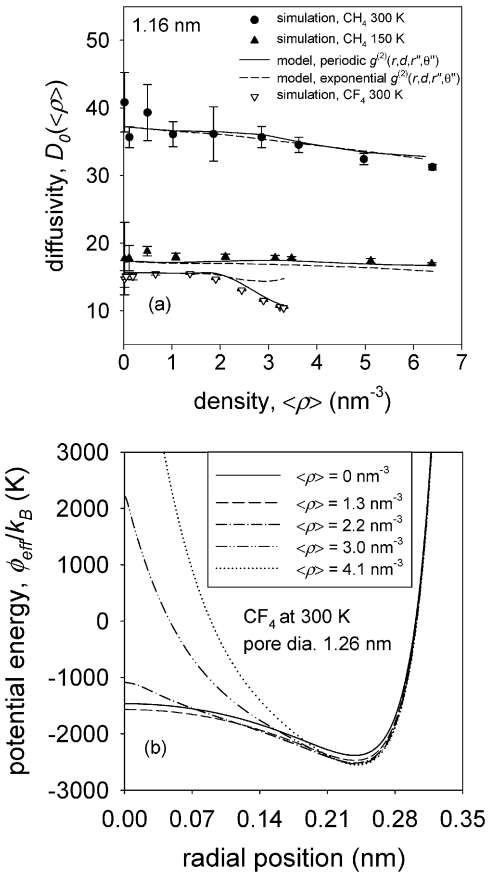

Fig. 18 (a) Variation of collective diffusivity of CH_4 with density, at 150 K and of CH_4 and CF_4 at 300 K, in pore of diameter 1.16 nm, and (b) effect of adsorbed density on potential energy profile for CF_4 at 300 K in pore of diameter 1.26 nm. From Bhatia and Nicholson.[189]

in the nearest neighbor treatment represents a good first approximation.

4.2.4 Permeation in adsorbents and membranes. The Oscillator model offers a useful and rather elegant tool for predicting the transport properties of membranes based on their known structural characteristics. Bhatia[65] has used the oscillator model along with the permeability model in eqn (12), to interpret the data of Tomita *et al.*[11] on the variation of the permeability with molecular size of the diffusing species, for a microporous DDR zeolite membrane of 0.63 nm average critical window size (center-to-center between surface oxygen atoms), at 301 K and 373 K. These authors investigated the transport of various molecules, covering a range of molecular size, and observed an unusual maximum in the permeability with molecular size. Fig. 19a depicts their data, taken over the linear region of the flux *versus* feed pressure relationship (thereby ensuring that the Henry's law region permeability applicable to low densities was obtained) and the results of Bhatia[65] using the Oscillator model. In the application of this model the narrow channel connecting the cages of the DDR zeolite which controls the flux was taken as a cylindrical pore having the critical size. In interpreting the data only a single unknown parameter γ/ε_p was adjusted for the whole data set covering all the molecules. While the crystal structure and

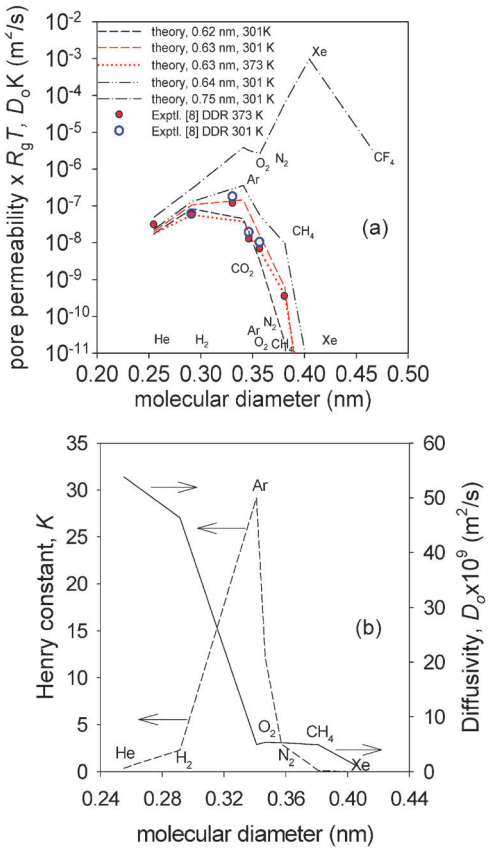

Fig. 19 (a) Comparison of Oscillator model prediction with experimental data of Tomita *et al.*[11] for variation of permeability with molecular size for DDR zeolite membrane, and (b) predicted variation of the Henry constant and diffusivity with molecular size at 301 K in 0.63 nm diameter channel. From Bhatia.[65]

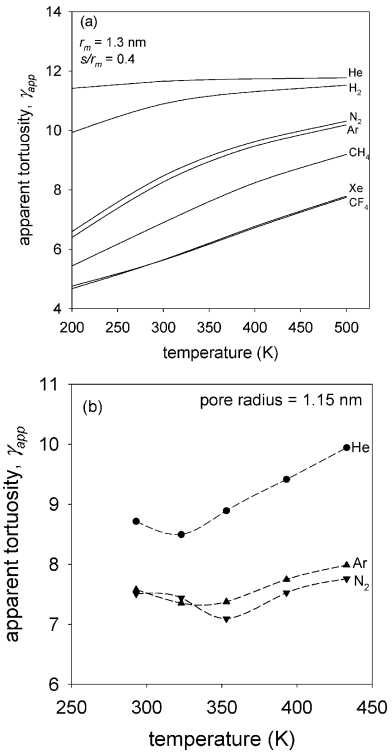

Fig. 20 Variation of the apparent tortuosity with temperature. (a) Theoretical results for various gases in a silica pore network having a Rayleigh pore size distribution of modal pore radius 1.3 nm, and relative standard deviation of 0.4. (b) Results from application of Oscillator model with the hybrid EMT–CRWT in eqn (10)–(12) to the data of Markovic *et al.*[86] for permeation in a 1.15 nm mean pore radius membrane. From Bhatia.[65]

therefore the porosity of DDR zeolite crystals is known, the channel volume is only a small part of the unknown membrane porosity. Further, in order to avoid leakage through inter-crystalline pores the crystallites comprising the membrane are highly inter-grown, leading to blockages and porosity loss. Thus, the value of the parameter γ/ε_p must be obtained by fitting at least one set of permeation data. The excellent agreement between the Oscillator model and data covering the whole range of molecular sizes using just this single parameter is a strong indicator of the applicability of the theory. An interesting feature of the data is the existence of a permeability maximum, which is reproduced by the theory, and has been shown by Bhatia[65] to be due to the combination of the adsorption equilibrium and transport coefficients in eqn (12), with the equilibrium constant having a strong peak for argon as seen in Fig. 19b. Another interesting feature, evident in Fig. 19a, is that small change in channel size to 0.63 nm or 0.64 nm leads to large variation in the permeability of the CH_4, illustrating the high sensitivity when the molecular size is comparable to the pore size. In this case the centre-to-centre channel diameter of 0.63 nm has an open diameter of about 0.37 nm (after accounting for a surface oxygen size of 0.37 nm), which is comparable to the LJ diameter of 0.38 nm of CH_4.

A rich variety of behavior is predicted for disordered adsorbents and membranes, upon application of the Oscillator model,[65] and is found to be consistent with experimental data. Such materials have a distribution of pore sizes, and large pores offer short circuit paths which reduce the flux in narrow pores. This increases the tortuosity and, most importantly, leads to a tortuosity that depends not only on the adsorptive but also on process conditions such as temperature. Fig. 20a depicts the variation of apparent tortuosity, based on eqn (12)–(14) with temperature for various gases in a silica pore network having coordination number, N, of 3, and with Rayleigh pore size distribution having uniform length pores with modal pore radius, r_m, of 1.3 nm and a standard deviation, s/r_m, of 0.4.[65] The tortuosity is seen to vary with the adsorption strength, with the most weakly adsorbed gas, He, having a high tortuosity in the range of 10–12, while the most strongly adsorbed gas, CF_4, has a tortuosity in the range of 5–7. Such behaviour cannot be predicted by the Knudsen model with $K = 1$, as discussed earlier, since the factor of $\sqrt{T/M}$ which embeds the effect of adsorptive and temperature cancels out on application of eqn (12)–(14). Results similar to those of Fig. 20a were obtained by Bhatia on interpreting the data of Markovic *et al.*[86] for permeation in disordered glass membranes using the Oscillator model with eqn (12)–(14). Fig. 20b[65] depicts one such result, illustrating the variation of apparent tortuosity with temperature for various gases for a 1.15 nm mean pore radius membrane, showing much similarity with the theoretical results in Fig. 20a. The increase in tortuosity with decrease in

temperature at lower temperatures was attributed to the intrusion of additional resistances at narrow pore necks, which can only be confirmed by more detailed structural characterization than was available. Further, while both theory and experiment show Ar and N_2 to have quite similar tortuosities, the change in order between them in Fig. 20b was attributed to enhanced adsorption due to electrostatic interactions of N_2 with the silica, which were noted by Markovic *et al.*,[86] but were not quantified. In related work, molecular size dependent tortuosities have also been predicted for carbons[192] and supported by analysis of experimental results[193] on the permeation of various gases in disordered mesoporous carbon membranes.

4.2.5 Apparent success of the Knudsen correlation. The simplicity of the Knudsen model in eqn (1) and the linearity of the low density diffusion coefficient with $\sqrt{T/M}$, as predicted by this model, makes it very attractive for use in the interpretation of experimental data. As a result there is a long history of its use[34,35] and remarkably, despite the hard-sphere assumption underlying the Knudsen model and the neglect of adsorption, linearity of the D_0 *versus* $\sqrt{T/M}$ correlation is frequently observed in experiments even in mesoporous materials. This linearity is commonly[85,86,100,194] taken as evidence in support of the Knudsen model. Recent work[192] has, however, shown that the correlation is deceptive, and conclusions regarding validity of the Knudsen model based on this can be misconceived. The crux of the argument is that experimental estimates of the diffusivity are invariably based on measurements that depend on the flux and therefore on the permeability. Consequently, following eqn (11) it is readily evident that any estimate of D_o while assuming $K = 1$, *i.e.* of D_k, is effectively an estimate of KD_o. Using the Oscillator model for D_o, Bhatia and Nicholson[192] have shown that KD_o correlates linearly with D_k, with only small deviation that is within the usual range of experimental error, when adsorption is not strong.

Fig. 21 depicts the KD_o-D_k correlation for a large number of gases in a 2.6 nm silica mesopore and a 4 nm carbon mesopore,[192] obtained using the Oscillator model with the solid–fluid interaction potential in eqn (5). It is clear that KD_o and D_k exhibit an approximately linear relationship for a wide range of conditions. Moreover, the results collapse into a single almost-linear correlation covering all gases, except for the more strongly adsorbed ones at low temperatures. The points in the ellipses correspond to data for which adsorption effects are so strong that the linear trend is lost. From these plots, it is clear why the Knudsen equation has appeared so successful in correlating experimental data.[85,86,100] In all cases a small but systematic deviation from linearity is observed, and such deviation is commonly overlooked as experimental error. The strong curvature in the low temperature data for several gases is similar to that observed in the literature, where such points are generally ruled out from the linear regression. It must be noted however that the slope is not unity; for the linear fitting in Fig. 21a the slope is 0.53, while in Fig. 21b it is 0.58. Therefore, the corresponding tortuosity will be overestimated by a factor of 1.88 for the silica and 1.72 for the carbon, explaining the overestimation of tortuosity when using the Knudsen model (*e.g.* Markovic *et al.*[86]). Bhatia and Nicholson[192] have shown that a similar explanation exists for the apparent success of the Knudsen correlation in the study of Gruener and Huber[194] on the transport of He and Ar in a silicon nanochannel, and that the reported 30% overestimation of the measured value of D_k by eqn (1) is consistent with the slope of the KD_o-D_k correlation for the 12 nm silicon nanochannel used.

4.3 Transport at finite density—the distributed friction approach

The difficulty of treating the many-body system while considering the non-uniformity inherent to fluids in nanopores has posed a significant challenge to statistical mechanicians, and a rigorous but tractable theory has proved elusive. In the pursuit of tractability the microscopic momentum balance in eqn (43), based on the classic Bearman–Kirkwood[120] formulation for bulk fluids, would appear to be a good starting point; although strictly speaking it loses rigor for strongly inhomogeneous systems where the length scale of density variations is comparable to the molecular size. A second, more vexing, issue

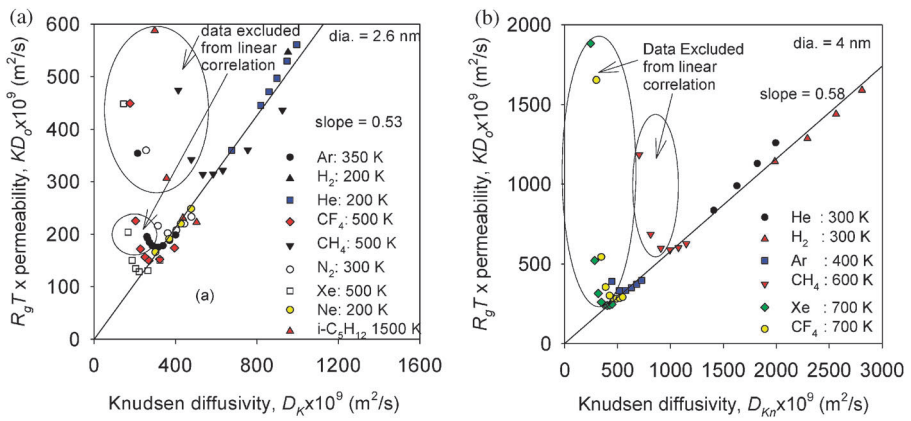

Fig. 21 Correlation of the value of KD_o as predicted using the Oscillator model with the Knudsen diffusivity, D_k, for diffusion of various gases in a (a) silica nanopore of diameter 2.6 nm, and a (b) carbon nanopore of diameter 4.0 nm. Data within the ellipses is not considered in the linear correlation. The temperature in the legend for any gas represents the minimum temperature for which the data for that gas is considered in the correlation. i-C_5H_{12} represents neopentane. From Bhatia and Nicholson.[192]

is that of a local constitutive model for the shear stress, as the usual choice of a Newtonian shear stress model, as in eqn (46) would also appear to be inaccurate in the presence of non-uniformity.[195] It has since been questioned based on results of molecular dynamics simulations in the presence of inhomgeneity[196] and strong variations in strain rate,[197] and instead a nonlocal linear constitutive expression, based on generalized hydrodynamics, has been suggested.[196,197] However, an expression for the nonlocal viscosity kernel based on molecular parameters is still awaited, and thus such a model has not been possible in a predictive approach. An alternate formulation, which allows for inhomogeneity, albeit retaining the Newtonian expression, is the locally averaged density model (LADM) of Bitsanis *et al.*,[198,199] in which the viscosity is estimated at a coarse-grained density locally averaged over a sphere of molecular dimensions, following

$$\tilde{\rho}_i(\mathbf{r}) = \frac{6}{\pi\sigma_{\mathrm{ff},i}^3}\int_{|\mathbf{r}'|<1/2\sigma_{\mathrm{ff},i}} \rho_i(\mathbf{r}+\mathbf{r}')d\mathbf{r}' \qquad (87)$$

This provides a nonlocal viscosity, which was found to accurately explain the couette flow MD simulations of Bitsanis *et al.*,[198,199] although it loses accuracy for very strongly inhomogeneous systems such as nanoscale films.[200] The approach of evaluating the viscosity at a locally smoothed density has found independent support.[146,147] Bitsanis *et al.*[198] also recommend the use of the locally averaged density in eqn (87) for diffusion coefficients, and this allows eqn (59) to overcome the issue of its validity in inhomogeneous systems (except for the very strongly non-uniform systems in which the inaccuracy observed by Bitsanis *et al.*[200] remains).

Besides the issue of treating inhomogeneity, any successful approach for transport at non-zero density based on eqn (43), while considering adsorption, must address the issue of the boundary condition in a manner that permits an accurate low density transport coefficient to be predicted. This becomes somewhat unclear in the absence of a well-defined surface at which molecule–wall reflections occur when soft intermolecular potentials (such as the LJ potential) are used. An initial approach by Bhatia and Nicholson[106,107] for single component transport, while adopting the LADM, arbitrarily considered diffuse reflection at the radial location, $r = r_o$, of the minimum of the fluid solid potential, and the frictional boundary condition

$$\xi_s\rho_o v_o = -\eta\frac{dv}{dz} \text{ at } r = r_o \qquad (88)$$

also used by de Gennes[201] in explaining large slip lengths on surfaces. This approach was heuristically used to extract the friction coefficient by comparison of the transport coefficient obtained upon solution of eqn (43) for a cylindrical capillary with that from MD simulations. While yielding friction coefficients that were only weakly dependent on density, the arbitrary assumption of reflection at the potential minimum location overlooks the penetration of the repulsive region beyond this position when a soft potential is used. A subsequent approach[55,62,108] adopted a DGM type superposition

$$D_o(\bar{\rho}) = D_o^{\mathrm{LD}} + D_{\mathrm{vis}}(\bar{\rho}) \qquad (89)$$

of the Oscillator model low-density transport coefficient with a viscous contribution obtained upon integrating eqn (43) in the core region, $0 < r < r_0$ assuming a no-slip boundary condition at $r = r_0$,

$$D_{\mathrm{vis}}(\bar{\rho}_i) = \frac{2k_BT}{\bar{\rho}r_p^2}\int_0^{r_{0i}}\frac{dr}{r\eta(\bar{\rho}(r))}\left(\int_0^r r'\rho(r)dr'\right)^2 \qquad (90)$$

Reasonably good agreement of single component transport coefficients with MD results was obtained; however, the arbitrary assignment of the viscous region to $0 < r < r_0$ poses difficulties in extending to mixtures, in which the location of the minimum of the fluid–solid interaction potential will be different for each species.

All of the above problems have been overcome in a recent modification of eqn (43) to not only incorporate the LADM with a Newtonian shear stress model, but also a distributed friction coefficient, leading to the equation of change for species *i*,[56,57]

$$\frac{1}{r}\frac{d}{dr}\left(r\eta_i(\tilde{\rho}_1(r),\tilde{\rho}_2(r),\ldots)\frac{dv_i}{dz}\right) = \rho_i(r)\frac{d\mu}{dz} + \rho_t(r)k_BT \times\sum_{j=1}^{n}\frac{x_ix_j(v_i-v_j)}{D_{ij}(\tilde{\rho}_1(r),\tilde{\rho}_2(r),\ldots)} + \xi_i\rho_i(r)a(r-r_{oi}) \qquad (91)$$

in which ξ_i is a uniformly distributed wall friction coefficient for species *i*, such that the last term on the right hand side of eqn (91) represents the rate of momentum loss due to molecule wall collisions in the repulsive region of the fluid–solid interaction potential, $r_{oi} < r < r_p$, where r_{oi} represents the location of the minimum of the fluid solid potential for species *i*, and $a(r - r_{oi})$ is the Heaviside function having the value of unity for $r > r_{oi}$ and zero otherwise. Fig. 22 illustrates this zone of friction in the steep repulsive region beyond the potential minimum location, in which molecules of different energy reflect at different positions, losing some or all of their axial momentum. Bhatia and Nicholson[57] showed that the species partial viscosity, η_i, must be related to the mixture viscosity, η, by $\eta_i = \omega_i\eta$, since the sum of the shear stresses on the different components must match the total shear stress on the mixture. This overcame a difficulty with the Bearman–Kirkwood equations that had persisted since their formulation in 1958,

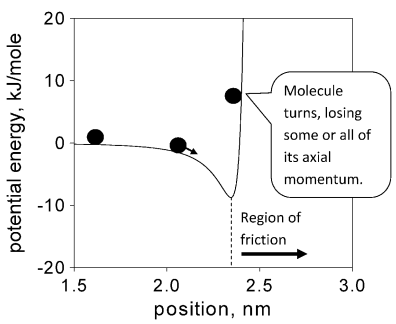

Fig. 22 Illustration of potential energy profile and region of friction corresponding to the repulsive part of the potential energy curve. From Bhatia and Nicholson.[56]

in which no simple prescription existed for the specification of this partial viscosity.

As has been discussed earlier with reference to Fig. 7, the density profiles during transport essentially match those at equilibrium, and can be determined by density functional theory or Monte Carlo simulation. Eqn (91) then represents a coupled boundary value problem for the streaming velocity profiles, $v_i(r)$, with boundary conditions $dv_i/dr = 0$ at $r = 0$ and $r = r_p$. The first of these represents the usual symmetry condition, while the second reflects the fact that at the centerline of the solid surface, *i.e.* at $r = r_p$, the fluid density and hence shear stress must decay to zero. Solution of eqn (91) was performed by converting it into an integral equation that was solved by a Picard iteration method. Since cross-sectional equilibrium essentially prevails during transport,[55,106] the axial chemical potential gradients $d\mu_i/dz$ are kept radially uniform during the integrations, as opposed to the usual practice of integrating the Navier–Stokes equation with a uniform pressure gradient over the cross-section. The latter, while approximately valid for a large pore where the density nonuniformity is confined to a relatively narrow region near the surface, violates the Gibbs–Duhem equation for nanopores where the length scale of the nonuniformity is comparable to the pore size.[55]

A convenient way to represent the cross-coupling of the different species in a multi-component system is the Onsager formulation of irreversible thermodynamics,[118,202] following

$$J_i = \sum_{j=1}^{n} \Omega_{ij}(-\nabla\mu_j) \qquad (92)$$

Upon expressing the pore flux (*cf.* eqn (24)) in terms of the chemical potential gradients in this way Bhatia and Nicholson[56,57] showed that the Onsager coefficients, Ω_{ij}, for the pore flux could be conveniently obtained from the solution of eqn (91). These coefficients can also be evaluated from EMD simulations through autocorrelation of the streaming velocities, and the Green–Kubo relation[102]

$$\Omega_{ij} = \frac{N_i N_j}{k_B T V} \lim_{x\to\infty} \int_0^x \langle \bar{v}_i(0) \cdot \bar{v}_j(t) \rangle dt \qquad (93)$$

Key to the above frictional model is the expression for the distributed friction coefficient

$$\xi_i = -\frac{k_B T \int_0^{r_p} r e^{-\phi_{fs,i}(r)/k_B T} dr}{D_{oi}^{LD} \int_{r_{oi}}^{r_p} r e^{-\phi_{fs,i}(r)/k_B T} dr} \qquad (94)$$

obtained upon matching the low density solution of eqn (91) with the Oscillator model.[56,57] This permits evaluation of the friction coefficients based on intermolecular interaction parameters, and makes the model fully predictive. It is also necessary to use suitable theories or correlations expressing the bulk mixture viscosity and the binary (*i.e.* mutual) diffusivities in terms of the species densities and molecular properties, which may be combined with the LADM for the inhomogeneous pore fluid. A number of such correlations, specifically developed for LJ as well as molecular fluids are available in the literature.[203–208]

An assumption in this friction-based approach is that the friction coefficient, ξ_i, is density and position independent. Although, in principle, ξ_i will be affected by intermolecular interactions and therefore vary with density and position, the success of the predictions of pure component transport coefficients, and binary Onsager coefficients, discussed below, suggests that this is a secondary effect, which is overshadowed by the wall repulsion. Thus, Bhatia and Nicholson[56,57] showed that the isothermal friction coefficient has a weak minimum value at the diameter corresponding to levitation, at which the low pressure transport coefficient has a local maximum value. They also showed that the friction coefficient has a strong minimum with respect to temperature, at about 300 K for CH_4 and 130–140 K for H_2, in silica mesopores, suggesting optimal temperatures are possible in nanofluidic operations.

4.3.1 Comparison with MD simulations. Fig. 23[56,57] depicts the comparison of the density dependence of the transport coefficients for H_2 and CH_4 at 300 K in MCM-41 silica pores of various diameter, as predicted by this new frictional approach, with that from MD simulations and from the superposition approximation in eqn (90). The frictional approach performs somewhat better than the approximation in eqn (89), capturing the decrease in diffusivity with increase in density in the small

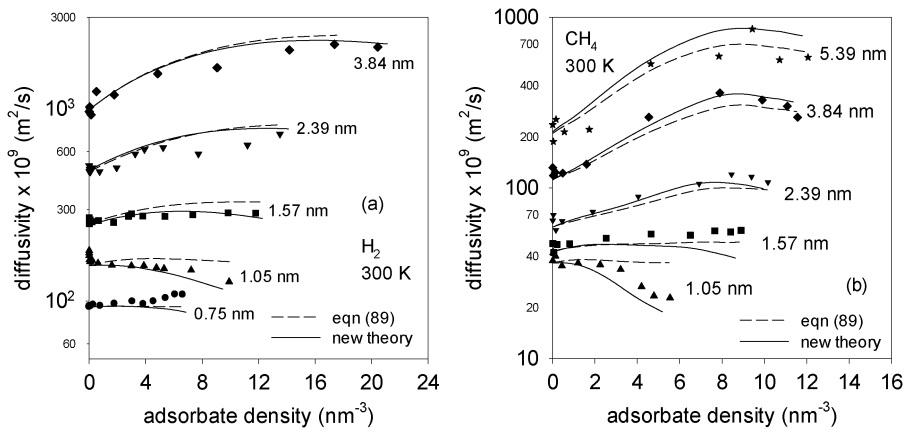

Fig. 23 Variation of transport coefficient with density at 300 K for (a) hydrogen, and (b) CH_4 in MCM-41 silica pores of various diameters. Symbols correspond to EMD simulation results, and lines to theory. From Bhatia and Nicholson.[56]

pore size of 1.05 nm. This decrease originates from an increased collision frequency and consequent momentum loss arising from the presence of only one statistical monolayer on the cylindrical pore surface at this pore size. It must be noted that, at this level of confinement, the adsorbate is not truly a 3-D fluid and the bulk fluid-based viscosity is strictly no longer appropriate. This explains the slight underprediction of the diffusivity, even when the locally-averaged densities are used. In this sense, the distributed friction model is more suitable for transport in pores larger than those where only one monolayer can be fitted (*i.e.* larger than 1.05 nm for CH_4). In such larger pores the intermolecular interactions can be described reasonably well, since the bulk viscosity is meaningful when momentum can be exchanged in all three dimensions between fluid molecules. For smaller pores the Oscillator model with the modified potential in eqn (84) and (85) is more appropriate, and is recommended.

Fig. 24[56] depicts the variation of the Onsager coefficients with methane density for a CH_4/H_2 mixture, in cylindrical silica pores of diameter 1.57 nm and 3.84 nm at 300 K for an adsorbed H_2 density of 1 nm^{-3}, calculated by means of the distributed friction model and by EMD simulations. Despite the widely different mobilities of H_2 and CH_4, the agreement of the model with simulation is excellent when the density distribution is accounted for (Fig. 24a and b), with the Onsager coefficients spanning three decades in magnitude. On the other hand, when the cross-section averaged density was employed instead of the density profile, considerable deviations were observed with respect to the EMD results (Fig. 24c and d), particularly for the more strongly inhomogeneous fluid of the narrower 1.57 nm pore, demonstrating the impact of fluid inhomogeneities on the transport behavior. Further, both simulation and theory yield $\Omega_{12} = \Omega_{21}$, as is to be expected based on microscopic reversibility of the cross interactions, indicating internal consistency of the model.

One of the key reasons for the success of the distributed friction model seen above is that it seamlessly integrates within a single theory, the *exact* low density Oscillator model with the viscous flow model which becomes increasingly more accurate at high density. Since viscous flow is vanishingly small at low density, any inaccuracy resulting from using the Newtonian model inherent to the LADM is negligible in this limit. Thus, the approach has the attributes of being accurate at both low and high density, and therefore serves as a good interpolation medium at intermediate densities.

While developed for the diffuse reflection boundary condition, the Oscillator model has been used to interpret MD results of rapid diffusion in carbon nanotubes,[129] using the superposition approach of eqn (90) modified to include the Smoluchowski factor as in eqn (3),

$$D_o(\bar{\rho}) = \frac{2-\alpha}{\alpha} D_o^{LD} + D_{vis}(\bar{\rho}) \qquad (95)$$

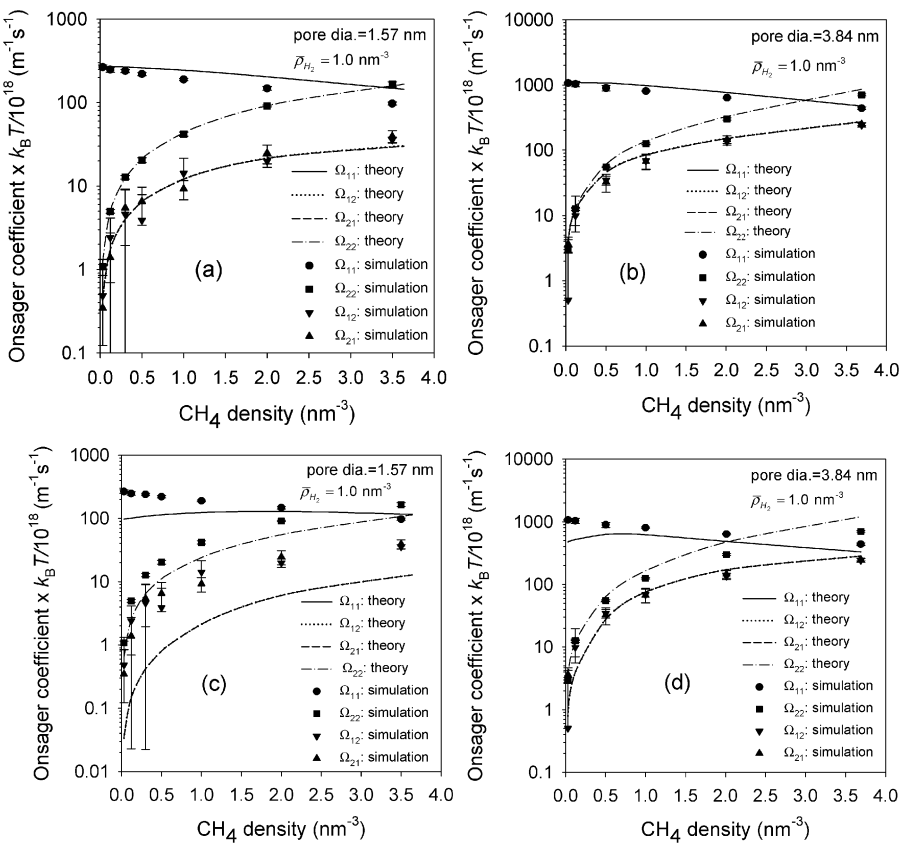

Fig. 24 Variation of the Onsager coefficients with methane density at 300 K and hydrogen density of 1.0 nm^{-3} in cylindrical silica pore of diameter (a) 1.57 nm, and (b) 3.84 nm. (c) and (d) depict the results when the densities are assumed uniform in the theory. From Bhatia and Nicholson.[56]

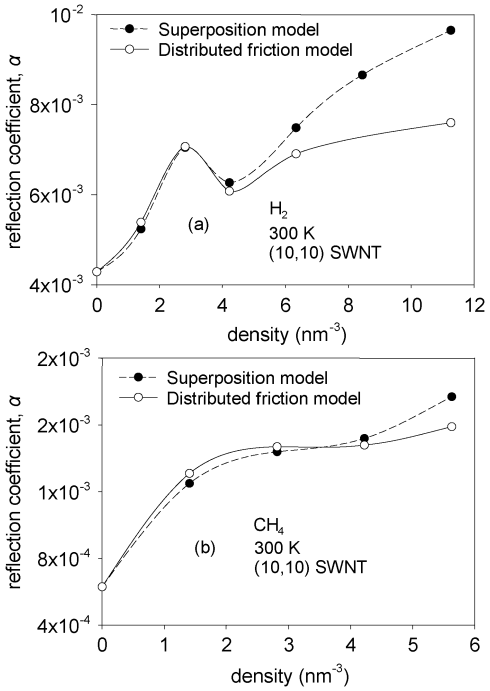

Fig. 25 Variation of momentum accommodation coefficient for (a) H_2, and (b) CH_4 in a (10,10) single wall carbon nanotube at 300 K.

The estimated momentum accommodation coefficients for H_2 and CH_4 in a (10,10) single wall carbon nanotube (SWNT) at 300 K were in line with those directly estimated by NEMD,[68] and were of the order of 10^{-3}, indicating a very smooth energetic landscape consistent with prior observations of Skoulidas *et al.*[69] These accommodation coefficients showed an increase with increase in density, suggesting that interaction of reflecting molecules with other molecules localized near the pore wall contributed to an apparent roughening of the surface. The reflection coefficient for H_2 was 5–7 times that of CH_4, showing that the smaller H_2 is more sensitive to the texture of the carbon surface, on which the inter-atomic spacing of the carbon of 0.142 nm is significantly smaller than the van der Waals size of about 0.29 nm for H_2 and 0.38 nm for CH_4. It is this tight packing of the covalently bonded carbons of the SWNT that leads to its apparent relatively smooth surface to the approaching molecules. Fig. 25 depicts the variation of the reflection coefficient for H_2 and CH_4 with density estimated earlier[129] and that obtained from the same MD data using the distributed friction model with the Smoluchowski correction incorporated in the low density transport coefficient in eqn (95). The distributed friction model leads to a much smaller variation of the accommodation coefficient with density after an initial increase, suggesting that the pure component accommodation coefficients may be used in modeling mixture transport. However, this has yet to be tested against MD simulation results for mixtures.

4.3.2 Comparison with generalised Maxwell–Stefan approach.

In the generalized Maxwell–Stefan approach of Krishna and co-workers,[48–50] viscous effects are treated as unimportant under high level of confinement, or are indirectly considered through the pure component transport coefficients which also carry information on the effects of adsorption fields and the resulting inhomogeneity. However, the accuracy of representing such effects on the mixture through pure component data alone may not necessarily be adequate for systems in which the different components have widely differing adsorption properties and mobilities.

Critical to the MS formulation is the recipe for the estimation of the binary diffusivities, $Đ^s_{ij}$, which has taken on several variations, discussed in Section 4.1. Most recently, Krishna and van Baten[110] have applied the MS approach to silica mesopores, taking the binary diffusivity to be the bulk fluid diffusivity following Bhatia and Nicholson.[56,57] Subsequently, a unified approach for application to any pore sizes has been proposed[109] in which this binary diffusivity is taken as a certain multiple, F, of the bulk fluid value. Based on MD simulations of CH_4–Ar and Ne–Ar mixtures in a variety of zeolites and metal–organic framework (MOF) materials, this factor, F, is empirically correlated with the degree of confinement, defined as the ratio of the binary LJ parameter σ_{ij} (arithmetic average of the σ values of i and j) to the channel dimension. Fig. 26[109] depicts this correlation, in which F is taken to be unity below a degree of confinement of about 0.2. However, significant outliers are observed, with the points within the ellipse termed as "rogue" behavior, obtained for zeolites LTA, CHA and DDR, underscoring the issue of uncertainty in specifying the binary diffusivity.

A comparison of the prediction of binary transport coefficients with MD results and the predictions of the distributed friction model of Bhatia and Nicholson,[56,57] depicted in Fig. 27, illustrates the complexity of the above issues. This figure shows the variation of the Onsager coefficients with CH_4 density for a H_2–CH_4 mixture in silica pores of 1.57 nm and 3.84 nm at H_2 densities of 1.0 nm^{-3} and 0.25 nm^{-3} at 300 K, respectively, for which the MD results and distributed friction model predictions were provided in Bhatia and Nicholson.[57] The distributed friction model (black lines) used the binary diffusivities obtained from the LJ fluid correlation of Reis *et al.*[207] based on fits of bulk MD data, and is seen to match the MD results very well. At the level of confinement of either

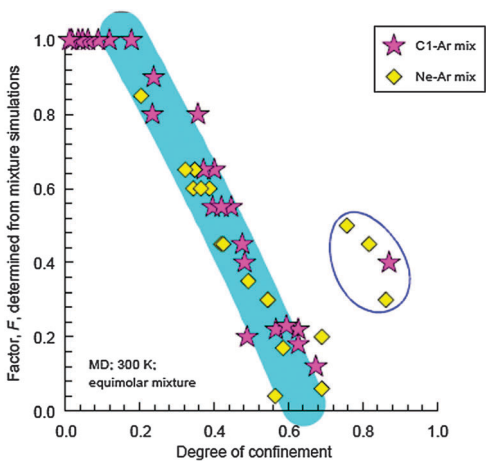

Fig. 26 Variation of factor F with degree of confinement. From Krishna and van Baten.[109]

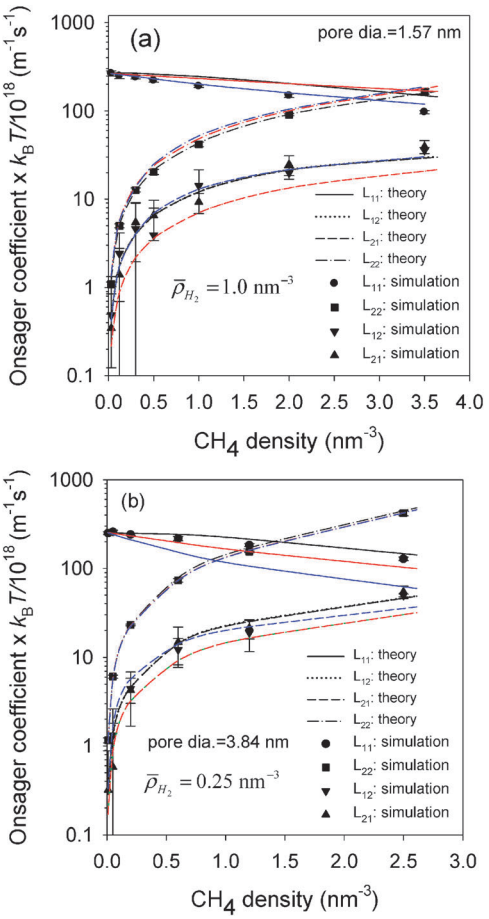

Fig. 27 Comparison of predictions of distributed friction-based model and generalised Maxwell–Stefan approach for variation of Onsager coefficients with CH_4 density, for (a) H_2 density of 1.0 nm^{-3} in pore of diameter 1.57 nm, and (b) H_2 density of 0.25 nm^{-3} in pore of diameter 3.84 nm. Symbols correspond to MD results, black lines to friction model and red lines to MS model. Blue lines correspond to MS model results when the binary diffusivity is taken to be half its true value.

pore size, the factor, F, is expected to be unity based on Fig. 26. However, when the MS model is used with bulk binary diffusivity evaluated at the overall pore densities of the components, as given by the Reis *et al*. correlation, it is found to severely underpredict the values of the Onsager cross parameter Ω_{12} in both cases (red lines). In the case of the 1.57 nm pore good agreement with MD is obtained when F is taken as 0.5 (blue lines), while use of this factor for the 3.84 nm pore leads to some improvement of the predictions of the MS model for the Onsager cross-parameter but deterioration of the prediction for Ω_{11}. Thus the factor F is not necessarily unity even for mesopores with low degree of confinement, and the case considered here, involving H_2 and CH_4, which have widely different molecular weights and mobilities as well as adsorption strengths, would also be classified as "rogue" behavior. Such deviation is most likely a result of confining all inhomogeneities and viscous effects in the pure component transport coefficients, which breaks down when the different components are significantly dissimilar in properties.

5. Concluding remarks and outlook

For over a century the Knudsen model has established itself as a key tool in our craft for the modelling of transport in narrow pores and confined spaces. However, with the emergence of molecular dynamics it is now possible to test theoretical approaches for transport, and an overwhelming body of evidence indicates that the Knudsen theory overestimates low pressure diffusivities. The principal source of the overprediction is the neglect of adsorptive fluid–solid interactions, which lead to deviation from the rectilinear trajectories of molecules that occur under the hard sphere interaction hypothesis inherent to the Knudsen theory. Although the literature is replete with apparently successful correlation of experimental diffusivities with $\sqrt{T/M}$ this is not an indication of validity of the Knudsen model. Such correlation is to be expected even under conditions involving some adsorption, because experimental diffusivities are invariably based on permeability-related measurements. Thus, when diffusivities are determined with adsorption neglected, they are really estimates of KD_o, and this quantity is found to correlate linearly with $\sqrt{T/M}$ except when adsorption is strong. The incorrect use of this correlation leads to high tortuosities in disordered solids, which vary with adsorptive gas and temperature, and are not a material property as is universally assumed. This deficiency arising from neglect of the adsorptive fluid–solid force field is inherited by the widely used Dusty gas model, which utilizes the Knudsen theory in modeling the momentum loss of fluid molecules on wall collision. In addition, the DGM suffers from internal theoretical inconsistencies arising from conflicting choices of frames of reference at different stages of its derivation.

More modern theories such as the generalized Maxwell–Stefan approach of Krishna and co-workers, and the statistical mechanics-based Oscillator model of Bhatia and co-workers combined with their distributed friction approach, offer more promising techniques that incorporate the effect of adsorption in a natural and rigorous way. Nevertheless, the MS-based approach has considerable uncertainty in the way binary mixture diffusivities, to which the results are highly sensitive, are specified. Attempts to relate these to pure component diffusivities at infinite dilution, as has been the method of choice, create inconsistencies with irreversible thermodynamics principles, in which the degrees of freedom are precisely specified and the binary diffusivities are to be independently determined based on cross-interactions. The distributed friction based model of Bhatia and Nicholson, while tested for LJ fluids, is extendable to more complex fluids if the low density diffusivities required for estimating the friction coefficient are available from MD simulations or from experiment. For LJ fluids they can be obtained from the exact Oscillator model, with the Smoluchowski correction used to incorporate non-diffuse reflection.

In recent years computing speeds have increased many-fold, and MD simulations for nanopores and mesopores are now possible with modest computing times (10–24 h even without the use of supercomputing facilities) for simple systems. However, theoretical calculations for such systems are orders of magnitude faster in execution (a few minutes), without sacrificing accuracy, and can be used predictively. Thus, they are much more readily integrated into process design practice,

and will remain the main option for routine use, and in applications, for some time.

Although our ability to model transport in nanoscale confinement in a tractable manner has seen major advances in recent years, significant difficulties remain that need to be addressed. Among these is the development of a suitable constitutive model for the shear stress that is applicable at the nanoscale, as the use of a Newtonian model, albeit considering inhomogeneity through the LADM, may not be appropriate at large Knudsen numbers. A similar development with respect to the binary diffusivities is also needed, to provide further advances over the existing methodology using the LADM with the distributed friction based model. Such developments will increase the predictive power and accuracy of this model for pores where only a monolayer or less can be accommodated. While the extension of the Oscillator model as discussed in Section 4.2.3 addresses the modeling for such pores, its adaptation for mixtures is not straightforward, as the concept of periodic motion of second nearest neighbors inherent to this development cannot be directly translated to this case.

As developed, the Oscillator model is valid for simple molecules that can be reasonably modeled as spherical LJ particles. While the theory can in principle be extended for more complex molecules, the additional degrees of freedom that would need to be considered will make the theory computationally impractical if not intractable. The estimation of the friction factor in the distributed friction approach, which is currently based on the Oscillator model, must therefore be done from alternate estimates of the low density transport coefficient, such as from MD simulations. However, this adaptation of the friction-based approach needs to be tested. Such adaptation must also move away from the diffuse reflection condition, which is ill-defined for non-spherical molecules. The application of the approach for non-spherical molecules and atomistic as well as rough surfaces must be therefore simultaneously addressed in the next stage of development of the approach.

Moving beyond the single pore level to that of a realistic material with a disordered structure will also require much further development, particularly for mixtures. Even with the obvious drawback of an idealized structure such as that of cylindrical or slit-like pores, the treatment of mixture transport in networks requires theoretical advances, as existing approaches[209,210] based on the effective medium theory are only applicable for non-adsorbing conditions in which the model equations can be cast in a form in which pore size and density are decoupled. Work is already underway in our laboratory extending the EMT–CRWT approach of eqn (10)–(12) to multi-component transport, and will be reported in due course.

Acknowledgements

We are grateful to the Australian Research council for support of our research, through a series of grants under the Discovery scheme. One of us (SKB) acknowledges an Australian Professorial Fellowship from the Australian Researches Council. We thank the High Performance Computing Unit of the University of Queensland, for access to supercomputing facilities.

References

1 W. Y. Zhou, X. D. Bai, E. G. Wang and S. S. Xie, *Adv. Mater.*, 2009, **21**, 4565–4583.
2 E. T. Thostenson, Z. F. Ren and T. W. Chou, *Compos. Sci. Technol.*, 2001, **61**, 1899–1912.
3 N. L. Rosi, J. Eckert, M. Eddaoudi, D. T. Vodak, J. Kim, M. O'Keeffe and O. M. Yaghi, *Science*, 2003, **300**, 1127–1129.
4 H. Furukawa, N. Ko, Y. B. Go, N. Aratani, S. B. Choi, E. Choi, A. O. Yazaydin, R. Q. Snurr, M. O'Keeffe, J. Kim and O. M. Yaghi, *Science*, 2010, **329**, 424–428.
5 V. I. Isaeva and L. M. Kustov, *Pet. Chem.*, 2010, **50**, 167–180.
6 C. T. Kresge, M. E. Leonowicz, W. J. Roth, J. C. Vartuli and J. S. Beck, *Nature*, 1992, **359**, 710–712.
7 H.-P. Lin, Y.-R. Cheng, C.-R. Lin, F.-Y. L. Li, C.-L. Chen, S.-T. Wong, S.-F. Cheng, S.-B. Liu, B.-Z. Wan, C.-Y. Mou, C.-Y. Tang and C.-Y. Lin, *J. Chin. Chem. Soc.*, 1999, **46**, 495–507.
8 P. Selvam, S. K. Bhatia and C. G. Sonwane, *Ind. Eng. Chem. Res.*, 2001, **40**, 3237–3261.
9 M. E. Davis, *Nature*, 2002, **417**, 813–821.
10 P. Kumar and V. V. Guliants, *Microporous Mesoporous Mater.*, 2010, **132**, 1–14.
11 T. Tomita, K. Nakayama and H. Sakai, *Microporous Mesoporous Mater.*, 2004, **68**, 71–75.
12 E. E. McLeary, J. C. Jansen and F. Kapteijn, *Microporous Mesoporous Mater.*, 2006, **90**, 198–220.
13 M. U. Niemann, S. S. Srinivasan, A. R. Phani, A. Kumar, D. Y. Goswami and E. K. Stefanakos, *J. Nanomater.*, **2008**, 950967.
14 S. K. Bhatia and A. L. Myers, *Langmuir*, 2006, **22**, 1688–1700.
15 B. Conway, *Electrochemical Supercapacitors: Scientific Fundamentals and Technological Applications*, Plenum Press, New York, 1999.
16 A. D. Sheehan, J. Quinn, S. Daly, P. Dillon and R. O'Kennedy, *Anal. Lett.*, 2003, **36**, 511–537.
17 J. C. T. Eijkel and A. van den Berg, *Microfluid. Nanofluid.*, 2005, **1**, 249–267.
18 S. G. Li, Z. G. Xu, A. Mazzeo, D. J. Burns, G. Fu, M. Dirckx, V. Shilpiekandula, X. Chen, N. C. Nayak, E. Wong, S. F. Yoon, Z. P. Fang, K. Youcef-Toumi, D. Hardt, S. B. Tor, C. Y. Yue and J. H. Chun, in *Mems, Moems, and Micromaching III*, ed. H. Urey, Spie-Int Soc Optical Engineering, Bellingham, 2008, vol. 6993, pp. F9930.
19 M. Knudsen, *Ann. Phys.*, 1909, **333**, 75–130.
20 M. Knudsen and W. J. Fisher, *Phys. Rev.*, 1910, **31**, 586–588.
21 M. Knudsen, *Ann. Phys.*, 1915, **351**, 641–656.
22 M. Knudsen, *Ann. Phys.*, 1915, **352**, 697–708.
23 M. Knudsen, *Ann. Phys.*, 1916, **355**, 472–488.
24 M. v. Smoluchowski, *Ann. Phys.*, 1910, **338**, 1559–1570.
25 M. v. Smoluchowski, *Ann. Phys. (Leipzig)*, 1911, **4**, 983–1004.
26 W. G. Pollard and R. D. Present, *Phys. Rev.*, 1948, **73**, 762.
27 R. B. Evans, G. M. Watson and E. A. Mason, *J. Chem. Phys.*, 1961, **35**, 2076–2083.
28 R. B. Evans, G. M. Watson and E. A. Mason, *J. Chem. Phys.*, 1962, **36**, 1894–1902.
29 E. A. Mason, R. B. Evans and G. M. Watson, *J. Chem. Phys.*, 1963, **38**, 1808–1826.
30 S. Chapman and T. G. Cowling, *Mathematical Theory of Non-Uniform Gases*, Cambridge University Press, Cambridge, 1939.
31 E. A. Mason, A. P. Malinauskas and R. B. Evans, *J. Chem. Phys.*, 1967, **46**, 3199–3216.
32 E. A. Mason and A. P. Malinauskas, *Gas Transport in Porous Media: The Dusty-Gas Model*, Elsevier Scientific Pub. Co., Amsterdam, 1983.
33 E. A. Mason and L. F. del Castillo, *J. Membr. Sci.*, 1985, **23**, 199–220.
34 R. Jackson, *Transport in Porous Catalysts*, Elsevier Sicentific Pub Co, Amsterdam, 1977.
35 R. E. Cunningham and R. J. J. Williams, *Diffusion in Gases and Porous Media*, Plenum Press, New York, 1980.
36 P. J. A. M. Kerkhof, M. A. M. Geboers and K. J. Ptasinski, *Chem. Eng. J.*, 2001, **83**, 107–121.
37 J. B. Young and B. Todd, *Int. J. Heat Mass Transf.*, 2005, **48**, 5338–5353.

38 J. Kärger and D. M. Ruthven, *Diffusion in Zeolites and Other Microporous Solids*, John Wiley and sons Inc., New York, 1992.
39 J. R. Xiao and J. Wei, *Chem. Eng. Sci.*, 1992, **47**, 1123–1141.
40 H. T. Davis, in *Fundamentals of inhomogeneous fluids*, ed. D. Henderson, Marcel Dekker, New York, 1992.
41 L. A. Pozhar and K. E. Gubbins, *Int. J. Thermophys.*, 1999, **20**, 805–813.
42 J. M. D. MacElroy, L. A. Pozhar and S. H. Suh, *Colloids Surf., A: Physicochemical and Engineering Aspects*, 2001, **187**, 493–507.
43 E. N. Lightfoot, *Transport in Living Systems*, Wiley, New York, 1974.
44 P. J. A. M. Kerkhof, *Chem. Eng. J. Biochem. Eng. J.*, 1996, **64**, 319–343.
45 E. Wicke and R. Kallenbach, *Kolloid-Z.*, 1941, **97**, 135–151.
46 R. M. Barrer and J. A. Barrie, *Proc. R. Soc. London, Ser. A*, 1952, **213**, 250–265.
47 R. Ash, R. W. Baker and R. M. Barrer, *Proc. R. Soc. London, Ser. A*, 1967, **299**, 434.
48 R. Krishna, *Chem. Eng. Sci.*, 1990, **45**, 1779–1791.
49 R. Krishna, *Chem. Eng. Sci.*, 1993, **48**, 845–861.
50 R. Krishna and J. A. Wesselingh, *Chem. Eng. Sci.*, 1997, **52**, 861–911.
51 J. H. Yang, J. Cermakova, P. Uchytil, C. Hamel and A. Seidel-Morgenstern, *Catal. Today*, 2005, **104**, 344–351.
52 M. P. Allen and D. J. Tildesley, *Computer simulation of liquids*, Oxford University Press, New York, 1987.
53 D. Frenkel and B. Smit, *Understanding Molecular Simulation: From Algorithms to Applications*, Academic Press, San Diego, 2nd edn, 2002.
54 O. G. Jepps, S. K. Bhatia and D. J. Searles, *Phys. Rev. Lett.*, 2003, **91**, 126102.
55 S. K. Bhatia, O. Jepps and D. Nicholson, *J. Chem. Phys.*, 2004, **120**, 4472–4485.
56 S. K. Bhatia and D. Nicholson, *J. Chem. Phys.*, 2008, **129**, 164709–164712.
57 S. K. Bhatia and D. Nicholson, *Phys. Rev. Lett.*, 2008, **100**, 236103.
58 P. J. A. M. Kerkhof and M. A. M. Geboers, *Chem. Eng. Sci.*, 2005, **60**, 3129–3167.
59 D. A. McQuarrie, *Statistical Mechanics*, University Science, Sausalito CA, 2000.
60 T. J. Grey, K. P. Travis, J. D. Gale and D. Nicholson, *Microporous Mesoporous Mater.*, 2001, **48**, 203–209.
61 J. M. D. MacElroy and S. H. Suh, *Microporous Mesoporous Mater.*, 2001, **48**, 195–202.
62 O. G. Jepps, S. K. Bhatia and D. J. Searles, *J. Chem. Phys.*, 2004, **120**, 5396–5406.
63 L. P. Ding and S. K. Bhatia, *AIChE J.*, 2003, **49**, 883–895.
64 X. J. Hu, S. Z. Qiao and D. D. Do, *Langmuir*, 1999, **15**, 6428–6437.
65 S. K. Bhatia, *Langmuir*, 2010, **26**, 8373–8385.
66 A. I. Skoulidas and D. S. Sholl, *J. Phys. Chem. A*, 2003, **107**, 10132–10141.
67 V. P. Sokhan, D. Nicholson and N. Quirke, *J. Chem. Phys.*, 2001, **115**, 3878–3887.
68 V. P. Sokhan, D. Nicholson and N. Quirke, *J. Chem. Phys.*, 2002, **117**, 8531–8539.
69 A. I. Skoulidas, D. M. Ackerman, J. K. Johnson and D. S. Sholl, *Phys. Rev. Lett.*, 2002, **89**, 185901.
70 J. C. Maxwell, *Philos. Trans. R. Soc. London*, 1879, **170**, 231–256.
71 G. Arya, H.-C. Chang and E. J. Maginn, *Phys. Rev. Lett.*, 2003, **91**, 026102.
72 J. W. Hiby and M. Pahl, *Z. Naturforsch., A: Phys. Sci.*, 1952, **7**, 533–541.
73 W. Gaede, *Ann. Phys.*, 1913, **346**, 337–380.
74 W. Gaede, *Ann. Phys.*, 1913, **346**, 289–336.
75 W. Gaede, *Ann. Phys.*, 1915, **351**, 357–392.
76 I. Langmuir, *Phys. Rev.*, 1916, **8**, 48.
77 L. Dunoyer, *Adv. Vac. Sci. Technol.*, 1960, **1**, 9–13.
78 R. G. Christian and J. H. Leck, *Vacuum*, 1966, **16**, 299–304.
79 E. B. Maxted, *J. Soc. Chem. Ind., London*, 1926, **45**, 323.
80 C. G. Sonwane and S. K. Bhatia, *Langmuir*, 1999, **15**, 2809–2816.
81 G. J. Tjatjopoulos, D. L. Feke and J. A. Mann, *J. Phys. Chem. A*, 1988, **92**, 4006–4007.
82 A. V. Neimark, P. I. Ravikovitch, M. Grün, F. Schüth and K. K. Unger, *J. Colloid Interface Sci.*, 1998, **207**, 159–169.
83 T. X. Nguyen, J. S. Bae, Y. Wang and S. K. Bhatia, *Langmuir*, 2009, **25**, 4314–4319.
84 W. A. Steele, *The Interaction of Gases with Solid Surfaces*, Pergamon, Oxford, 1974.
85 S. Higgins, W. DeSisto and D. Ruthven, *Microporous Mesoporous Mater.*, 2009, **117**, 268–277.
86 A. Markovic, D. Stoltenberg, D. Enke, E. U. Schlünder and A. Seidel-Morgenstern, *J. Membr. Sci.*, 2009, **336**, 17–31.
87 S. Z. Qiao and S. K. Bhatia, *Microporous Mesoporous Mater.*, 2005, **86**, 112–123.
88 S. Z. Qiao and S. K. Bhatia, *Ind. Eng. Chem. Res.*, 2005, **44**, 6477–6484.
89 S. K. Bhatia, *Chem. Eng. Sci.*, 1986, **41**, 1311–1324.
90 Q. Huang, R. Qamar and M. Eić, *Adsorption*, 2010, **17**, 27–38.
91 C. L. Cavalcante, N. M. Silva, E. F. Souza-Aguiar and E. V. Sobrinho, *Adsorption*, 2003, **9**, 205–212.
92 S.-S. Chong, H. Jobic, M. Plazanet and D. S. Sholl, *Chem. Phys. Lett.*, 2005, **408**, 157–161.
93 J. Kärger, C. Chmelik, L. Heinke and R. Valiullin, *Chem. Ing. Tech.*, 2010, **82**, 779–804.
94 H. Jobic, M. Bée and G. J. Kearley, *Zeolites*, 1992, **12**, 146–151.
95 W. Heink, J. Karger, H. Pfeifer, K. P. Datema and A. K. Nowak, *J. Chem. Soc., Faraday Trans.*, 1992, **88**, 3505–3509.
96 S. Kirkpatrick, *Rev. Mod. Phys.*, 1973, **45**, 574–588.
97 P. D. Deepak and S. K. Bhatia, *Chem. Eng. Sci.*, 1994, **49**, 245–257.
98 S. Ismadji and S. K. Bhatia, *Appl. Surf. Sci.*, 2002, **196**, 281–295.
99 H. M. Alsyouri and J. Y. S. Lin, *J. Phys. Chem. B*, 2005, **109**, 13623–13629.
100 D. M. Ruthven, W. J. DeSisto and S. Higgins, *Chem. Eng. Sci.*, 2009, **64**, 3201–3203.
101 S. K. Bhatia and D. Nicholson, *Chem. Eng. Sci.*, 2010, **65**, 4519–4520.
102 *Molecular Simulation of Transport in a Single Micropore*, ed. D. Nicholson and K. Travis, Elsevier, Amsterdam, 2000.
103 D. S. Sholl, *Acc. Chem. Res.*, 2006, **39**, 403–411.
104 D. Dubbeldam and R. Q. Snurr, *Mol. Simul.*, 2007, **33**, 305–325.
105 K. E. Gubbins, Y.-C. Liu, J. D. Moore and J. C. Palmer, *Phys. Chem. Chem. Phys.*, 2011, **13**, 58–85.
106 S. K. Bhatia and D. Nicholson, *Phys. Rev. Lett.*, 2003, **90**, 016105.
107 S. K. Bhatia and D. Nicholson, *J. Chem. Phys.*, 2003, **119**, 1719–1730.
108 S. K. Bhatia and D. Nicholson, *AIChE J.*, 2006, **52**, 29–38.
109 R. Krishna and J. M. van Baten, *Chem. Eng. Sci.*, 2009, **64**, 3159–3178.
110 R. Krishna and J. M. van Baten, *Chem. Eng. Sci.*, 2009, **64**, 870–882.
111 N. E. Fernandes and G. R. Gavalas, *Ind. Eng. Chem. Res.*, 1999, **38**, 723–730.
112 S. Yashonath and P. Santikary, *J. Phys. Chem.*, 1994, **98**, 6368–6376.
113 A. V. Anil Kumar and S. K. Bhatia, *J. Phys. Chem. B*, 2006, **110**, 3109–3113.
114 A. I. Skoulidas and D. S. Sholl, *J. Phys. Chem. B*, 2002, **106**, 5058–5067.
115 J. O. Hirschfelder, C. F. Curtiss and R. B. Bird, *Molecular theory of gases and liquids*, John Wiley, New York, 1954.
116 J. A. Wesselingh and R. Krishna, *Mass Transfer in Multicomponent Mixtures*, Delft University Press, Delft, The Netherlands, 2000.
117 Y. Wang and M. D. LeVan, *J. Phys. Chem. B*, 2008, **112**, 8600–8604.
118 D. Fitts, *Nonequilibrium Thermodynamics: A Phenomenological Theory of Irreversible Processes in Fluid Systems*, McGraw-Hill, New York, 1962.
119 V. Zhdanov, Y. Kagan and A. Sazykin, *Sov. Phys. JETP*, 1962, **15**, 596–602.
120 R. J. Bearman and J. G. Kirkwood, *J. Chem. Phys.*, 1958, **28**, 136–145.
121 F. M. Snell, R. Aranow and R. A. Spangler, *J. Chem. Phys.*, 1967, **47**, 4959–4971.

122 F. M. Snell and R. A. Spangler, *J. Phys. Chem.*, 1967, **71**, 2503–2510.
123 B. K. Annis, *Phys. Fluids*, 1971, **14**, 269–277.
124 R. Datta and S. A. Vilekar, *Chem. Eng. Sci.*, 2010, **65**, 5976–5989.
125 P. J. A. M. Kerkhof and M. A. M. Geboers, *AIChE J.*, 2005, **51**, 79–121.
126 R. B. Bird, W. E. Stewart and E. N. Lightfoot, *Transport Phenomena*, John Wiley & Sons, New York, 1960.
127 J. C. Maxwell, *Philos. Trans. R. Soc. London*, 1879, **170**, 231–256.
128 E. A. Mason and L. A. Viehland, *J. Chem. Phys.*, 1978, **68**, 3562–3573.
129 S. K. Bhatia, H. Chen and D. S. Sholl, *Mol. Simul.*, 2005, **31**, 643–649.
130 E. A. Mason and L. F. Delcastillo, *J. Membr. Sci.*, 1985, **23**, 199–220.
131 V. Hejtmánek, P. Capek, O. Solcová and P. Schneider, *Chem. Eng. J.*, 1998, **70**, 189–195.
132 J.-H. Moon, J.-H. Bae, Y.-S. Bae, J.-T. Chung and C.-H. Lee, *J. Membr. Sci.*, 2008, **318**, 45–55.
133 W. Chang and T. Y. Lee, in *Process Systems Engineering 2003, Pts A and B*, ed. B. Chen and A. W. Westerberg, Elsevier Science Bv, Amsterdam, 2003, vol. 15, pp. 1159–1164.
134 R. S. Todd, P. A. Webley, R. D. Whitley and M. J. Labuda, *Adsorption*, 2005, **11**, 427–432.
135 J. T. F. Keurentjes, A. E. M. Janssen, A. P. Broek, A. Van der Padt, J. A. Wesselingh and K. Van' T. Riet, *Chem. Eng. Sci.*, 1992, **47**, 1963–1971.
136 E. M. Scattergood and E. N. Lightfoot, *Trans. Faraday Soc.*, 1968, **64**, 1135–1146.
137 L. B. Rothfeld, *AIChE J.*, 1963, **9**, 19–24.
138 P. Schneider, *Chem. Eng. Sci.*, 1978, **33**, 1311–1319.
139 P. Kerkhof, M. A. M. Geboers and K. J. Ptasinski, *Chem. Eng. J.*, 2001, **83**, 107–121.
140 V. M. Zhdanov and V. I. Roldughin, *Colloid J.*, 2002, **64**, 1–24.
141 D. Nicholson and J. H. Petropoulos, *Ber. Bunsen-Ges. Phys. Chem. Chem. Phys.*, 1975, **79**, 796–798.
142 D. Nicholson and J. H. Petropoulos, *J. Colloid Interface Sci.*, 1981, **83**, 420–427.
143 D. Nicholson, J. Petrou and J. H. Petropoulos, *J. Colloid Interface Sci.*, 1979, **71**, 570–579.
144 D. Nicholson and J. H. Petropoulos, *J. Colloid Interface Sci.*, 1985, **106**, 538–546.
145 S. T. Hwang and K. Kammermeyer, *Ind. Eng. Chem. Fundam.*, 1968, **7**, 671–672.
146 L. A. Pozhar and K. E. Gubbins, *J. Chem. Phys.*, 1991, **94**, 1367–1384.
147 L. A. Pozhar and K. E. Gubbins, *J. Chem. Phys.*, 1993, **99**, 8970–8996.
148 R. Zwanzig, *Phys. Rev.*, 1961, **124**, 983.
149 H. Mori, *Prog. Theor. Phys.*, 1965, **33**, 423–455.
150 L. A. Pozhar, *Transport Theory of Inhomogeneous Fluids*, World Scientific, Singapore, 1994.
151 E. Akhmatskaya, B. D. Todd, P. J. Daivis, D. J. Evans, K. E. Gubbins and L. A. Pozhar, *J. Chem. Phys.*, 1997, **106**, 4684–4695.
152 Z. Guo, T. S. Zhao and Y. Shi, *Phys. Rev. E: Stat. Phys., Plasmas, Fluids, Relat. Interdiscip. Top.*, 2005, **71**, 035301.
153 Z. Guo, T. S. Zhao, C. Xu and Y. Shi, *Int. J. Comput. Fluid Dyn.*, 2006, **20**, 361–367.
154 U. M. B. Marconi and S. Melchionna, *J. Chem. Phys.*, 2011, **134**, 064118–064115.
155 P. L. Bhatnagar, E. P. Gross and M. Krook, *Phys. Rev.*, 1954, **94**, 511.
156 L. J. P. Van Den Broeke, S. A. Nuhuis and R. Krishna, *J. Catal.*, 1992, **136**, 463–477.
157 E. Tylianakis and G. E. Froudakis, *J. Comput. Theor. Nanosci.*, 2009, **6**, 335–348.
158 R. Krishna, *Chem. Phys. Lett.*, 2002, **355**, 483–489.
159 R. Krishna and R. Baur, *Chem. Eng. J.*, 2004, **97**, 37–45.
160 R. Krishna and J. M. van Baten, *J. Phys. Chem. B*, 2005, **109**, 6386–6396.
161 F. J. Keil, R. Krishna and M. O. Coppens, *Rev. Chem. Eng.*, 2000, **16**, 71–197.
162 A. I. Skoulidas, D. S. Sholl and R. Krishna, *Langmuir*, 2003, **19**, 7977–7988.
163 D. D. Fitts, *Nonequilibrium Thermodynamics: A Phenomenological Theory of Irreversible Processes in Fluid Systems*, McGraw-Hill, New York, 1962.
164 J. Yang, J. Cermáková, P. Uchytil, C. Hamel and A. Seidel-Morgenstern, *Catal. Today*, 2005, **104**, 344–351.
165 M. Hanebuth, R. Dittmeyer, G. T. P. Mabande and W. Schwieger, *Catal. Today*, 2005, **104**, 352–359.
166 A. Tuchlenski, P. Uchytil and A. Seidel-Morgenstern, *J. Membr. Sci.*, 1998, **140**, 165–184.
167 S. K. Bhatia, *Transport of Gases Containing Condensables in Porous Solids*, in *Advances in Transport Processes IX*, ed. A. S. Mujumdar and R. A. Mashelkar, Elsevier, Amsterdam, 1993.
168 R. J. R. Uhlhorn, K. Keizer and A. J. Burggraaf, *J. Membr. Sci.*, 1989, **46**, 225–241.
169 R. Valiullin, P. Kortunov, J. Karger and V. Timoshenko, *J. Chem. Phys.*, 2004, **120**, 11804–11814.
170 M. Dvoyashkin, R. Valiullin, J. Kärger, W.-D. Einicke and R. Gläser, *J. Am. Chem. Soc.*, 2007, **129**, 10344–10345.
171 L. Herrera, C. Fan, D. D. Do and D. Nicholson, A revisit of the Gibbs dividing surfaces and helium adsorption, *Adsorption*, Submitted.
172 F. J. Keil, *J. Univ. Chem. Technol. Metall.*, 2010, **45**, 161–168.
173 A. Argönül and F. J. Keil, *Period. Polytech., Chem. Eng.*, 2008, **52/2**, 37–55.
174 D. Nicholson and S. K. Bhatia, *Mol. Simul.*, 2009, **35**, 109–121.
175 H. B. Chen, J. K. Johnson and D. S. Sholl, *J. Phys. Chem. B*, 2006, **110**, 1971–1975.
176 M. Majumder, N. Chopra, R. Andrews and B. J. Hinds, *Nature*, 2005, **438**, 44–44.
177 M. Whitby and N. Quirke, *Nat. Nanotechnol.*, 2007, **2**, 87–94.
178 T. X. Nguyen, J. S. Bae and S. K. Bhatia, *Langmuir*, 2009, **25**, 2121–2132.
179 J.-S. Bae, T. X. Nguyen and S. K. Bhatia, *J. Phys. Chem. C*, 2009, **114**, 1046–1056.
180 M. R. Bonilla, J. S. Bae, T. X. Nguyen and S. K. Bhatia, *J. Phys. Chem. C*, 2010, **114**, 16562–16575.
181 T. X. Nguyen, S. K. Bhatia, S. K. Jain and K. E. Gubbins, *Mol. Simul.*, 2006, **32**, 567–577.
182 S. K. Jain, R. J. M. Pellenq, J. P. Pikunic and K. E. Gubbins, *Langmuir*, 2006, **22**, 9942–9948.
183 T. X. Nguyen, N. Cohaut, J.-S. Bae and S. K. Bhatia, *Langmuir*, 2008, **24**, 7912–7922.
184 G. Arya, H. C. Chang and E. J. Maginn, *Mol. Simul.*, 2003, **29**, 697–709.
185 E. G. Derouane, J. M. Andre and A. A. Lucas, *J. Catal.*, 1988, **110**, 58–73.
186 A. V. A. Kumar and S. Yashonath, *J. Phys. Chem. B*, 2000, **104**, 9126–9130.
187 S. Y. Bhide and S. Yashonath, *J. Am. Chem. Soc.*, 2003, **125**, 7425–7434.
188 B. J. Borah, H. Jobic and S. Yashonath, *J. Chem. Phys.*, 2010, **132**, 144507.
189 S. K. Bhatia and D. Nicholson, *J. Chem. Phys.*, 2007, **127**, 124701.
190 S. K. Bhatia, *Langmuir*, 1998, **14**, 6231–6240.
191 S. K. Bhatia, *Langmuir*, 2002, **18**, 6845–6856.
192 S. K. Bhatia and D. Nicholson, *Chem. Eng. Sci.*, 2011, **66**, 284–293.
193 M. Yoshimune, T. Yamamoto, M. Nakaiwa and K. Haraya, *Carbon*, 2008, **46**, 1031–1036.
194 S. Gruener and P. Huber, *Phys. Rev. Lett.*, 2008, **100**, 064502.
195 D. J. Evans and J. P. Morris, *Statistical Mechanics of Non-equilibrium Liquids*, Academic Press, London, 1990.
196 K. P. Travis, B. D. Todd and D. J. Evans, *Phys. Rev. E: Stat. Phys., Plasmas, Fluids, Relat. Interdiscip. Top.*, 1997, **55**, 4288.
197 B. D. Todd, J. S. Hansen and P. J. Daivis, *Phys. Rev. Lett.*, 2008, **100**, 195901.
198 I. Bitsanis, J. J. Magda, M. Tirrell and H. T. Davis, *J. Chem. Phys.*, 1987, **87**, 1733–1750.
199 I. Bitsanis, T. K. Vanderlick, M. Tirrell and H. T. Davis, *J. Chem. Phys.*, 1988, **89**, 3152–3162.

200 I. Bitsanis, S. A. Somers, H. T. Davis and M. Tirrell, *J. Chem. Phys.*, 1990, **93**, 3427–3431.
201 P. G. de Gennes, *Langmuir*, 2002, **18**, 3413–3414.
202 J. O. Hirschfelder, C. F. Curtiss and B. R. B., *Molecular Theory of Gases and Liquids*, Wiley, New York, 1954.
203 T. H. Chung, M. Ajlan, L. L. Lee and K. E. Starling, *Ind. Eng. Chem. Res.*, 1988, **27**, 671–679.
204 D. M. Heyes, *J. Chem. Phys.*, 1992, **96**, 2217–2227.
205 C. Dariva, L. A. F. Coelho and J. V. Oliveira, *Braz. J. Chem. Eng.*, 1999, **16**, 213–227.
206 G. Galliéro, C. Boned and A. Baylaucq, *Ind. Eng. Chem. Res.*, 2005, **44**, 6963–6972.
207 R. A. Reis, R. Nobrega, J. V. Oliveira and F. W. Tavares, *Chem. Eng. Sci.*, 2005, **60**, 4581–4592.
208 S. M. Ali, *Mol. Phys.: Int. J. Interface Chem. Phys.*, 2007, **105**, 387–393.
209 V. N. Burganos and S. V. Sotirchos, *AIChE J.*, 1987, **33**, 1678–1689.
210 S. V. Sotirchos and V. N. Burganos, *AIChE J.*, 1988, **34**, 1106–1118.